



Forschungsberichte
aus
dem Institut
für Höchstfrequenztechnik
und Elektronik
der
Universität Karlsruhe

Herausgeber:
Prof. Dr.-Ing. W. Wiesbeck

Jürgen v. Hagen

**Wide Band Electromagnetic
Coupling to a Cavity:
An Integral Representation
Based Model**

Copyright: Institut für Höchstfrequenztechnik und Elektronik
Universität Karlsruhe, 1997

alle Rechte vorbehalten

Druck: Druckerei Ernst Grässer, 76131 Karlsruhe, Tel. (07 21) 61 50 50

ISSN: 0942-2935

Vorwort des Herausgebers

Die Kombination von Elektromagnetischer Verträglichkeit (EMV) mit numerischer Feldtheorie stellt für beide Bereiche eine Herausforderung dar. Dies insbesondere auch deshalb, weil die räumlichen Dimensionen in der EMV die heute bekannte Leistungsfähigkeit der numerischen Feldtheorie bis an die Grenzen auslasten. Diese Grenzen werden weniger durch das technische Verständnis, als vielmehr durch Speichergrößen und Rechenleistung gesetzt. Während nun die analytische Feldtheorie a priori das Verständnis um die Felder und Wellen unterstützt, ist bei der numerischen Feldtheorie eine intensive Interpretation der Ergebnisse unabdingbar. In Verbindung mit der erst seit wenigen Jahren intensiv betrachteten elektromagnetischen Verträglichkeit ergeben sich hieraus ebenso umfangreiche theoretisch-mathematische Aufgabenstellungen, wie Interpretationsanforderungen.

In der vorliegenden Arbeit sind die Problemstellungen, die Lösungsmöglichkeiten und die Ergebnisse für die Einkopplung ebener elektromagnetischer Wellen in geschlossene Gehäuse mit im Vergleich zur Wellenlänge kleiner Öffnungen umfassend untersucht. Es zeigt sich, daß von der Vielzahl numerischer Feldberechnungsverfahren für spezifische Anwendungen auch spezifische Codes nur optimale Ergebnisse liefern. Nicht globale, sondern lokale Verfahren, speziell adaptiert an das Problem, führen zum Ziel. In diesem Sinne liefert die vorliegende Arbeit beispielhaft Ein- und Ansichten zum Einsatz numerischer Feldberechnungsverfahren in der elektromagnetischen Verträglichkeit.

Prof. Dr.-Ing. Werner Wiesbeck

- Institutsleiter -

**Forschungsberichte aus dem
Institut für Höchstfrequenztechnik und Elektronik
der Universität Karlsruhe (TH)**

Herausgeber: Prof. Dr.-Ing. Werner Wiesbeck

- Band 1 Daniel Kähny
Modellierung und meßtechnische Verifikation polarimetrischer, mono- und bistatischer Radarsignaturen und deren Klassifizierung
- Band 2 Eberhardt Heidrich
Theoretische und experimentelle Charakterisierung der polarimetrischen Strahlungs- und Streueigenschaften von Antennen
- Band 3 Thomas Kürner
Charakterisierung digitaler Funkssysteme mit einem breitbandigen Wellenausbreitungsmodell
- Band 4 Jürgen Kehrbeck
Mikrowellen-Doppler-Sensor zur Geschwindigkeits- und Wegmessung - System-Modellierung und Verifikation
- Band 5 Christian Bornkessel
Analyse und Optimierung der elektrodynamischen Eigenschaften von EMV-Absorberkammern durch numerische Feldberechnung
- Band 6 Rainer Speck
Hochempfindliche Impedanzmessungen an Supraleiter / Festelektrolyt-Kontakten
- Band 7 Edward Pillai
Derivation of Equivalent Circuits for Multilayer PCB and Chip Package Discontinuities Using Full Wave Models
- Band 8 Dieter J. Cichon
Strahlenoptische Modellierung der Wellenausbreitung in urbanen Mikro- und Pikofunkzellen
- Band 9 Gerd Gottwald
Numerische Analyse konformer Streifenleitungsantennen in mehrlagigen Zylindern mittels der Spektralbereichsmethode
- Band 10 Norbert Geng
Modellierung der Ausbreitung elektromagnetischer Wellen in Funksystemen durch Lösung der parabolischen Approximation der Helmholtz-Gleichung
- Band 11 Torsten C. Becker
Verfahren und Kriterien zur Planung von Gleichwellennetzen für den Digitalen Hörrundfunk DAB (Digital Audio Broadcasting)
- Band 12 Friedhelm Rostan
Dual polarisierte Microstrip-Patch-Arrays für zukünftige satellitengestützte SAR-Systeme

**Forschungsberichte aus dem
Institut für Höchstfrequenztechnik und Elektronik
der Universität Karlsruhe (TH)**

- Band 13 Marcus Demmler
Vektorkorrigiertes Großsignal-Meßsystem zur nichtlinearen Charakterisierung von Mikrowellentransistoren
- Band 14 Andreas Froese
Elektrochemisches Phasengrenzverhalten von Supraleitern
- Band 15 Jürgen v. Hagen
Wide Band Electromagnetic Aperture Coupling to a Cavity: An Integral Representation Based Model

**Wide Band Electromagnetic Aperture
Coupling to a Cavity :
An Integral Representation Based Model**

Zur Erlangung des akademischen Grades eines

DOKTOR-INGENIEURS

von der Fakultät für
Elektrotechnik
der Universität Karlsruhe

genehmigte

DISSERTATION

von

Dipl.-Ing. Jürgen v. Hagen
aus München

Tag der mündlichen Prüfung :

18. November 1997

Hauptreferent :

Prof. Dr.-Ing. Werner Wiesbeck

Korreferent :

Prof. Docteur es Sciences Walid Tabbara

La présente dissertation est née de mes travaux menés conjointement à l'Institut für Höchstfrequenztechnik und Elektronik de l'Université de Karlsruhe (TH) en Allemagne et dans la Division Ondes du Laboratoire des Signaux et Systèmes (LSS), unité mixte du Centre National de la Recherche Scientifique (CNRS) et de l'École Supérieure d'Électricité (Supélec) en France.

J'exprime mes cordiaux remerciements à Monsieur Professor Dr.-Ing. Werner WIESBECK, Université de Karlsruhe, pour avoir accepté d'assumer la charge de directeur de thèse, pour ses remarques et ses critiques ainsi que pour son aide efficace lors des difficultés que j'ai pu rencontrées.

Je remercie très spécialement Monsieur le Professeur Walid TABBARA, LSS, pour les suggestions et les idées avec lesquelles il a nourri mon travail, son conseil professionnel et personnel en toutes circonstances ainsi que son aide toujours aimable.

Je remercie vivement mes parents, ma belle-sœur et mon frère pour leur soutien constant quelles que soient mes décisions et pour leurs encouragements. Sans eux je n'aurais peut-être jamais abouti.

Que mes collègues et amis en France, entre autres Bernard DUCHÊNE, Jean-Michel GEFFRIN, Alain JOISEL, Marc LAMBERT, Jean LEFÈBVRE, Amélie LITMAN, et comment ne pas oublier Christophe ROZIER, ainsi que mes collègues en Allemagne Frank DEMMERLE, Jens HAALA, Norbert GENG, Stefan KERN, Frederik KÜCHEN et Thomas ZWICK soient remerciés pour leur amitié et pour les discussions que nous avons pu avoir. Je tiens aussi à remercier Laurence FRÉMY et Renate WYPYCH pour leur aide toujours aimable et efficace.

Finalement je voudrais exprimer ma joie d'avoir pu contribuer à l'entente et amitié franco-allemande. Je voudrais également remercier Carine d'avoir changé d'avis sur les Allemands en me donnant ainsi un sens profond à mon séjour.

Die vorliegende Arbeit entstand während meiner Forschungstätigkeit am Institut für Höchstfrequenztechnik und Elektronik der Universität Karlsruhe (TH) in Deutschland und der Division Ondes des Laboratoire des Signaux et Systèmes (LSS) als gemeinsame Einrichtung des Centre National de la Recherche Scientifique (CNRS) und der École Supérieure d'Électricité (Supélec) in Frankreich.

Mein herzlicher Dank gilt Herrn Professor Dr.-Ing. Werner Wiesbeck, Universität Karlsruhe, für die Übernahme des Hauptreferats, seine kritischen Anmerkungen zu meiner Arbeit und seine pragmatische und flexible Unterstützung bei der Lösung aller Probleme.

Herrn Professeur Walid Tabbara, LSS, danke ich ganz besonders für seine vielen Anregung zu dieser Arbeit, seinen fachlichen und persönlichen Rat in jeder Lage und seine umfassende, stets lebenswürdige Hilfestellung.

Meinen Eltern, meiner Schwägerin und meinem Bruder gilt mein aufrichtiger Dank für ihre Unterstützung bei all meinen Entscheidungen und ihre Aufmunterung in guten und weniger guten Zeiten. Ohne sie wäre diese Arbeit wohl nicht möglich gewesen.

Meinen Kollegen und Freunden in Frankreich, unter anderen Bernard Duchêne, Jean-Michel Geffrin, Alain Joisel, Marc Lambert, Jean Lefebvre, Amélie Litman, und, wie könnte ich nur vergessen, Christophe Rozier sowie in Deutschland Frank Demmerle, Jens Haala, Norbert Geng, Stefan Kern, Frederik Küchen und Thomas Zwick möchte ich vielen Dank sagen für ihre Freundschaft und viele hilfreiche Diskussionen. Laurence Frémy und Renate Wypych möchte ich für ihre immer schnelle und lebenswürdige Hilfe danken.

Abschließend möchte ich meine Freude zum Ausdruck bringen, daß ich durch meine Tätigkeit in den beiden Ländern einen kleinen Beitrag zur deutsch-französischen Freundschaft leisten konnte. Und ich möchte Carine danken, daß sie ihre Meinung über die Deutschen geändert hat und mir dadurch einen tieferen Sinn für alles gab.

Contents

Contents	v
Table of Symbols and Variables	ix
1. Introduction	1
1.1. Motivation	1
1.2. The Problem at Issue	2
1.3. Structure	4
2. Electromagnetic Compatibility	7
2.1. Basic Notions	8
2.1.1. Sources of Perturbations	8
Natural Sources	8
Man Made Noise	8
Nuclear Sources (Electromagnetic Pulse, EMP)	9
2.1.2. Coupling Mechanisms	10
Cables	10
Screens and Housings	11
Apertures	12
2.2. Laws and Standards	13
2.2.1. Legal Framework	15
2.2.2. Standards	15
2.3. Testing Procedures	16
2.4. Numerical Modelling in EMC	18
2.5. Conclusions	19

3. Numerical Modelisation	21
3.1. A Survey on Possible Solutions	21
3.1.1. Finite Difference - Finite Integration	22
Application of MAFIA	26
3.1.2. Finite Elements - HFSS	28
3.1.3. Integral Equations	33
3.1.4. The Method of Moments	34
3.1.5. Choice of the Green's Functions	36
3.2. Separation of Interior and Exterior	37
3.3. Source Fields at the Exterior	39
3.4. The Green's Functions of a Rectangular Cavity	43
3.5. Reformulation of the Integral Equation	48
3.6. Conclusions	52
4. Implementation and Sample Cases	53
4.1. Application of MoM	53
4.1.1. Efficient Computation of the Triple Series	54
4.1.2. Double Surface Integration	56
4.1.3. Basis and Testing Functions	58
Strictly Local Functions	58
Semi-Global Functions	61
4.1.4. Lumped Loads and Sources	64
4.1.5. Inversion of the Impedance Matrix	65
4.2. Experimental Setup	66
4.3. Sample and Test Cases	66
4.3.1. The Wire in the Cavity	69
4.3.2. Plates in the Cavity	73
4.3.3. Changing the Shape of the Cavity	74
4.4. Acceleration of Computation Times	77
4.4.1. Different Algorithms for Computing Acceleration	77
4.4.2. Wide Band Data from Sample Frequencies	78

5. Applications	83
5.1. Interaction Plate–Monopole	83
5.2. Statistical Methods in EMC	90
5.3. Conclusion	94
6. Conclusion and Outlook	97
A. Polarisabilities of Small Apertures	101
A.1. Circular Aperture	101
A.2. Elliptic Aperture	101
A.3. Narrow Elliptic Aperture ($w \ll l$)	102
A.4. Narrow Slit ($w \ll l$)	102
A.5. Various Shapes	102
B. Reaction of Cavity and Objects	103
B.1. Electric Dipole	103
B.2. Magnetic Dipole	106
B.3. Example	106
C. The Elements of the Impedance Matrix	109
C.1. Z_{JJ}	109
C.2. Z_{JE}	110
C.3. Z_{JH}	110
C.4. Z_{EJ}	111
C.5. Z_{EE}	112
C.6. Z_{EH}	112
C.7. Z_{HJ}	112
C.8. Z_{HE}	112
C.9. Z_{HH}	113
C.10. Integrals	113
C.10.1. Local Basis Functions	113
C.10.2. Global Basis Functions	116

D. Algorithm for the Interpolation by Rational Functions	119
Bibliography	121
Curriculum Vitae	129

Table of Symbols and Variables

The present table summarizes the symbols and variables used in the following. Numerical figures were taken from DIN 1324, Part 1 (1988).

A	cavity size in \vec{e}_x	m
α_e	electric polarisability	m^3
$\bar{\alpha}_m$	magnetic polarisability	m^3
B	cavity size in \vec{e}_y	m
C	cavity size in \vec{e}_z	m
c_0	speed of light in vacuum, $c_0 = 2.997925 \cdot 10^8 \frac{\text{m}}{\text{s}}$	$\frac{\text{m}}{\text{s}}$
$\vec{e}_x, \vec{e}_y, \vec{e}_z$	unit vectors in the three space coordinates	
\vec{E}	electric field	$\frac{\text{V}}{\text{m}}$
ε	permittivity of a medium, $\varepsilon = \varepsilon_0 \varepsilon_r$	$\frac{\text{V s}}{\text{A m}}$
ε_0	permittivity of the vacuum, $\varepsilon_0 = \frac{1}{\mu_0 c_0^2} \approx 8.854187817 \cdot 10^{-12} \frac{\text{V s}}{\text{A m}}$	$\frac{\text{V s}}{\text{A m}}$
ε_r	relative permittivity	
f	frequency	Hz
Γ	general: surface	
\bar{g}_e	Green's function for the electric field due to magnetic current	m^{-2}
\bar{g}_F	Green's function for the electric vector potential	m^{-1}
\bar{g}_h	Green's function for the magnetic field due to magnetic current	m^{-3}
\bar{G}_A	Green's function for the magnetic vector potential	m^{-1}

$\bar{\bar{G}}_e$	Green's function for the electric field due to electric current	m^{-3}
$\bar{\bar{G}}_h$	Green's function for the magnetic field due to electric current	m^{-2}
\vec{H}	magnetic field	$\frac{\text{A}}{\text{m}}$
$\bar{\bar{I}}$	unit dyad	
j	imaginary unit, $j^2 = -1$	
\vec{J}	volume current density	$\frac{\text{A}}{\text{m}^3}$
\vec{J}	surface current density	$\frac{\text{A}}{\text{m}^2}$
k	wave number, $k = \frac{2\pi}{\lambda}$	m^{-1}
\vec{M}	magnetic current density	$\frac{\text{V}}{\text{m}^2}$
μ	permeability, $\mu = \mu_0 \mu_r$	$\frac{\text{V s}}{\text{A m}}$
μ_0	permeability of the vacuum, $\mu_0 = 4\pi 10^{-7} \frac{\text{V s}}{\text{A m}}$	$\frac{\text{V s}}{\text{A m}}$
μ_r	relative permeability	
ν	intrinsic wave impedance, $\nu = \sqrt{\frac{\mu}{\epsilon}}$	Ω
ω	angular frequency $\omega = 2\pi f$	s^{-1}
Q	quality factor of a resonant system	
λ	wavelength, $\lambda = c/f$	m
$L(\cdot)$	linear operator	
\vec{n}	normal vector of a surface	
\vec{r}	general: point in space	m
\vec{r}'	source point	m
S	scattering matrix	
t	time	s
X	normalisation constant for general variable x	

Chapter 1

Introduction

1.1. Motivation

After the invention of the transistor and subsequently of the integrated circuit, electronics have moved more and more into everyday life. Producers tend to include more and more ‘intelligent’ features into most basic appliances, even if an objective advantage is not obvious: toasters with microcontrollers clocked at a rate of several MHz [1], washing machines with fuzzy logic controller, vacuum cleaners with electronic suck control. The list goes on. Moreover, more and more electronic applications facilitate our life: microwave ovens, computers, mobile phones came only recently, but are today indispensable. And electronic devices control the functioning of systems, watch over our life and make it more secure: for cars, we have seen electronic injection or non blocking brakes and will, perhaps, see anti collision radars and automatic guidance systems in a near future. Already today, up to 48 microprocessors and 62 electric motors are integrated into S-class cars of Mercedes-Benz.

Not always, however, the designers of systems accounted for the fact that any equipment is to function in an electromagnetic environment which is far from perfect. The oblivion of this parameter leads to inexplicable performances, sometimes with serious consequences: lorries start their engine, the medical apparatus fails during resuscitation allegedly because a doctor uses his mobile phone in the ambulance [2], during the Vietnam war, the American army loses aircrafts while approaching the aircraft carrier.

To redress the errors, two possibilities exist and have been chosen simultaneously: the first is to forbid what should not happen, as the “don’t use a cellular phone if you have a pacemaker” in [3]. The other is to impose

certain characteristics on all electric and electronic equipment not to perturb and not to become perturbed. This gave birth to regulations, quite early for military applications, more recently also for civil ones.

Most regulations were issued by national bodies and were applicable only to one specific country. Common markets need common rules, however. This is true not only for the abolishment of restraints, but also for the undisturbed coexistence of various equipments together in a common environment. This is why the European Union enacted a directive uniquely concerning EMC. National laws as well as European and national standards followed so as to fix common European testing procedures and limits.

Manufacturers and producers were hence obliged to harden their systems against possible perturbations, and to develop them in a way that the emission of perturbations would be as small as possible. In the beginning, EMC was considered only late during the design cycle, until it was realised that late corrections are more expensive than an early inclusion of EMC notions in the development. Nowadays, EMC experts take part in every stage of the development.

Due to the experimental character, EMC was widely a domain of experimental work. While computers and software become faster and faster, have a wider applicability with simultaneously falling prices, EMC continues to be an experimental area due to the tremendous complexity of the systems and the symptoms. Even with modern mainframes, parallel machines or vector computers, a modellisation of an EMC problem remains expensive in time or money.

The present work does not intend to solve one well defined problem. It aims more on two other points. The first is the physical understanding of phenomena: what happens and why. The other main point is closely related to hereto. Knowing more about the phenomena, what should be respected to reduce possible perturbations.

1.2. The Problem at Issue

The problem at issue is based on a natural necessity: even with a perfect shielding in a housing, a connection of the equipment to the exterior is

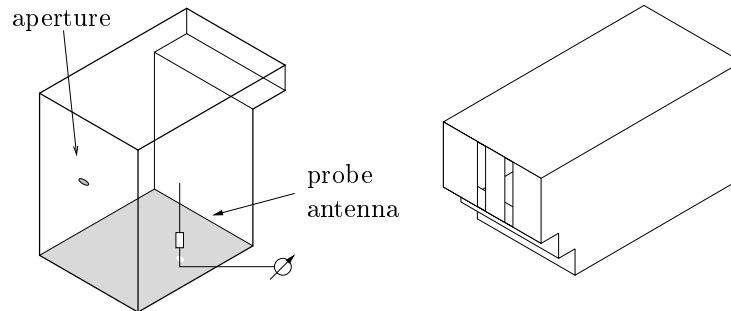


Figure 1.1.: Generic metallic housing with probe antenna and flight warning calculator Airbus A 320

necessary. The problem at issue picks up this necessity and treats the interaction of a wave with a metallic housing. The wave enters the housing through a hole like in fig. 1.1. A numerical method computes the currents induced and predicts the interaction. The amount of coupling is measured at the base of an antenna, which allows to compare easily with the experimentations. Pure field measurements are quite sensitive to errors and are therefore excluded from the present work.

An exact drawing of the generic structure is shown in fig. 1.2. The cavity has the dimensions A , B and C in the x , y and z directions respectively. The origin for all dimensions is the lower front corner of the cavity, shown as a circle in the figure. The aperture is in the $x = 0$ wall, its coordinates are hence $(0, y_{ap}, z_{ap})$. It is described by a characteristic dimension as the radius r or the surface S . The objects placed in the cavity are defined by two corners, the bottom corner and the top corner. The coordinates are $(x_{bot}, y_{bot}, z_{bot})$ and $(x_{top}, y_{top}, z_{top})$ respectively.

The computation of wave interaction with this generic structure is not a pure academic problem. Most housings resemble it like the flight warning calculator of the Airbus A 320 plane (fig. 1.1). Furthermore, a study of the understanding of physical effects should concentrate more on general phenomena than on the immediate solution of a concrete problem which always remains one specific case only.

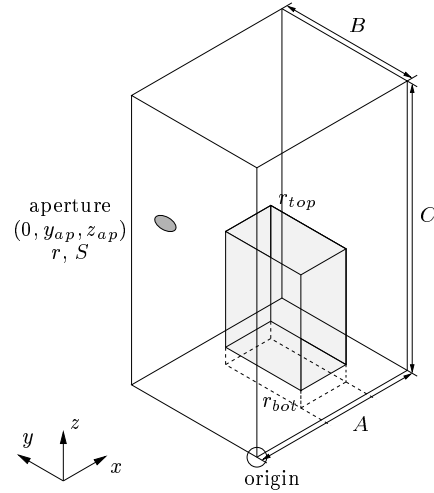


Figure 1.2.: Generic structure and dimensions

Each numerical method has its strong points, but also its restrictions. An application of a method without careful and critical interpretation of the results can lead to failure and wrong results. After considering several methods, an Integral Equation formulation solved by a Method of Moments has been chosen.

Numerical methods tend to be slow and to demand large amount of memory. During the development of the method, this was also to be respected.

1.3. Structure

The present work is organised as follows: after this introduction, a description of what makes Electromagnetic Compatibility (EMC) a wide domain is given in chapter 2. For this, it is necessary to provide a common vocabulary: basic notions in EMC form a major part of the chapter. An overview of the European standards with special weight on radiated perturbations and testing methods follows. Recent applications of numerical methods on

problems in EMC are at the end of that chapter. Numerical methods are the topic of chapter 3. Three of the most popular methods are: Finite Difference Time Domain, Finite Element Method and Integral Equation Method. By analysing the three, the Integral Equation Method shows to be more adapted to the problem at issue. The general Integral Equations are reformulated under consideration of the problem at issue at the end of the chapter. Chapter 4 presents the details of the numerical implementation and sample cases showing the domain of validity of the method. Two types of functions are presented and compared with respect to implementation and effectiveness. This comparison was until now incomplete in the literature and is here presented in a unified way. A new method for gaining broad band data in strongly resonant structures ends the chapter. A physical interpretation of some phenomena, as well as possible applications of the method are found in chapter 5. The use of statistical methods in conjunction with the present numerical method for fast predictions in EMC is a further part of that chapter. Chapter 6 summarises the present work, and gives an outlook.

The appendix is a collection of most of the mathematical work. It contains the polarizabilities for various apertures (appendix A), the way to compute the expressions for reaction of the cavity (appendix B), the elements of the moment matrix (appendix C) and the algorithm for the interpolation by rational functions in appendix D.

Finally a comment on the presentation: Even though written in British English, this text is inspired by a certain German ‘taste’. Unless directly issued by computer software, figures were drawn as suggested in the German standards. DIN 5 [4] was underlying for perspective pictures, DIN 461 [5] for curves in coordinate systems. DIN 1324 [6] gives a broad basis for quantities in electromagnetics. Finally, the document was formatted using the German ‘Koma-script’ package of \LaTeX .

Chapter 2

Electromagnetic Compatibility

Electromagnetic compatibility (EMC) is defined as the ability of an equipment to function in a given electromagnetic environment without emitting perturbations possibly causing disturbances for other equipment present in the same environment. Hereby a possible impairment of biological tissues by electromagnetic fields is related to it, is, however, not subject of the present work. The two major parts of EMC are called immunity as the ability to continue to function, and emission as the fact of not perturbing other equipment.

EMC becomes more and more an important issue for manufacturers due to legal regulations and also to fear of legal suits. During the design of new systems, aspects of EMC must be included already in an early stage in order to reduce costs arising from late corrections. To date, recommendations exist for the design of systems so that they are less prone to perturbations. They concern mainly the grouped arrangement of the different analog and fast and slow digital circuits, the design of printed circuit boards, grounding schemes, the wire layout, position and size of orifices, shielding practice etc., and are based both on long-time experience and physical considerations. The latter are the result of the nature of the different phenomena, the sources, and the coupling mechanisms. During and after the design stage, the new equipment is subject to tests checking if it complies with the requirements of the constructor, the customer and/or national standards.

This chapter will concentrate on some of the above items: first some basic notions of EMC are introduced. Characteristic sources and possible coupling mechanisms give an idea of the range of EMC considerations. Protection measures for radiated perturbations as well as the transmission of electromagnetic energy through apertures build another part of the basic notions. The growing importance of national and international standards

are the reason for an overview over European standards in EMC. These standards define also measurement techniques presented in a further part of this chapter. Finally, some recent examples of numerical modellisation in EMC follow. Additional informations much beyond the scope of the present work can be found in [7–10].

2.1. Basic Notions

2.1.1. Sources of Perturbations

The sources of electromagnetic perturbations are usually subdivided according to their origin into natural and man made sources, the latter further subdivided into industrial and nuclear sources. Most natural sources, lightning apart, have a low power level, and are thus only important for specific equipments.

Natural Sources

Natural low power sources are electromagnetic noise by electrical discharges in the atmosphere during thunderstorms and cosmic noise. This noise has a long grasp and therefore a permanent character. Sources with a short lifetime are electrostatic discharges, and lightnings. Direct strokes of lightnings cause not only electric, but also thermic and mechanic damages. Static discharges are accompanied by electric fields up to 3 MV/m with a rise time of several nanoseconds and a total time of several hundred nanoseconds. Lightnings cause electric fields of several hundred V/m with a rise and total time in the order of microseconds.

Man Made Noise

Unintentional and intentional artificial emitters of electromagnetic energy compose the man made noise. Unintentional and undesired signals are produced by all sorts of electric and electronic systems like power lines, transformers, electric motors in home appliances, ignition systems of combustion engines, industrial applications like welding or cleaning, neon tubes

and many others. Most of them have a spectrum spread over a wide range of frequencies. Emitters of intentional signals are for instance radio and television transmitters, information transmission systems using electromagnetic waves in space or on wires, inductive heating systems, systems for telemetry, etc., with a signal ideally confined to a very narrow frequency band. Digital equipments constitute a source of electromagnetic noise due to high clock rates and short rise times. This source of electromagnetic noise becomes more and more important. The whole frequency spectrum of common environments reaches from kHz to GHz with field strengths from mV/m to V/m. Ambient electric fields in urban areas in the order of 0.1 V/m [9] from short waves to VHF were reported.

Considering the bandwidth of the perturbation and the useful bandwidth of the victim, the perturbation can also be referred to as being a small or wide band perturbation.

Nuclear Sources (Electromagnetic Pulse, EMP)

Nuclear sources, or better perturbations caused by explosions of nuclear weapons in the atmosphere or in high altitude, are of minor importance for civil equipment, the direct effects of the ionising radiation being much more important. Explosions in high altitudes are nevertheless of relevance not only for armed forces, but also for civil electronic or electric applications like power lines installations, transmission systems, etc. due to the large spatial range they have. The electromagnetic effects after such explosions also allow the surveillance of the nuclear activities in the world.

The electromagnetic radiation which concerns EMC is a result of the interaction of the nuclear radiation with matter, either the atmosphere or the soil, producing free charges by the photoelectric effect, Compton effect, or formation of electron-positron pairs. Mathematical models exist for the representation of electromagnetic fields after nuclear explosions. Typical rise times are hereby in the order of nanoseconds, the total duration of the phenomenon is several hundred nanoseconds.

Additional effects on electronic and electric devices, not directly related with the EMP, but rather with ionising radiation, are the SGEMP (System Generated Electromagnetic Pulse, caused by direct irradiation of enclos-

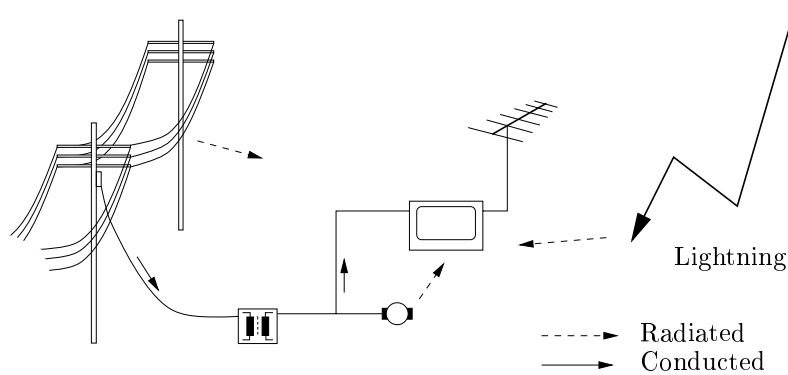


Figure 2.1.: Coupling paths by radiation and conduction

ures) and the TREE (Transient Radiation Effects on Electronics, direct effect of ionising radiation on components).

2.1.2. Coupling Mechanisms

The electromagnetic interference effects caused by the various sources propagate on various paths to a given equipment. Fig. 2.1 shows the two paths of coupling: radiation and conduction. Cables and wires play a major role for both types of perturbations. One considers that for frequencies below 30 MHz (corresponding to a wavelength of 10 m), the perturbations are predominantly conducted ones, whereas above 30 MHz the radiated type predominates.

Cables

Cables are the elements which cause most of the radiation. Even cables normally not intended to carry RF currents, can radiate like presented in [11] where the power supply cable of a computer screen radiates most of the energy at certain frequencies. Also, a conducted perturbation can be the result of a wave which couples to a cable or wire far away from the actual equipment or system, then conducted into the system.

The coupling by radiation in the near field of the source is either a predominantly magnetic field coupling or an electric field coupling. The far field of a source may be considered as an electromagnetic wave, at very large distances as plane wave. The actual perturbation finally happens when the field couples to the system. The cable layout has a major influence on the nature and amount of the coupling. To reduce perturbations by radiation, the systems and interconnecting cables are provided with a shield which must be continuous to be effective. However, the shields of coaxial cables are rarely perfect. Flexible cables with their woven shields with small holes deteriorate the shielding effectiveness. Furthermore, even with a very effective shielding, the shield itself can act as an antenna, and radiate or receive a considerable amount of energy, then coupled into a system via inappropriate connectors.

Inside a system, more specifically between different wires and cables and also printed lines on printed circuit boards (PCB), the coupling is called crosstalk, and caused by mutual inductances or inter-circuit capacitance. The wires being the source are clock or other digital lines, power lines or current carrying grounds. The common impedances in the conducting path possibly have a reactive part, resulting in resonances with strong increase or decrease of the current. Design recommendations exist for the layout of PCBs, where to place high speed circuits, analog devices, connectors to other PCBs or the exterior, etc. Further down on the design level, decoupling capacitances, the capacitances between the different layers of the PCB, line widths etc. are parameters for decoupling the system components mutually [1].

Screens and Housings

Systems are usually shielded by metallic housings. An electromagnetic wave impinging onto a conductor induces a current on it. For a perfect conductor this current is a surface current, and entirely confined to the surface. An enclosure made of perfect conducting material would annihilate the field in the interior, and hence perturbation by direct irradiation would be impossible. On real materials for enclosures with finite conductivity, 63.2 % of the total induced current are confined to the skin depth on the

irradiated surface. The skin depth depends on the media and frequency and is given by

$$\delta = \sqrt{\frac{2}{\kappa\mu\omega}} \quad (2.1)$$

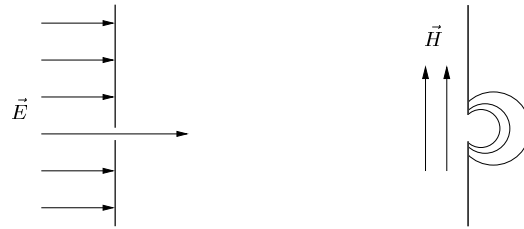
with μ permeability, κ conductivity of the shielding material. Hence, the shielding effectiveness depends on the material, its thickness and the frequency of the incoming wave. One sees that for high frequencies the skin depth decreases, the shielding becomes more efficient.

As plastic or resins are isolating media, enclosures made of these materials must be doubled by conducting coatings due to the isolating properties of the plastic. The coatings usually consist of an isolating base material with conducting fillers as carbon black, metallized glass, or others. The requirements for the coatings are manifold. They must, among others, be mouldable, light, and persistent. By using these modern composite materials, transparent openings with shielding properties are possible.

Apertures

By adequate shielding, the attenuation of external fields can be made as strong as necessary. However, as every equipment must communicate with the exterior in a way or another, openings or orifices are inevitable for ventilation, viewing displays, connectors for power and signal cables which are intentional openings. Maintenance traps of small equipments and access doors to large scale systems are usually sealed electromagnetically by joints, which constitute unintentional and unexpected apertures after degradation due to aging or improper use. Therefore, coupling through apertures is a very important issue in electromagnetic compatibility.

Fig. 2.2 shows the \vec{E} and \vec{H} field coupling through small apertures in thin walls [9]. For design purposes, apertures are usually modelled by the basic equivalent dipole principle. This principle replaces the aperture by a set of dipoles on both sides of the enclosure wall. This basic, but important concept will be used to model the aperture, and yields very good results. The reaction, which is the field coupled back to the aperture, is neglected, can however cause at certain frequencies high resonances as shown in the

(a) \vec{E} field coupling(b) \vec{H} field couplingFigure 2.2.: Coupling of \vec{E} or \vec{H} through an aperture

examples in chapter 4. In that chapter the equivalent dipole principle is extended to include the reaction fields.

The exponential attenuation of a wave in a waveguide below cut-off together with thick walls helps to reduce the transmission of electromagnetic energy through apertures. The attenuation constant is $\alpha \approx \frac{2\pi f_c}{c}$ for low frequencies compared to f_c (cut-off frequency of the waveguide formed by the aperture through the wall), therefore the cross section of the opening should be as small as possible, with a length corresponding to a intended attenuation. This is exploited in honeycomb air vent filters where the whole section of the orifice is subdivided into small tubes by metallic lamellas.

2.2. A Survey on Laws and National and International Standards

In the following a short introduction into the area of standards is given. This section also provides an idea of how EMC is currently regulated. The presentation is limited to the standards issued by the CENELEC (Comité Européen de Normalisation Electrotechnique), the standardisation institute of the European Union for civil applications. Due to European laws they have to be and were issued as national standards, e.g. in Germany by the VDE (Verband Deutscher Elektrotechniker) in the DIN (Deutsches Institut für Normung e.V.), or in France by the AFNOR (Association Française de Normalisation). The standards are based on international

CISPR (Comité International Spécial pour les Perturbations Radioélectriques) recommendations, so that the knowledge of the European standards is a good starting point also for other regions of the world.

The different limits and methods of measurement are elaborated and published by several CISPR subgroups. They are

CISPR 11, for industrial, scientific and medical equipments

CISPR 11A

CISPR 12 for ignition systems for motor vehicles

CISPR 13 for receivers for radio and television

CISPR 14 for electrical motor operated and thermal appliances for household and similar purposes, electric tools and similar electric apparatus

CISPR 15 for radio disturbance characteristics of electrical lighting and similar equipment

CISPR 20 for immunity of sound and television broadcast receivers and associated equipment

CISPR 22 for information technology equipment

The above mentioned CISPR recommendations were adopted as European standards, the corresponding classification mark is EN 550., “..” being the appropriate CISPR number. German standards are prefixed with DIN.

Another set of standards elaborated by the IEC, or International Engineering Consortium, are the IEC 801 standards which describe limits and methods of measurement. They are now being replaced by the IEC 1000 standards, taken over by the European EN 61000 with part and section appended to the number. The different parts determine e.g. the methods of measurement or the environment, whereas the sections determine among other things the limits for measurements of immunity characteristics, for tests concerning static electricity, high frequency fields, bursts, magnetic fields, bulk currents, and others. In section 2.3 some of the methods of measurement are detailed.

In other parts of the world, like North America or Asia, other standards are applicable. They can be based on the same CISPR standards as the European ones, as are for instance the American ANSI or FCC standards, or be totally different.

Another field, not considered here, are standards and special specifications for the various armies. They can vary between the different forces. They are not normalised in Europe, let alone in the world. As they can be very different in content, and difficult to inspect due to understandable security issues, this topic is not broached.

2.2.1. Legal Framework

The legal obligation to respect the standards is given by the European directives 89/336/EEC and 93/68/EEC. They were translated into national law, in Germany in the *Gesetz über die elektromagnetische Verträglichkeit* dating November 9th, 1992 and furthermore in *Erstes Gesetz zur Änderung des Gesetzes über die elektromagnetische Verträglichkeit* from August 30th, 1995. These laws concern all manufacturers of any equipment likely to cause electromagnetic perturbations or to be disturbed electromagnetically. An equipment is here a product with a characteristic function in contrast to a system (e.g. a microcomputer) as an assembly of several equipments with a common function, or to a plant as an assembly of several systems. Systems are covered by the directive, whereas plants are only covered in so far as the systems composing the plant are concerned. Components as elements for products or systems are not covered either. Explicitly excluded from the requirements of the law are equipments covered by other directives like today motor vehicles (72/245/EEC), telecommunication equipments (91/263/EEC), or equipments for satellite broadcast (93/97/EEC).

The main statement of the directive is that the producer is responsible that his product conforms with the corresponding European standards. The fact that the equipment fulfils the requirements is signed by marking the equipment with the *CE* sign. The European standards in their German version are shortly described below.

2.2.2. Standards

All equipment fall under the generic standards EN 50081, part 1 and 2 and 50082, part 1 and 2. EN 50081 treats the emission, EN 50082 the immunity. Of either standard, part 1 is for residential, commercial and light industry

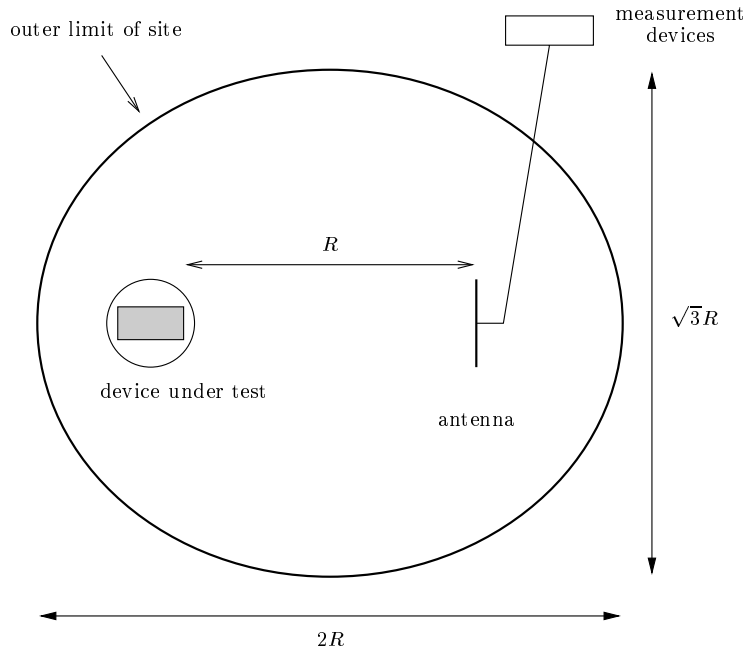


Figure 2.3.: Measuring site as defined in EN 55020

environments, part 2 for industrial environment. The four standards are not applicable to equipment for which specific product or product family standards exist. EN 50081 and 50082 refer to other standards (mainly the above CISPR or IEC standards in their European form) for fixing limits and methods of measurement. They further describe how to mark the product and which technical documentation must be available to the customer.

For some equipments, respective product or product family standards exist. Their number is continuously growing.

2.3. Testing Procedures

Each of the above mentioned perturbations needs specific testing procedures, the limits are then imposed on the thereby measured values. Defined

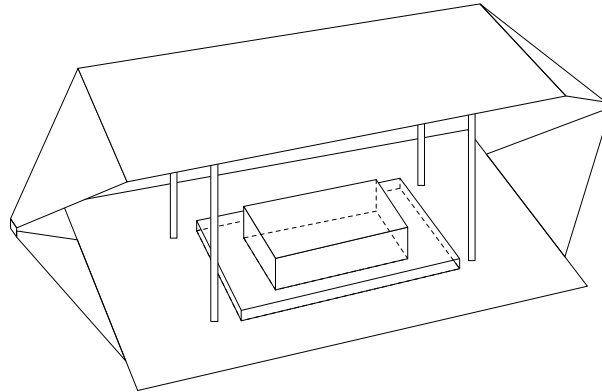


Figure 2.4.: Open stripline TEM cell as sketched in EN 55020

are measurement methods for conducted and radiated perturbations. As the problem at issue is related to radiated perturbations these are the only ones presented.

Radiated perturbations must be carried out on a site which satisfies the dimensions as defined in EN 55022 and sketched in fig. 2.3: the distance between the device under test (DUT) and the antenna is 10 m, the test area is now defined as an area limited by an ellipse with the small axis of approximately 17 m and the large axe of 20 m. Also possible is a distance of 3 m, the axes of the ellipse then being 6 m and 5.2 m. The space inside the ellipse and above the area, must be free of reflecting objects. Usually only open area test sites fulfil the requirements, but have sometimes a noise level above the legal limits for perturbations. The standards (CISPR 16 and 22) also authorise alternative test sites with precise requirements for the site attenuation.

Open area test sites and alternative test sites are, however, not always available. Especially for smaller elements subject to immunity tests, stripline TEM cells (fig. 2.4) are used as defined in EN 55020. The wave limited by the upper and lower plate is sufficiently homogeneous in approximately a third of the TEM cell volume. The TEM cells can attain dimensions of more than 50 m as e.g. the SSR site of the Direction Générale de l'Armement,

so that tests on large scale systems like airplanes or vehicles are possible.

The basic requirement for all test sites is the homogeneity of the field on the device under test. For anechoic chambers, this is an important property. A possibility would be to use monoconic antennas with a metallic floor, the wave close to the floor would be almost plane and hence homogeneous. This type of test area is not included in the standards, will however be used for comparative measurements within this work.

2.4. Numerical Modelling in EMC

EMC is a domain where numeric modelling is not yet widely used. Standards only define test procedures, no numeric tools are mentioned. Development departments of manufacturers rely more on rules of thumb, experience and testing as on numerical modelling. Small and medium companies can not afford the high investments state of the art tools would demand.

However, large systems or test sites require sometimes even higher investments. Numerical modellisations in early stages reduce considerably the high costs wrong or unsuitable designs can cause.

Big companies were hence the first to apply numerical tools. Levilain [12] presented the use of numerical tools at the Aerospatiale. A Finite Difference Time Domain code called **GORF 3D** was used for the design of lightning conductors on the launch site of the Ariane rockets. For one type of the Airbus airplane family, numerical methods were called on for the accreditation process concerning electromagnetic compatibility and lightning.

Manufacturers of automobiles have used numerical tools for a long time in the domain of crash tests. For the optimisation of combustion in engines or crash tests, finite element tools like **NASTRAN** are widely in use. Electromagnetic simulations are not yet commonly used, essentially due to limited computer resources. A modelling of a medium sized car like a Peugeot 306 with, as an example, the boundary element code **ASERIS** of the Aerospatiale ([13] and private communication) demands several days for the meshing and several weeks for a simulation.

Printed circuit boards are a field where numerical tools begin to emerge. Programs developed for the investigation of signal integrity are now adapted to predict the radiation of boards. The quality of the simulated values compared to measured values is, however, not satisfying due to the more than simple models used. A thorough board simulation by 2^{1/2} or 3D tools like Momentum or Microwave Explorer demands powerful PCs or workstations. A recent paper reports the use of the numerical code NEC (Numerical Electromagnetics Code) for simple test cases of the emission of microstrip lines with view on physical understanding and educational clearness [14].

The numerical modellisation of housings were the subject of a PhD thesis of the University of Karlsruhe [15, 16]. Housings with finite conductivity with or without holes were treated using the TLM method. For reasonable execution times the TLM algorithm was parallelised and executed on a workstation cluster. Housings with small apertures, however, cause convergence problems.

Test sites demand a great effort in time and financial means. Numerical modellisations can assist the builder during the design. The assessment and possible optimisation of open area sites was presented based on Method of Moments and Finite Difference Time Domain computations [17]. The modellisation of semianechoic chambers and the possible improvement were treated using the Finite Integration Technique in another PhD thesis of the University of Karlsruhe [18]. There the homogeneity of the field incident on the device under test (DUT) was computed, additional absorbers were suggested in strategic places to optimise the electromagnetic properties of the chamber.

2.5. Conclusions

In this chapter, a short and necessarily incomplete overview of the domain of EMC, the phenomena, the legal framework and standards, as well as testing procedures was given. Some emerging numerical applications show the growing interest to use computers for EMC. The main attention is hereby more and more directed towards the understanding of the underlying physics and educational clearness.

The presentation is necessarily only an incomplete collection of what can be concerned, many things are missing. Hopefully the reader is now aware of the large field of EMC and its growing importance in today's industrial developments. The following chapters pick out of the various elements the problem presented in chapter one.

Chapter 3

Numerical Modelisation

This chapter will present the criteria for choosing from some potential numerical methods. No method is able to tackle the whole problem. The separation of interior and exterior cuts the problem into two and allows to consider interior and exterior separately by adapted methods. The selected method is finally examined more closely.

3.1. A Survey on Possible Solutions

The determination of a solution for Maxwell's equations with a set of boundary conditions is only sometimes possible in an analytical way. In early times approximations were made in order to solve problems with a reasonable accuracy. With the advent of digital computers new methods were developed to tackle different problems. As each of these numerical methods has its own strong points, but also its weaknesses, it is best suited only for a certain class of problems. A "general problem solver" is not yet known, and will, in my opinion, never be found. In the following an overview over some of the most well-known methods (Finite Difference Time Domain FDTD and Finite Integration Technique FIT, Finite Element Method FEM and the Method of Moments MOM for the solution of the Electric Field Integral Equation) is given. Further indicated are well-suited problems and the reasons for choosing one of these rather than another. In doing so, no details on each method will be given, but rather the criteria which led to the final decision for the method used in the present work. For further informations the reader is kindly invited to refer to the bibliography. Beside books specialised on one or more methods (like [19–22]), journals regularly publish special issues on numerical methods like [23], [24] or most recently [25]. In these special issues the reader will find interesting

and useful introductions, up-to-date informations as well as references for technical details.

The problem presented in chapter 1 exhibits some very interesting features which are important for the choice of the appropriate solution technique. Several details have to be taken into consideration:

- The cavity under test is placed in free space with a plane wave coming onto the structure.
- The wave interacts with the cavity whose size spans from only fractions of a wavelength at very low frequencies to several wavelengths at high frequencies. At the same time the characteristic dimensions of the aperture are very small compared to the dimensions of the cavity and hence of the wave.
- The antenna measuring the amount of coupling into the cavity has only a very small radius compared to the dimensions of the cavity
- At first, the cavity is only fitted with metallic objects. A deformation of the cuboidal cavity remains possible.
- The only losses for the cavity looked at as a resonator are the losses through the small aperture and the ohmic losses in the antenna impedance. Therefore, the Q-factor of the system is very high.

One has to bear in mind these constraints when considering a method. In the following section some of the best known methods are confronted with the present problem. First, the FDTD, the FIT and the FEM methods show how they can tackle the present problem. This highlights their interest and weaknesses. The codes chosen are the MAFIA and the HFSS codes respectively.

3.1.1. Finite Difference - Finite Integration

The most straightforward way to introduce a numerical method for the solution of Maxwell's equations is perhaps the Finite Difference Time Domain (FDTD) approach. Starting with initial conditions for the electric and

magnetic field $\vec{E}(\vec{r}_0, t_0)$ and $\vec{H}(\vec{r}_0, t_0)$, one advances the time t step by step while updating the fields under consideration of the boundary conditions. The most spread scheme is the scheme proposed by Yee in 1966 [26]. For this scheme one applies central-difference approximations to the time and space derivatives in Maxwell's curl equations. This procedure is a sampling scheme accurate to the second order. The sampling points for the electromagnetic fields (continuous in space and time) are chosen so that the discretisation error stays within some previously fixed bounds. Hereby the discretisations in space and time are not independent, but have to satisfy the so-called stability-condition for numerical stability and least numerical dispersion. Furthermore the components of the electric and magnetic fields are interleaved in time and space so as to be able to fulfill the appropriate boundary conditions at media interfaces. As the update process is explicit, there is no need for setting up or solving a set of linear equations, the required computer storage and running time are hence proportional to the computational volume and time interval.

Another method closely related to the FDTD is the Finite Integration Method (FIT) developed by Weiland [27] and commercially available as MAFIA computer code. Each of the four Maxwell equations in integral form is transformed to an equivalent matrix expression on a Yee lattice. The integrations are simple multiplications by the cell size [18]. According to the authors, the method is widely equivalent to the FDTD and shall therefore be treated within the same section.

According to Taflové [28], the FDTD-method has among others the following strong points:

- The method was validated by comparisons to analytical and experimental results for three-dimensional conducting bodies in the range of 0.1 to 30 wavelengths. Meshes with non-constant cell sizes are possible. Due to limitations for the non-constant discretisation steps in space, the proportion of the smallest detail to the biggest extent is not arbitrary, but limited.
- It is easily applicable to complex surface shapes and/or closed geometries with internal structures. As the discretisation is directed in the three coordinate directions, only rectangular shapes can be

meshed exactly. Arbitrarily shaped structures will be meshed with a certain error, generally considered as neglectable. So-called Fuzzy-cells at curved boundaries allow to reduce further this error.

- A variety of waveforms is available for the excitations by waves or discrete sources. The number of complete cycles of the wave needed for a converging solution is proportional to the Q factor of the structure or phenomenon being modelled which can lead to very long computation times for highly resonant cavity-structures near the resonance [29].
- The number of unknowns of the fields can be very high, several hundreds of thousands are usual. As however the entire volume has to be discretised, this number is higher than for surface discretisations.
- The computation of problems involving non-linearities, time-varying media properties or pulse responses is straightforward.
- Frequency dependent properties of media involve in the time domain convolutions. Some types of frequency dependence (Debye) can be taken into consideration by recursive convolutions [22].

In the following the capabilities of the Finite Difference Time Domain method are compared to the constraints of the problems at issue.

As the entire computational volume of the problem has to be discretised, the lattice has to be truncated at some distance from the cavity. The outgoing wave must not be reflected at this lattice truncation so as to model free space. This truncation problem is solved by application of absorbing boundary conditions of different types [30]. The Mur ABCs approximates locally the wave equation at the cells at the lattice truncation by a Taylor expansion. One assumes hereby that the wave is an outgoing plane wave perpendicular to the boundary, thus necessitating a considerable distance to all scatterers. Another possibility is the perfectly matched layer introduced by J.P. Berenger [31, 32] as a “layer of media” with an impedance suitably chosen so that waves are totally absorbed. The truncation can then be much closer as with classic Mur absorbing boundaries. A cavity with a size of approximately one third of a wavelength, e.g. 0.5 m for 200 MHz, has to be put into a volume of about one wavelength for the classic

ABC. Thus, the interior of the cavity, which makes up the most interesting part, is only a ninth of the total computational volume. Furthermore the computation of near field quantities as surface current densities necessitates for each angle of incidence a totally new computation.

The Finite Difference method was originally used with constant discretisation steps. For the meshing of small sized details in larger problems the number of unknowns would be rather high as the mesh in less interesting regions would be unnecessary fine. Non-constant meshes allow to sample precisely places of interest and the remaining parts more sparsely. The ratio of the sizes of adjacent cells is usually limited to a value between 0.8 and 1.2. A constant expanding or contracting factor yields cell sizes according to a geometric series law.

The most difficult part to mesh is the small aperture. Tests show that at least nine mesh points are needed on the aperture to accurately account for it. Additionally, the wall with the aperture must have a finite thickness as the investigated FDTD codes are not capable to model plates with zero thickness. At low frequencies the amount of the wave coupled into the cavity is very low. The aperture in the wall acts like a waveguide below cut-off and attenuates further the coupling. Therefore, the wall thickness should be small, necessitating a fine sampling in the direction normal to the wall. In the vicinity of the aperture the meshing is therefore very fine compared to a mesh needed for the rest of the cavity. Taflov proposed a modification of the basic FDTD algorithm in order to include also apertures and gaps whose size is much smaller than a lattice cell [33]. This method is not yet available in commercial codes.

For very small scatterers like wires with diameters much smaller than the discretisation step, several efforts are reported in the literature. One possibility is to modify the FDTD update equations and to include the charge and the current present on the wire. The electric and magnetic fields of the cells just around the wire are then modified correspondingly [34]. Another possibility especially for wire bundles introduced in [29] is the application of Faraday's law with a contour integral for the looping magnetic field adjacent to the wire or wire bundle. For this, the wire or the wire bundle is replaced by a single wire with an equivalent radius. Then, the equivalent wire is placed into a volume delimited by a virtual surface

coinciding with a mesh border of the FDTD lattice. On this surface the electromagnetic fields are computed via a FDTD and then applied in an electric field integral equation (EFIE) to compute the accurate current distribution on every single wire. Again, the thin wire formulation is not yet available in many commercially available codes. If available, the previously mentioned antenna could be modelled using one of these thin wire approximations.

Metallic objects of finite thickness, dielectric bodies and cavities of arbitrary shape are well suited problems for the FDTD

Application of MAFIA

The Finite Integration Method is commercially available in the package MAFIA. It contains a mesh generator, two time-domain modules for two-dimensional and for three-dimensional computations, a frequency-domain module, and finally a postprocessor. The frequency domain module does not include absorbing boundary conditions so that free-space computations are not possible. The ABC in the time-domain module are only classic ones using the approximation of the wave-equation at the boundaries, Berenger-ABCs are not available. Wires treated as perfect electric conductors are possible, but approximated by polygons through mesh points.

The incident field can be created by electric dipoles, a plane wave, or electric and magnetic fields defined as initial fields. The fields can be probed, measurements of currents however are “subject to a beta version, so check [...] results carefully” [35].

Nevertheless, it was possible to model the problem of chapter 1 by this commercial code, version 3.20. The time domain module `t3` was used as the frequency domain module `f3` does not allow free-space computations. Fig. 3.1 shows a sample mesh for a rectangular cavity with a small aperture centred on the front wall. The long side of the cavity is $\lambda/3$ long, the short ones $\lambda/5$. The aperture has a size of only $\lambda/20$. Clearly to see is the fine mesh around the aperture with 16 mesh points lying in the aperture plane. The front wall has a thickness of one cell size. The remaining inner volume of the cavity is meshed with a larger step size. Absorbing boundary conditions of the first order are placed at a distance of $\lambda/3$ from the outer

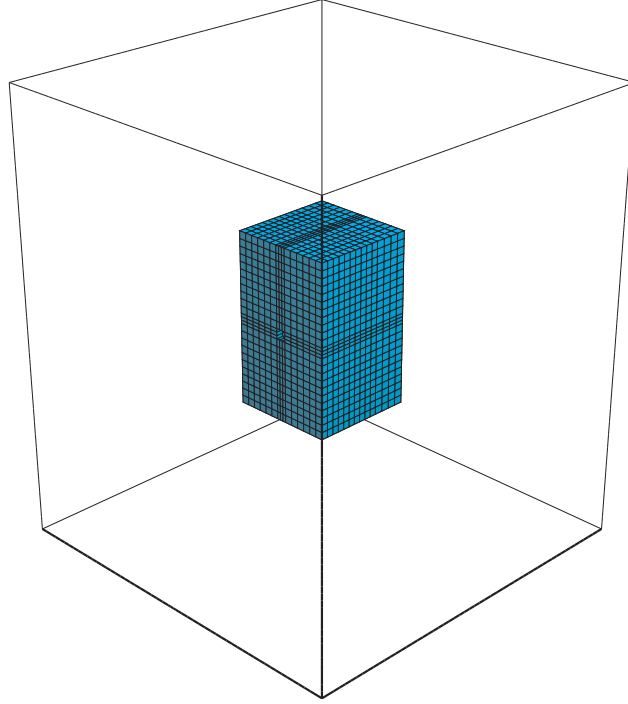


Figure 3.1.: Example of a mesh generated for the MAFIA code

walls of the cavity. The frequency of the incoming wave is well below the first resonance of the cuboidal cavity. There are no objects inside the cavity.

Fig. 3.2 shows the z -component of the electric field right behind the aperture for a monochromatic incident plane wave. One sees that the system only reaches the steady state very slowly. In fact, there is no noticeable attenuation of the high-frequency components. This is the major drawback of time-domain solutions for the case of resonant structures: a very long computation time is necessary to achieve the steady state. For the present case of a cavity with very high Q -factor the computation times are not acceptable (computation time for fig. 3.2 several hours).

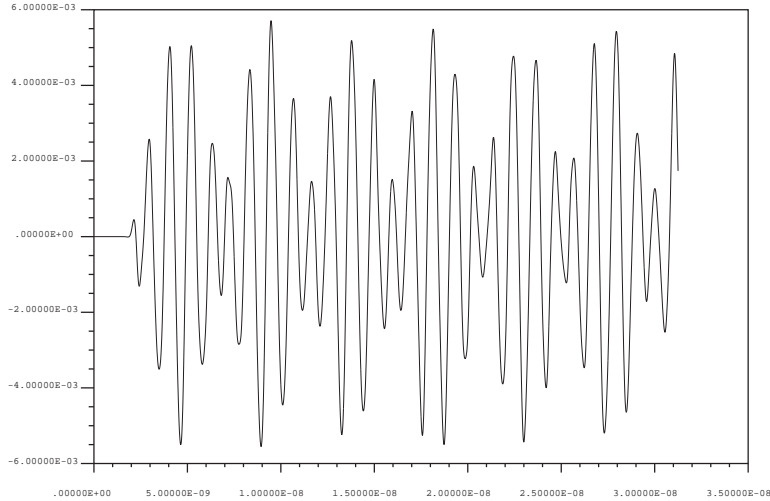


Figure 3.2.: Electric field inside a cuboidal cavity (E_z/Vm^{-1} over t/s)

These problems encountered during the modelling with Finite Difference and Finite Integration Methods suggested not to use these methods. A possibility to perform computations of coupling to cavities is proposed by [36]. There, the exterior and the interior of the cavity are separated by application of the Schelkunoff-principle. The incident field on the outside of the cavity is determined by a Method of Moments, then the interaction of the equivalent aperture field inside the cavity is computed by a FDTD scheme. This method, however, requires a profound modification of the FDTD codes.

3.1.2. Finite Elements - HFSS

Another code, commercialised by Hewlett-Packard, is the so-called High Frequency Structure Simulator (HFSS). It is based on the Finite Element Method (FEM) in the frequency domain. No details will be given here, only the application of version 4.1 of the above programme to the present problem.

The Finite Element Method discretises the whole computational space by tetrahedra and interpolates the electric field between the nodes by polynomials, called basis functions. The solution of the field quantities involves a matrix inversion for each frequency or each mesh. With fixed frequency, the mesh is refined in an iterative process until a user defined error for the field or for therefrom derived quantities as the scattering parameters is achieved. ABC are again needed for free-space simulations. The ABC are here called “radiation boundaries”, and normally used for computing far fields and radiation patterns. The boundary must lie at some distance from all scatterers, at least a quarter of a wavelength [37].

Further restrictions concern the overall size of the problem. [38] states several general rules for problems that are within the scope of the software’s analytical capabilities. Among other things, the structure should be electrically small, i.e. only a few wavelengths long. Another important issue for the modellisation of structures is again the ratio of smallest and largest dimensions. [37] advises not to use ratios greater than three orders of magnitude (details of 1 mm are not advised for structures with dimensions of 1 m).

Two options are available for scattering parameter S computations in a certain frequency band. One option is to explicitly solve for the S parameters at every frequency point using the mesh generated for the so-called *adaptive frequency*. This mesh reduces the difference of the field between the previous iteration and the present one to the user defined value. Another option is the “fast sweep” option where the solution at the adaptive frequency is extrapolated to the entire frequency band by an asymptotic waveform evaluation. The accuracy of the solution is obviously best near the adaptive frequency [37].

A difficulty arises when one attempts to compute currents on metallic surfaces. The magnetic field is derived from the simulated electric field by a discrete derivation $\vec{H} = \frac{1}{-j\omega\mu} \nabla \times \vec{E}$. The current again is equal to the curl of the magnetic field $\vec{J} = \nabla \times \vec{H}$ [37]. By twice deriving numerically the simulated quantity, the values for the current are inaccurate if one does not take into account many iterations. Direct current measurements were therefore excluded.

In a first step a completely closed, perfectly conducting box in free space

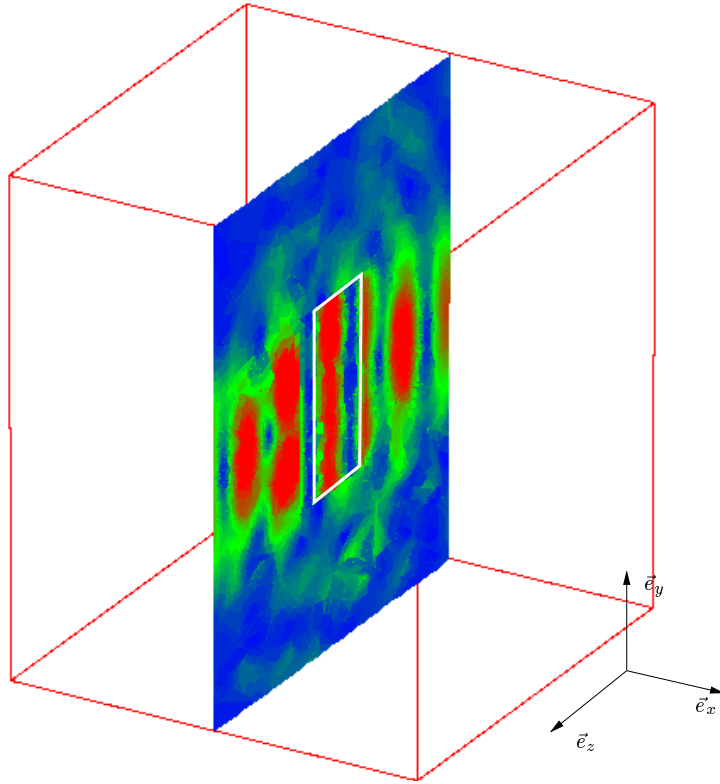


Figure 3.3.: HFSS: completely closed, perfectly conducting box in a plane wave field

was simulated. A plane wave directed in $+z$ direction at a frequency well below the first resonance impinges on the front wall. The electric field is shown in fig. 3.3, the shape of the box is drawn in white. This obviously wrong field reaches values inside the box ten times higher than the incident field. The technical support mentioned that this was a known problem of the method and confirmed that the method was not applicable to boxes in free space.

Among the most suited problems to be tackled with HFSS are com-

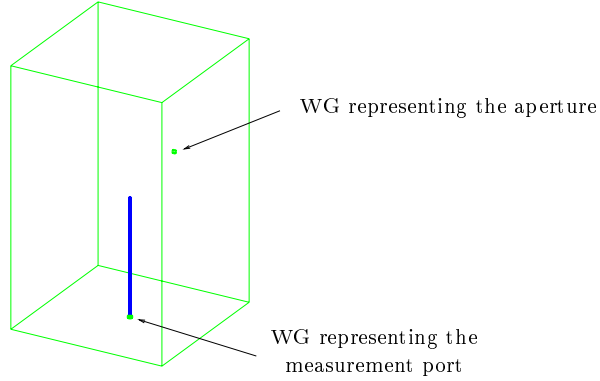


Figure 3.4.: S_{21} simulation without free space

putations of the scattering matrix S of multiports. The present problem of wave interaction is now looked as the determination of the scattering matrix S of a two port, one port representing the small aperture, the other one being the monopole antenna. Each port has to be connected to a short homogeneous waveguide. As the dimensions of the waveguide associated with the aperture are very small, this waveguide is operated below cut-off. The wave travelling down the waveguide is therefore strongly attenuated which causes high differences for the field strength values, and thus numerical problems when inverting the system matrix. Waveguides should therefore be held as short as possible in these cases. Fig. 3.4 shows a sample drawing of a rectangular cavity with at the back the small aperture. The monopole antenna is modelled as a perfect conductor which ends in a coaxial waveguide with impedance 50Ω representing the input of a network analyser. Both the sweep and the fast sweep option for a wide band computation were used. Fig. 3.5 shows the graphs of the sweep and the fast sweep solution of HFSS for the scattering coefficient S_{21} between the two waveguides. For comparison also plotted is a Method of Moments solution described further down for the interaction of a plane wave to the cavity through a small hole. As the coupling through the aperture is not equivalent to the coupling through a waveguide, the absolute values are

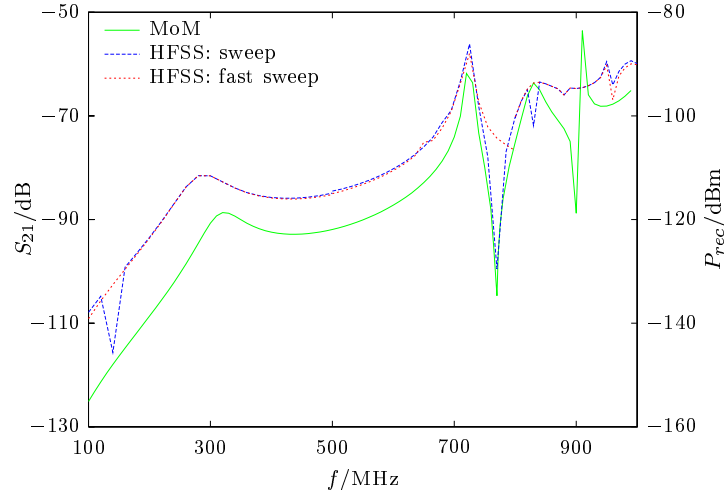


Figure 3.5.: Sweep and fast sweep solution as well as Method of Moments solution

not comparable. On the left-hand y -axis applicable to the HFSS-results, the magnitude of S_{21} is shown. On the right-hand axis the received power computed by the MoM for an incident plane wave of unity electric field strength is shown. The agreement in shape and progression, specially for the resonances, is satisfying.

As a result, the above stated problems show that the FEM is not entirely suited for the problem at issue. In [39] a separation of exterior from the interior is proposed which at least would solve the problems related to a plane wave incident on objects in unbounded space. This demands however the inclusion of magnetic currents which is not provided in HFSS. A complete rewriting of the FEM part would be necessary. Still, the question of computing currents from the electric field is not addressed. Not having the required competence and experience with the FEM, the already present EFIE/MoM code [40] was chosen to be extended to three-dimensional objects.

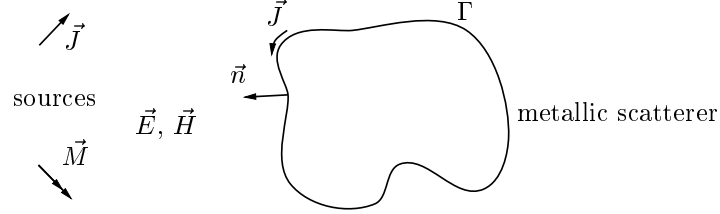


Figure 3.6.: Metallic scatterer in electromagnetic field

3.1.3. Integral Equations

One more family of methods is based on the field representation by Maxwell's equations in integral form. For perfect electric conductors, the Electric Field Integral Equation method (EFIE), exclusively involving the electric field, is used. In the following a very short introduction to this method will be given, and leave further informations to literature, e.g. [41] or [42].

Consider fig. 3.6: a perfect conducting scatterer in free space with surface Γ with outward pointing normal vector \vec{n} is placed in an incident electromagnetic field $(\vec{E}_{inc}, \vec{H}_{inc})$ created by some sources \vec{J}, \vec{M} . The total electric field (\vec{E}, \vec{H}) is the sum of the incident field and the scattered field:

$$\vec{E} = \vec{E}_{inc} + \vec{E}_{sca} \quad \vec{H} = \vec{H}_{inc} + \vec{H}_{sca} \quad (3.1)$$

The scattered field \vec{E}_{sca} is created by the currents on the scatterer

$$\vec{E}_{sca} = \frac{j}{\omega \epsilon} (\nabla^2 + k^2) \int_{\Gamma} \vec{G}_A(\vec{r}, \vec{r}') \vec{J}(\vec{r}') dr' \quad (3.2)$$

where k is the free-space wave number $k = \frac{2\pi}{\lambda}$, \vec{r}' a point on Γ and \vec{G}_A is the Green's function for the vector potential. The Green's function is, as Collin [43] says,

“basically [...] the solution to a given differential equation, together with specified boundary conditions, with the source being a source of unit strength and localised at a point in space.”

The actual geometry, which could be, to name but a few, free space, a half space bordered by a perfect conducting plane, rectangular or cylindrical

cavities, or stratified media, imposes the boundary conditions. Eqn (3.2) states that if the currents are known, the integration of the Green's functions over the currents will yield the field in any point of space under consideration of the boundary conditions specified by the Green's functions. By changing the Green's function, it is possible to investigate the radiation of the sources in the corresponding space.

For a general field problem however, the currents on the scatterers are not known, so that the scattered field can not be determined. The boundary condition for the electric field on a perfect conductor $\vec{n} \times \vec{E} = 0$ gives us the additional condition needed for the total field. Eqn. (3.1) and (3.2) can now be combined to give:

$$\vec{n} \times \vec{E}_{inc} = -\vec{n} \times \vec{E}_{sca} = -\vec{n} \times \left(\frac{j}{\omega \varepsilon} \right) (\nabla^2 + k^2) \int_{\Gamma} \vec{G}_A(\vec{r}, \vec{r}') \vec{J}(\vec{r}') dr' \quad (3.3)$$

The currents in this equation are still unknown. They are, however, related to the incident field by an integral equation. Once the currents are obtained, the fields can be computed in every point of the domain. The most popular method for solving eqn. (3.3) is the Method of Moments (MoM).

3.1.4. The Method of Moments

In general, the Method of Moments is a method to solve linear functional equations. Here, only the MoM applied to the solution of the electric field integral equation eqn. (3.3) is of interest. Further general considerations about the method can be found e.g. in [21], [41] or [44].

Eqn. (3.3) is an inhomogeneous functional equation which can be written in the form

$$L(f) = g \quad (3.4)$$

with L being a linear operator, g a known function and f a function to be determined. The MoM consists of several steps. First one identifies the operator L , its domain (the functions f on which it operates) and its range

(the functions g for any given f). For the present work, L is an integral operator with kernel $(\nabla^2 + k^2)\bar{G}_A$, its range is the field created by the currents in the space of the Green's functions. The domain of L are the currents which can physically exist on the metallic objects.

The next step is the expansion of the unknown function f in a series of known functions f_1, f_2, f_3, \dots in the domain of L as

$$f = \sum_n \alpha_n f_n \quad (3.5)$$

where the f_n are the so-called *basis functions*, and α_n the projections of f on the f_n . As f is unknown, the α_n are unknown as well. The sum is for exact solutions usually infinite, to be able to solve a given problem with finite resources, one has to truncate the sum at some index N . Applying (3.5) to (3.4), it becomes

$$L(f) = \sum_n \alpha_n L(f_n) = g \quad (3.6)$$

as the operator L is linear.

The next step is to define a set of *weighting* or *testing functions* w_1, w_2, w_3, \dots in the range of L and a suitable inner product $\langle \phi, \psi \rangle$. This inner product is then applied to eqn. (3.6) with each w_m

$$\sum_n \alpha_n \langle L(f_n), w_m \rangle = \langle g, w_m \rangle \quad (3.7)$$

for each $m = 1, 2, 3, \dots$. The resulting set of equations can be written in matrix form as

$$\mathbf{L}\alpha = \mathbf{g} \quad (3.8)$$

with the matrix \mathbf{L} and vectors α and \mathbf{g} as:

$$\mathbf{L} = \begin{pmatrix} \langle L(f_1), w_1 \rangle & \langle L(f_2), w_1 \rangle & \cdots \\ \langle L(f_1), w_2 \rangle & \langle L(f_2), w_2 \rangle & \cdots \\ \langle L(f_1), w_3 \rangle & \langle L(f_2), w_3 \rangle & \cdots \\ \dots\dots\dots\dots\dots\dots\dots \end{pmatrix} \quad (3.9)$$

$$\alpha = \begin{pmatrix} \alpha_1 \\ \alpha_2 \\ \vdots \end{pmatrix} \quad \text{and} \quad \mathbf{g} = \begin{pmatrix} \langle g, w_1 \rangle \\ \langle g, w_2 \rangle \\ \vdots \end{pmatrix}$$

The matrix \mathbf{L} is called the moment-matrix whose name is derived from the original name n^{th} -moment of f for the expression $\int f(x)x^n dx$. After replacing x^n by the f_n , the integral keeps the name of *moment*.

If \mathbf{L} is nonsingular, its inverse \mathbf{L}^{-1} exists, the α_n are then given by

$$\alpha = \mathbf{L}^{-1} \mathbf{g} \quad (3.10)$$

f is then the linear combination of the $\alpha_i f_i$ as in eqn. (3.6). Depending on f , the f_n and w_m , the solution for f may be exact or approximate.

From a practical point of view, the series (3.5) and (3.7) must always be truncated at some index. The inversion of the matrix \mathbf{L} is then always possible.

3.1.5. Choice of the Green's Functions

The electric field integral equation method is depending on the Green's functions $\bar{\bar{G}}_A$ applicable for a large range of problems. Until now usually only the free-space Green's functions were used, some authors as [44] distinguished between MoM solutions using the free-space functions and MoM solutions using Green's functions for other geometries, the latter even calling hybrid MoM/Green's function methods. FEKO, e.g., a commercial MoM program developed at the University of Stuttgart, Germany, contains not only the free-space Green's functions, but also the ones for a dielectric sphere in free space. The latter is used for computations of biological effects of cellular telephones near human heads. Other Green's functions again would enable field computations in other spaces.

For a long time the Green's functions for rectangular or cylindrical cavities have been known [45–48]. If one separated the interior of the cavity from the exterior, the problem would effectively be cut into two smaller ones: the first is the wave interacting with a metallic cavity in free space, and the second the resulting field inside the cavity in presence of metallic scatterers. This separation allows the use of two different Green's functions for the two regions, thus making profit of the advantage that the Green's functions already include the boundary conditions. In free space no artificial absorbing boundary conditions are needed, only the metallic scatterer is discretised, and therefore the number of unknowns remains quite small. On the other hand, the Green's functions of a cavity already include the boundary conditions on the cavity walls, thus again reducing the number of unknowns to the scatterers.

3.2. Separation of Interior and Exterior

[43] presents how to separate two regions: two waveguides are coupled through a small aperture. It is based on a theory originally developed by H.A. Bethe based on theorems by Schelkunoff [49]¹. The theorems provide a formulation to replace apertures by equivalent electric and magnetic current sheets. For apertures with dimensions small compared to wavelength, an approximate theory states that the aperture is equivalent to a combination of electric and magnetic dipoles whose moments are proportional to the field at the aperture. In the following Schelkunoff's theorems is touched upon, the equivalent dipole theory follows from that.

Schelkunoff's ideas in the case of a perfect electric conductor are as follows. Consider a perfect electric conductor with sources inside and an aperture whose surface will be denoted by Γ_a . When the aperture Γ_a is closed with a perfect electric conductor, the sources produce the field E_0, H_0 , the field outside is zero as there is no leakage through the conductor. On Γ_a the electric tangential field E_{tan} vanishes and is therefore continuous.

¹The decoupling of interior and exterior mentioned in sections 3.1.1 and 3.1.2 is based on the same theorems, suggesting that this separation and subsequent use of the EFIE for the exterior is in fact the best suited method for wave interaction of boxed objects in unbounded media.

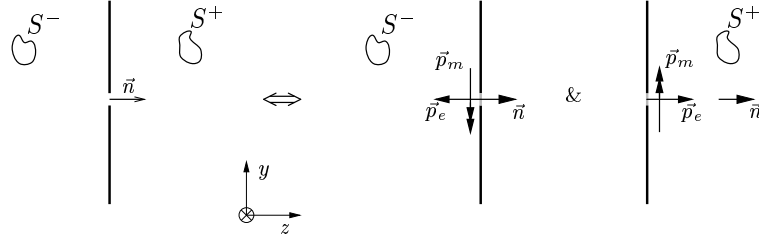


Figure 3.7.: Small aperture equivalent problems

On the other hand, H_{tan} is discontinuous by the electric current density $\vec{J} = -\vec{n} \times \vec{H}_0$ on Γ_a .

The aperture being open, the field produced by the same sources is the sum of E_0, H_0 and the field produced by an electric current sheet of density $n \times H_0$ over Γ_a . This is because the discontinuity in H_{tan} is eliminated and the continuity of E_{tan} is preserved. The resultant field satisfies all boundary conditions for the field produced by the given sources in the conductor with aperture.

By virtue of the theorem the aperture can be replaced by a perfect electric conductor and a set of sources provided that E_{tan} is continuous and H_{tan} is discontinuous.

Based on this theory, Bethe and later van Bladel and others [50–52] investigated the coupling through small apertures. They found that small apertures can be approximated by two dipoles, one electric perpendicular to the aperture plane and one magnetic in the aperture plane. The original theory concerns small apertures in infinite screens separating two homogeneous half spaces with electric characteristics ε, μ like in fig. 3.7. Sources S^- and S^+ are located in both half spaces on the left and the right side of the screen respectively. If the aperture placed at \vec{r}' is closed by a perfect electric conductor, the field on the two sides of the screen is $\vec{E}_{sc}^-, \vec{H}_{sc}^-$ and $\vec{E}_{sc}^+, \vec{H}_{sc}^+$ respectively. The field due to the aperture can now

be approximated for the right side by

$$\vec{p}_e = \varepsilon \alpha_e \left(\vec{E}_{sc}^-(\vec{r}'-) \cdot \vec{n} - \vec{E}_{sc}^+(\vec{r}'+) \cdot \vec{n} \right) \cdot \vec{n} \quad (3.11)$$

$$\vec{p}_m = -\bar{\alpha}_m \left(\vec{H}_{sc}^-(\vec{r}'-) - \vec{H}_{sc}^+(\vec{r}'+) \right) \quad (3.12)$$

where \vec{r}' is the location of the aperture, $\vec{r}'+$ a point at a small distance in direction of \vec{n} , and $\vec{r}'-$ at some small distance in the direction of $-\vec{n}$. The polarizabilities α_e and $\bar{\alpha}_m$ describe the size and shape of the aperture. They are available for small apertures with different shapes [43, 51, 53, 54]. The polarizabilities for circular apertures with radius r in a screen normal to \vec{e}_z are e.g.:

$$\alpha_{e,z} = \frac{4}{3}r^3 \quad \text{and} \quad \bar{\alpha}_m = \frac{8}{3}r^3 (\vec{e}_x \vec{e}_x + \vec{e}_y \vec{e}_y)$$

For other shapes the dyad for the magnetic polarizability is possibly no longer symmetric. The polarizabilities for some shapes are specified in appendix A, others can be found in literature.

As the equivalent dipole principle provides a suitable interface between the interior and the exterior, a separate computation of the fields in the two regions is now possible. The exterior problem is solved by the program FEKO which uses a hybrid method of moments for integral equations and physical optics solution of scattering in free space. For the interior the already existing theory [40] for wire scatterers is extended to three-dimensional scatterers of arbitrary number. The following two sections will treat the source fields in the exterior and the Green's functions of a rectangular cavity. The last section will finally reformulate properly the integral equation.

3.3. Source Fields at the Exterior

Originally the front wall of the cavity was considered as an infinite metallic screen [40]. One could also consider that the cavity is mounted behind a screen thus assuring a constant electric and magnetic field on the side of incidence. In this case the total field is easily computed by the boundary

conditions on a perfect electric conductor

$$\begin{aligned}
 \vec{n} \times \vec{H} &= \vec{J}_s \\
 \vec{n} \times \vec{E} &= 0 \\
 \mu \vec{n} \cdot \vec{H} &= 0 \\
 \varepsilon \vec{n} \cdot \vec{E} &= \rho_s = \frac{j}{\omega} \nabla \cdot \vec{J}_s
 \end{aligned} \tag{3.13}$$

with \vec{n} normal vector pointing outward from the conductor and \vec{J}_s and ρ_s surface current density and surface charge respectively. Depending on the polarisation of the incident wave the scattered field is then readily computed [55]. A wave polarised parallelly to the cavity wall, for instance, would generate at the conducting plane a zero electric field and a magnetic field twice as strong as the incident one.

The assumption of an infinite plane at the exterior is less valid for low frequencies where, in addition to the fact that the aperture is very small compared with wavelength, the cavity corners and edges are quite close to the location of the aperture speaking in terms of wavelength. A numerical determination of the exterior fields is therefore included in the present work. Fig. 3.8(a) shows the surface current density on a perfect conducting box at low frequency where the box dimensions are a tenth and a sixth of the wavelength respectively. At higher frequencies, the box becomes bigger in terms of wavelengths, the assumption for the aperture being in an infinite plane becomes more valid, the current becomes more uniform on the front side as in fig. 3.8(b).

In order to determine the surface current density and hence the magnetic and electric field at the aperture location a numerical method is necessary. Having in mind the above characteristics of numerical field computation methods, the obvious choice is a MoM code with the Green's functions of free space. An additional advantage compared to the procedures described before is that even for multiple incidence angles and polarisations it only necessitates one determination of the matrix elements in eqn. (3.8). After setting up the matrix, the surface currents on the scatterers can be determined for several conditions of incidence like angle or polarisation. The already mentioned program FEKO was used for the

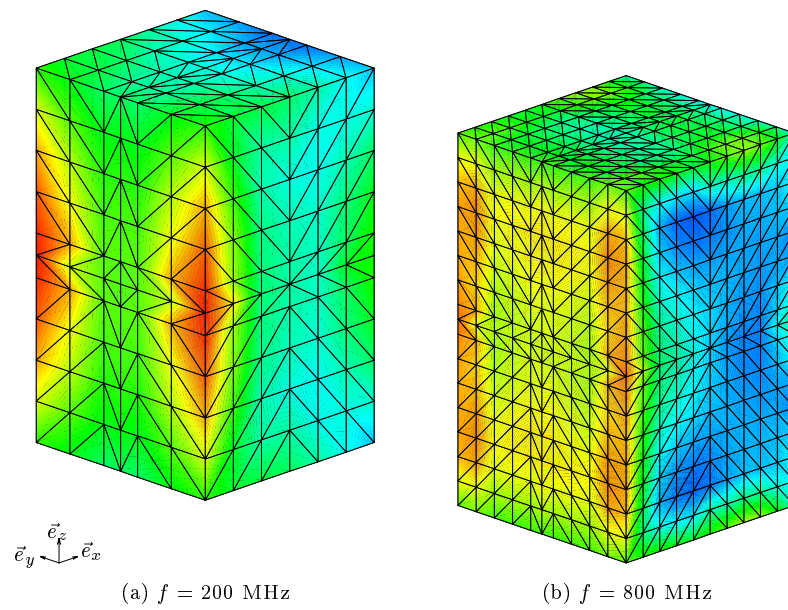


Figure 3.8.: Current distribution on a box in free space. The plane wave travels in \vec{e}_x and is polarised in \vec{e}_z

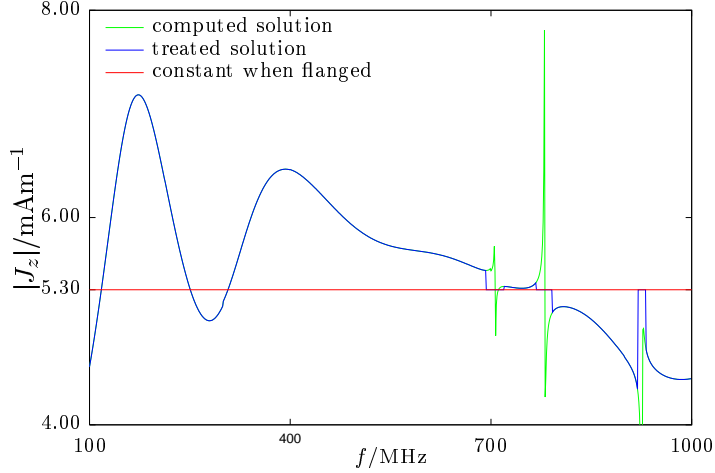


Figure 3.9.: Surface current J_z at aperture

computation of the incident field. It is a fast and accurate tool for computing the required quantities. From the surface currents, the electric and magnetic field strengths at the metallized aperture are derived.

The subsequent examples consider a perfect conducting box in a field created by a plane wave. The typical test case is a box with dimensions 0.3 m, 0.3 m and 0.5 m in a plane wave field polarised in \vec{e}_z and propagating in \vec{e}_x like the ones shown in fig. 3.8. Due to the polarisation parallel to the cavity wall, there is no normal electric field and hence no surface charge density at the aperture. The aperture will be placed centred on the wall directly exposed to the wave as in subsequent numerical and experimental studies. The only surface current of importance in this case is the one in \vec{e}_z as the one in \vec{e}_y is zero due to the polarisation. The surface current J_z computed with FEKO is shown in fig. 3.9 together with the constant value when accepting that the front wall of the cavity is comparable to an infinite plane. For low frequencies, the surface current density at the aperture is slowly evolving, the body is not small compared with the wavelength. At the resonances of the box at 705 MHz (1,1,0), 770 MHz (1,1,1), 924

MHz (1,1,2), a numerical difficulty of the Integral Equations is seen. At the internal resonances of the object, the solution is not physical, but a arbitrary linear combination of the external physical solution and of parasitic solutions of the internal problem [56]. The currents on the surfaces are non physical, the electric field inside the box is not zero as it should be. In contrary to the non physical solution touched upon in section 3.1.2 for the Finite Element Method, this occurs only very close to the resonances of the internal problem, here the rectangular cavity. A solution based on the Combined Field Integral Equation involving the electric type and the magnetic type equation would yield correct results, is, however, not available in FEKO. Therefore, values in vicinity of the three strong resonance lines in fig. 3.9 are to be interpreted with care. Being aware of the fact that they are wrong, I used the values of the assumption of a cavity flanged behind a wall for the subsequent calculations. These values are wrong in the interpretation of the cavity in free space, but at least one is well aware of the error. The three intervals are [693; 719] MHz, [768; 791] MHz and [920; 931] MHz.

The magnetic exterior field H_y is equal (but opposite in phase) to this surface current density and can now be used in eqn. (3.11) and eqn. (3.12) to give the sources for the interior problem.

3.4. The Green's Functions of a Rectangular Cavity

The determination of the Green's functions for the interior of the cavity can be found in [45–48]. In the following only a short sketch of this derivation is given.

The Green's function for the potentials and fields are dyadic and, as expected, singular in the source region. In the following uppercase G will denote a Green's function for fields due to an electric current source, and lowercase g the Green's functions connected with a magnetic current source. The index $_e$ designates the electric field, while $_h$ stands for magnetic field.

The dyadic Green's functions for the magnetic vector potential are

$$\bar{G}_A = \frac{1}{ABC} \sum_{m,n,l=0}^{\infty} \frac{\varepsilon_m \varepsilon_n \varepsilon_l}{K_{mnl}^2 - k^2}$$

$$\begin{pmatrix} (cc)_x(ss)_y(ss)_z & 0 & 0 \\ 0 & (ss)_x(cc)_y(ss)_z & 0 \\ 0 & 0 & (ss)_x(ss)_y(cc)_z \end{pmatrix}$$

(a) for the magnetic vector potential

$$\bar{g}_F = \frac{1}{ABC} \sum_{m,n,l=0}^{\infty} \frac{\varepsilon_m \varepsilon_n \varepsilon_l}{K_{mnl}^2 - k^2}$$

$$\begin{pmatrix} (ss)_x(cc)_y(cc)_z & 0 & 0 \\ 0 & (cc)_x(ss)_y(cc)_z & 0 \\ 0 & 0 & (cc)_x(cc)_y(ss)_z \end{pmatrix}$$

(b) for the electric vector potential

with: A, B, C cavity size in x, y and z $(cc)_i = \cos(k_i i) \cos(k_i i')$, and $(ss)_i = \sin(k_i i) \sin(k_i i')$, for $i = x, y, z$, primed coordinates source points,

unprimed coordinates observation points

 $k_x = \frac{m\pi}{A}$, $k_y = \frac{n\pi}{B}$, $k_z = \frac{l\pi}{C}$, $K_{mnl}^2 = k_x^2 + k_y^2 + k_z^2$,and finally $\varepsilon_i = 1$ when $i = 0$ and $\varepsilon_i = 2$ when $i \neq 0$.

Table 3.1.: Dyadic Green's function for the vector potentials of a rectangular cavity

$$\bar{G}_e = \frac{1}{ABC} \sum_{m,n,l=0}^{\infty} \frac{\varepsilon_m \varepsilon_n \varepsilon_l}{K_{mnl}^2 - k^2} \begin{pmatrix} (k^2 - k_x^2)(CC)_x(SS)_y(SS)_z & -k_x k_y (CS)_x(SC)_y(SS)_z & -k_x k_z (CS)_x(SS)_y(SC)_z \\ -k_x k_y (SC)_x(CS)_y(SS)_z & (k^2 - k_y^2)(SS)_x(CC)_y(SS)_z & -k_y k_z (SS)_x(CS)_y(SC)_z \\ -k_x k_z (SC)_x(SS)_y(CS)_z & -k_y k_z (SS)_x(SC)_y(CS)_z & (k^2 - k_z^2)(SS)_x(SS)_y(CC)_z \end{pmatrix}$$

(a) for the electric field

$$\bar{G}_h = \frac{1}{ABC} \sum_{m,n,l=0}^{\infty} \frac{\varepsilon_m \varepsilon_n \varepsilon_l}{K_{mnl}^2 - k^2} \begin{pmatrix} 0 & -k_z(SS)_x(CC)_y(CS)_z & k_y(SS)_x(CS)_y(CC)_z \\ k_z(CC)_x(SS)_y(CS)_z & 0 & -k_x(CS)_x(SS)_y(CC)_z \\ -k_y(CC)_x(CS)_y(SS)_z & k_x(CS)_x(CC)_y(SS)_z & 0 \end{pmatrix}$$

(b) for the magnetic field

Table 3.2.: Dyadic Green's functions for the fields due to an electric current source

$$\bar{g}_e = \frac{1}{ABC} \sum_{m,n,l=0}^{\infty} \frac{\varepsilon_m \varepsilon_n \varepsilon_l}{K_{mnl}^2 - k^2} \begin{pmatrix} 0 & -k_z(cc)_x(ss)_y(sc)_z & k_y(cc)_x(sc)_y(ss)_z \\ k_z(ss)_x(cc)_y(sc)_z & 0 & -k_x(sc)_x(cc)_y(ss)_z \\ -k_y(ss)_x(sc)_y(cc)_z & k_x(sc)_x(ss)_y(cc)_z & 0 \end{pmatrix}$$

(a) for the electric field

$$\bar{g}_h = \frac{1}{ABC} \sum_{m,n,l=0}^{\infty} \frac{\varepsilon_m \varepsilon_n \varepsilon_l}{K_{mnl}^2 - k^2} \begin{pmatrix} (k_x^2 - k_x^2)(ss)_x(cc)_y(cc)_z & -k_x k_y (sc)_x(cs)_y(cc)_z & -k_x k_z (sc)_x(cc)_y(cs)_z \\ -k_x k_y (cs)_x(sc)_y(cc)_z & (k^2 - k_y^2)(cc)_x(ss)_y(cc)_z & -k_y k_z (cc)_x(sc)_y(cs)_z \\ -k_x k_z (cs)_x(cc)_y(sc)_z & -k_y k_z (cc)_x(cs)_y(sc)_z & (k^2 - k_z^2)(cc)_x(cc)_y(ss)_z \end{pmatrix}$$

(b) for the magnetic field

Table 3.3.: Dyadic Green's functions for the fields due to a magnetic current source

defined by

$$\begin{aligned} (\nabla^2 + k^2) \bar{\bar{G}}_A(\vec{r}, \vec{r}') &= -\bar{\bar{I}} \delta(\vec{r}, \vec{r}') \\ \vec{n} \times (k^2 \bar{\bar{I}} + \nabla \nabla) \cdot \bar{\bar{G}}_A &= 0 \quad \text{on } \Gamma \end{aligned} \quad (3.14)$$

where $k = \frac{2\pi}{\lambda}$ is the wave number of the homogeneous, isotropic medium inside the cavity, \vec{r} the observation point and \vec{r}' the source point. $\bar{\bar{I}}$ is the identity dyad and \vec{n} an inward directed unit normal vector on the surface of the cavity Γ . Tai and Rozenfeld [47] determined the dyad $\bar{\bar{G}}_A$ using the vector wave functions \bar{L} , \bar{M} and \bar{N} , it is shown in table 3.1(a). With $\bar{\bar{G}}_A$, the dyads $\bar{\bar{G}}_e$ and $\bar{\bar{G}}_h$ for the electric and magnetic field due to an electric current source can be derived by

$$\bar{\bar{G}}_e = (k^2 \bar{\bar{I}} + \nabla \nabla) \cdot \bar{\bar{G}}_A \quad (3.15)$$

$$\bar{\bar{G}}_h = \nabla \times \bar{\bar{G}}_A \quad (3.16)$$

They are given in [48] and recapitulated in table 3.2(a) and 3.3(b).

The Green's dyad for the electric vector potential is defined by

$$\begin{aligned} (\nabla^2 + k^2) \bar{\bar{g}}_F(\vec{r}, \vec{r}') &= -\bar{\bar{I}} \delta(\vec{r}, \vec{r}') \\ \left. \begin{aligned} \vec{n} \cdot \bar{\bar{g}}_F &= 0 \\ \vec{n} \times \nabla \bar{\bar{g}}_F &= 0 \end{aligned} \right\} \quad \text{on } \Gamma \end{aligned} \quad (3.17)$$

$\bar{\bar{g}}_F$ is given in [48] and show in table 3.2(b). Now with $\bar{\bar{g}}_F$ determined, the dyads for the electric and magnetic field due to a magnetic current source can be determined by

$$\bar{\bar{g}}_e = -\nabla \times \bar{\bar{g}}_F \quad (3.18)$$

$$\bar{\bar{g}}_h = (k^2 \bar{\bar{I}} + \nabla \nabla) \bar{\bar{g}}_F \quad (3.19)$$

The dyads have the interesting property that the ones for the electric field due to a magnetic current and the ones for the magnetic field due to an electric current are antisymmetric

$$\bar{\bar{g}}_e(\vec{r}, \vec{r}') = -\bar{\bar{G}}_h^T(\vec{r}, \vec{r}') \quad (3.20)$$

The above dyads are the same as the ones presented in [47] and [46]. Their authors have taken great care to completely include the singularity in the expansion functions for $\bar{\bar{G}}_e$ in the source region. The agreement shows that completeness is ensured by using potentials and deriving the fields therefrom.

3.5. Reformulation of the Integral Equation

Using the above Green's functions, the approximation for the aperture as well as the relationship between the incident wave, the obstacle and the sources for the aperture approximation, the general integral equation (3.3) is reformulated. The starting point is

$$\vec{n} \times \vec{E}_{inc} = -\vec{n} \times \vec{E}_{sca} = -\vec{n} \times \left(\frac{j}{\omega \varepsilon} \right) (\nabla^2 + k^2) \int_{\Gamma} \bar{\bar{G}}_A \vec{J} dr \quad (3.21)$$

The incident field inside the cavity $\vec{E}_{inc}, \vec{H}_{inc}$ is generated by the equivalent dipoles which in turn are related to the fields at the aperture in the exterior and the interior as explained in eqn. (3.11) and eqn. (3.12):

$$\vec{p}_e = \varepsilon \alpha_e \left(\vec{E}_{sc}^-(\vec{r}'-) \cdot \vec{n} - \vec{E}_{sc}^+(\vec{r}'+) \cdot \vec{n} \right) \cdot \vec{n} \quad (3.22)$$

$$\vec{p}_m = -\bar{\alpha}_m \left(\vec{H}_{sc}^-(\vec{r}'-) - \vec{H}_{sc}^+(\vec{r}'+) \right) \quad (3.23)$$

The exterior field has been determined in 3.3 by a numerical method. The different contributors of the interior field are identified in the following. The image theory removes the metallic walls by placing an image for every interior source at the corresponding place. The sources to be imaged are the dipoles and also the currents to be determined in the process. The field created by the sources and their images is then the field inside the former cavity. The interior field $\vec{E}_{sc}^+(\vec{r}'+), \vec{H}_{sc}^+(\vec{r}'+)$ is now the one created by all these sources except the original dipoles at the aperture. It represents the reaction and hence the coupling to the aperture of cavity walls and objects.

To evaluate the field at the aperture two possibilities exist. One is to directly sum the contributions of all sources using the free space Green's functions. A better and more consistent way is to use again the Green's

functions of the cavity. This is straightforward for the contribution of the currents on the scatterers where the sources are on the surface of the obstacles and the field point is at the aperture. The computation of the field radiated by the images of the dipoles at the aperture however would demand an evaluation of the Green's functions at the source where they diverge. Therefore, more analytic work is needed for this contribution.

The field created by all images of the dipoles except the original ones can be determined by using the Green's functions of the cavity when removing the original or self term of the function:

$$\bar{\bar{G}}_A^r(\vec{r}, \vec{r}') = \bar{\bar{G}}_A(\vec{r}, \vec{r}') - \bar{I} \frac{e^{-jkR}}{2\pi R} \quad (3.24)$$

$$\bar{\bar{g}}_F^r(\vec{r}, \vec{r}') = \bar{\bar{g}}_F(\vec{r}, \vec{r}') - \bar{I} \frac{e^{-jkR}}{2\pi R} \quad (3.25)$$

where $R = |\vec{r} - \vec{r}'|$ is the distance of the observation point to the source. $\bar{\bar{G}}_A^r$ and $\bar{\bar{g}}_F^r$ will be called the reaction Green's functions as they represent the reaction of the field on the dipoles in the cavity. The Green's functions for the electric and magnetic field due to an electric and a magnetic current source arise by derivation of the above Green's functions from eqn. (3.15) and eqn. (3.18) for the electric field and eqn. (3.16) and eqn. (3.19) for the magnetic field. Note that all expressions individually diverge at the aperture as one evaluates the Green's functions at the source point. However, the difference of the two is bounded as it is a bounded solution of the homogeneous wave equation at the point \vec{r}' . Moreover, Daniele [57] showed that the singular part of the dyadic Green's function for a homogeneous medium which is bounded by a perfectly conducting surface equals the singular part of the free space Green's functions, the remainder is analytic. The value of this analytic part as the reaction was previously determined by interpolation of $\bar{\bar{G}}_A^r$ and $\bar{\bar{g}}_F^r$ and a subsequent discrete derivation [48]. In this thesis, new paths will be treated: the derivation will be done analytically, the resulting expression will then be extrapolated to the aperture. The exact procedure is shown in appendix B.

The interior field can finally be written as:

$$\vec{E}_{sc}^+(\vec{r}'+) = \frac{1}{\varepsilon} \bar{G}_e^r \vec{p}_e + j\mu\omega \bar{g}_e^r \vec{p}_m - \frac{j}{\omega\varepsilon} \int_{\Gamma} \bar{G}_e(\vec{r}, \vec{r}') \vec{J} ds' \quad (3.26)$$

$$\vec{H}_{sc}^+(\vec{r}'+) = j\omega \bar{G}_h^r \vec{p}_e + \bar{g}_h^r \vec{p}_m + \int_{\Gamma} \bar{G}_h(\vec{r}, \vec{r}') \vec{J} ds' \quad (3.27)$$

The incident field on the objects is created by the dipoles as already described

$$\vec{E}_{inc} = \frac{1}{\varepsilon} \bar{G}_e(\vec{r}, \vec{r}') \vec{p}_e + j\mu\omega \bar{g}_e(\vec{r}, \vec{r}') \vec{p}_m \quad (3.28)$$

Introduce now the difference between the interior and exterior field as two more unknown field quantities

$$\Delta E = \vec{E}_{sc}^- \cdot \vec{n} - \vec{E}_{sc}^+ \cdot \vec{n} \quad (3.29)$$

$$\Delta \vec{H} = \vec{H}_{sc}^- - \vec{H}_{sc}^+ \quad (3.30)$$

which yield with the expressions for the dipoles eqn. (3.11) and eqn. (3.12)

$$\vec{p}_e = \varepsilon \alpha_e \Delta E \quad (3.31)$$

$$\vec{p}_m = -\bar{\alpha}_m \Delta \vec{H} \quad (3.32)$$

Put these into eqn. (3.26) and (3.27) to get

$$\begin{aligned} \vec{E}_{sc}^+ \cdot \vec{n} &= \vec{E}_{sc}^- \cdot \vec{n} - \Delta E \\ &= \alpha_e \bar{G}_e^r \Delta E \vec{n}\vec{n} - j\omega\mu \bar{g}_e^r \bar{\alpha}_m \Delta \vec{H} \vec{n} - \frac{j}{\omega\varepsilon} \int_{\Gamma} \bar{G}_e \vec{J} ds \vec{n} \end{aligned}$$

from which follows

$$\vec{E}_{sc}^- \cdot \vec{n} = (1 + \alpha_e \bar{G}_e^r \vec{n}\vec{n}) \Delta E - j\omega\mu \bar{g}_e^r \bar{\alpha}_m \Delta \vec{H} \vec{n} - \frac{j}{\omega\varepsilon} \int_{\Gamma} \bar{G}_e \vec{J} ds \vec{n} \quad (3.33)$$

Similar, for the magnetic field holds

$$\vec{H}_{sc}^- = j\omega\varepsilon \alpha_e \bar{G}_h^r \Delta E \vec{n} + (1 - \bar{g}_h \bar{\alpha}_m) \Delta \vec{H} + \int_{\Gamma} \bar{G}_h \vec{J} ds \quad (3.34)$$

Note that for the two unknowns ΔE and $\Delta \vec{H}$ only three field components are necessary, the normal electric field and the tangential magnetic field. They are taken into account in the matrix for the Method of Moments. This system to be set up and solved is finally

$$\begin{pmatrix} Z_{JJ} & Z_{JE} & Z_{JH} \\ Z_{EJ} & Z_{EE} & Z_{EH} \\ Z_{HJ} & Z_{HE} & Z_{HH} \end{pmatrix} \cdot \begin{pmatrix} J \\ \Delta E \\ \Delta \vec{H} \end{pmatrix} = \begin{pmatrix} 0 \\ \vec{E}^- \cdot \vec{n} \\ \vec{H}^- \end{pmatrix} \quad (3.35)$$

Different choices are possible for ΔE and $\Delta \vec{H}$: the approximated values under the assumption of a cavity flanged to an infinite plane, or the numerically determined values for a box in free space. In the examples both possibilities to investigate the domain of validity of the approximation are presented. By virtue of the method of moments each of the submatrices describes a physical contribution of the currents and fields. They are in detail

- Z_{JJ} coupling of the different currents between themselves (N -by- N matrix). The field radiated by the surface currents is sampled by the different testing functions.
- Z_{JE} incident electric field radiated by the electrical dipole weighted by the testing functions (N -by-1 matrix)
- Z_{JH} incident electric field radiated by the magnetic dipole weighted by the different testing functions (N -by-2 matrix)
- Z_{EJ} reaction of the surface currents, or radiation of the currents onto the electric dipole at the aperture (1-by- N matrix)
- Z_{EE} relationship between the difference of the electric field and the electric incident field (scalar): $1 + \alpha_e \bar{G}_e^r \vec{n} \vec{n}$
- Z_{EH} reaction of the magnetic dipole onto the electric dipole (1-by-2 matrix): $-j\omega\mu\bar{g}_e^r \bar{\alpha}_m \vec{n}$
- Z_{HJ} reaction of the surface currents onto the electric dipole at the aperture (2-by-1 matrix)
- Z_{HE} reaction of the electric dipole onto the magnetic dipole (1-by-2 matrix): $j\omega\varepsilon\alpha_e \bar{G}_h^r \vec{n}$
- Z_{HH} relationship between the difference of the magnetic field and the magnetic incident field (2-by-2 matrix): $\bar{I} - \bar{g}_h^r \bar{\alpha}_m$

The individual expressions for each of the submatrices are obtained from the above equations. They are given in detail in appendix C.

Some notes should be added concerning the submatrices Z_{EJ} , Z_{EE} , Z_{EH} , Z_{HJ} , Z_{HE} and Z_{HH} . The two matrices Z_{EJ} and Z_{HJ} describe the reaction of the object onto the aperture. Neglecting the coupling is equivalent to set all elements to zero. Similar consideration hold for the four other matrices Z_{EE} , Z_{EH} , and Z_{HE} , Z_{HH} . When neglecting the reaction of the cavity onto the aperture, Z_{EH} and Z_{HE} are zero matrices and Z_{EE} and Z_{HH} are identity matrices.

3.6. Conclusions

In this chapter three major numerical methods for the solution of electromagnetic field problems were discussed under consideration of the geometry to be treated. From the proposed Finite Difference Time Domain, Finite Element Method and the Integral Equation Method the last one was chosen because of its capabilities in respect to the problem at issue and the ease of implementation. Further presented were a method to separate the interior from the exterior, and the Green's functions of a rectangular cavity. The electric integral equation was reformulated so as to account for the geometry as well as the sources. In the following chapter we will present details of the implementation and some representative examples with comparisons to previous numerical and new experimental results.

Chapter 4

Implementation and Sample Cases

In the previous sections the subdivision of the coupling problem into two subproblems was shown. The subproblems are the exterior problem as the interaction of a wave with a totally closed metallic box, and the interior problem as the field inside a totally closed cavity, possibly fitted with metallic objects. The relation between the two is provided by Schelkunoff's theorem, in form of the small aperture theory relating the fields in the exterior and the interior by a set of dipoles. The exterior problem will be regarded as solved, the following exclusively treats the interior problem. The method chosen for this task is the Method of Moments using the Green's functions of the cavity due to the considerations in the previous chapter. This chapter will present details of the numerical method, the experimental setup used for measurements, numerical and experimental data for sample cases, and finally a new method to speed up wide band simulations in resonant structures.

4.1. The Application of the Method of Moments to the Interior Problem

In section 3.5 the basic Electric Field Integral Equation was reformulated to take into consideration the actual geometry of the problem. The final equation (3.35) relates the known exterior fields to the unknown interior fields and surface currents. The elements Z_{JJ} involve the expansion in basis functions of the unknown surface currents on the objects, and the sampling of the resulting field by the testing functions. This is accomplished mathematically by a double integration of the Green's functions over the basis and testing functions. If one restricts the objects to have only surfaces parallel to the three coordinate planes, the integrations involve only two of the

three spatial dimensions. For certain classes of functions these integrations can be carried out analytically, thus reducing the computational effort.

Another artifice to reduce the computation time and also to gain numerical accuracy is to reduce the triple indexed Green's function series to series with only two indices. This is accomplished by eigenfunction expressions or Fourier series.

4.1.1. Efficient Computation of the Triple Series

Consider the following correspondences:

$$\sum_{m=1}^{\infty} \frac{1}{k_x^2 + \alpha^2} \sin k_x x \sin k_x x' = \frac{X}{2\alpha \sinh \alpha X} \sinh \alpha x_{<} \sinh \alpha (X - x_{>}) \quad (4.1)$$

$$\sum_{m=0}^{\infty} \frac{\varepsilon_m}{k_x^2 + \alpha^2} \cos k_x x \cos k_x x' = \frac{X}{\alpha \sinh \alpha X} \cosh \alpha x_{<} \cosh \alpha (X - x_{>}) \quad (4.2)$$

$$\sum_{m=1}^{\infty} \frac{k_x}{k_x^2 + \alpha^2} \cos k_x x_{<} \sin k_x x_{>} = \frac{X}{2 \sinh \alpha X} \cosh \alpha x_{<} \sinh \alpha (X - x_{>}) \quad (4.3)$$

$$\sum_{m=1}^{\infty} \frac{k_x}{k_x^2 + \alpha^2} \sin k_x x_{<} \cos k_x x_{>} = \frac{-X}{2 \sinh \alpha X} \sinh \alpha x_{<} \cosh \alpha (X - x_{>}) \quad (4.4)$$

with $\varepsilon_m = 1/2$ if $m = 0, 1$ elsewhere, $x_{<} = \min(x, x')$, $x_{>} = \max(x, x')$, X real normalisation constant in x , $k_x = \frac{m\pi}{X}$ and α arbitrary constant. These expressions derived in [43, 48] using Fourier series and eigenfunction expansions permit to replace one summation of the series by the corresponding analytical expression. We thus sum not over three indices, but only over two, however with an additional multiplier depending on the two indices. Therefore not only the computation time is reduced, but in the same time the numerical accuracy is increased. This is especially important for the slowly converging series 4.3 and 4.4. An important property of

the analytical expressions on the right hand side is that they decrease for α real and large and for $x_<$ different $x_<$ asymptotically like an exponential.

As an example consider the reduction in x of a cavity's Green's function. The cavity dimension A in \vec{e}_x of the cavity plays the role of the above normalisation constant X . k_x , k_y and k_z are the wave numbers of the modes in the cavity corresponding to the indices l , m , n of the Green's function expression, and α^2 equals $k_y^2 + k_z^2 - k_0^2$ with k_0 free-space wave number. If the mode corresponding to the triplet k_x , k_y and k_z has a wave number K_{mnl} with $K_{mnl}^2 = k_x^2 + k_y^2 + k_z^2$ higher than k_0 , the mode is below cut-off, the field due to that mode is then exponentially attenuated. α is in this case real and positive and increases with m , n and l . In that case, the expressions on the right in 4.1 - 4.4 decrease as mentioned exponentially like:

$$F(\alpha, A) \cdot \exp(-\alpha(x_> - x_<)) \quad (4.5)$$

The physical picture for that is that as at high frequencies the respective mode is not propagative, the field is attenuated exponentially and the closer confined to the region of the source the higher the frequency. In other words, the field at a point is less determined by modes with a high wave number than the ones with a low wave number possibly being propagative.

An efficient way of summing up the Green's functions can now be found if one takes advantage of this property. For high α the double indexed series will be multiplied by a term proportional to $\exp(-\alpha)$ which improves the convergence over the α^β -factor in the denominator of eqn. (4.1) - (4.4). Now the different modes k_y and k_z are sorted so that α increases, the most important modes being the ones with a low wave number. This is shown in fig. 4.1: the first term to be taken into account is the one with $k_y = k_z = 0$, α is then imaginary. The subsequent values for n and l lie between ellipses with half axes $\frac{B(q+\frac{1}{2})}{\max(B,C)}$ and $\frac{C(q+\frac{1}{2})}{\max(B,C)}$, with B and C cavity dimensions in \vec{e}_y and \vec{e}_z respectively as shown in fig. 1.2. The first 10 resulting ellipses and the corresponding (n, l) -pairs are shown in fig. 4.1 for $B = 500$ mm and $C = 300$ mm. Once the wave number K_{mnl} of a mode exceeds k_0 , the convergence will be exponential like in eqn. (4.5).

On the other hand, the exponential factor eqn. (4.5) depends also on the distance $x_> - x_<$ in \vec{e}_x of the source and the field point. The larger

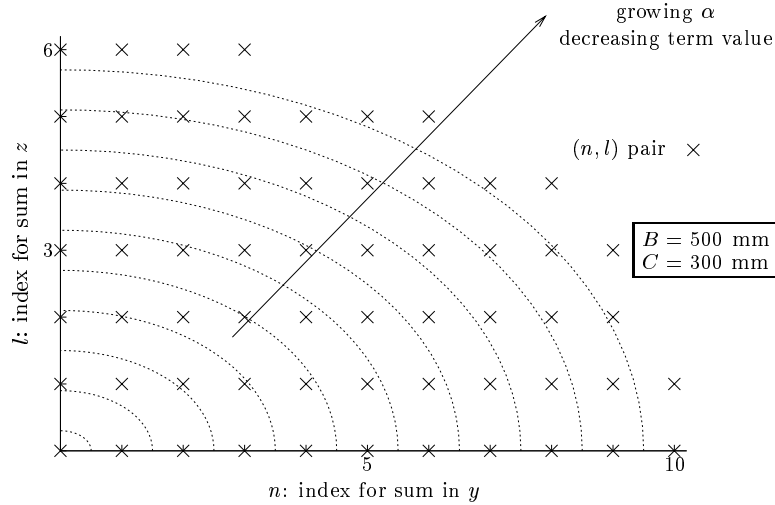


Figure 4.1.: Sorting algorithm for efficient calculation of the Green's functions

the distance of the two points, the faster the series will converge as the absolute value of the argument of the exponential is larger. For points close to each other more terms will be necessary, the convergence will be slower. If the two points lie on one x -plane, the exponential factor does no longer speed up convergence, a high number of terms will be necessary to obtain convergence.

The above considerations remain valid if the reduction of the triple sum is performed in either x , y or z . The decision which series to replace by its correspondence is made upon which part of the series is written in the form of one of (4.1) - (4.4), mainly the one not involved in any integration. Also important is to reduce for the largest distance $x_> - x_<$, $y_> - y_<$ or $z_> - z_<$.

4.1.2. Double Surface Integration

The integration of the kernel of the integral equation eqn. (3.7) is performed for the source coordinates \vec{r}' after the expansion of the unknown

surface currents. This first integration involves a surface integration over one expansion function and results in the field radiated by this function. The next step is the sampling of the field by each testing function using a suitable inner product. This is defined as

$$\langle \psi, \phi \rangle = \int \psi(\vec{r}) \bar{\phi}(\vec{r}) dr \quad (4.6)$$

with $\bar{\phi}$ complex conjugate of ϕ . The integration has to be carried out over the domain of definition of ϕ and ψ which again is a surface. As both the field radiated by an expansion function, symbolised by ϕ , and the testing functions, symbolised by ψ , are real for the cavity case, the inner product defined in 4.6 becomes a purely real operation and involves no complex conjugate.

Both integrations are combined to a double surface integration and executed term by term. As the objects only will have surfaces parallel to the coordinate planes, the surface integrations are uncoupled and therefore separable in the two directions. They will be carried out independently. The functions are now written as a product of two one-dimensional functions, e.g. for a surface parallel to the $x = 0$ -plane:

$$\psi(\vec{r}) = \psi(x, y, z) = \psi_y(y)\psi_z(z) \quad (4.7)$$

It remains to define suitable basis and testing functions and to examine their respective properties.

Important criteria on the properties of the functions depend on the nature of the integral equation and are given in [58]: in this paper the authors conclude that

1. in direction of the current the sum of the orders of differentiability of the basis and the testing function must be equal or greater than one, but
2. orthogonal thereto any piecewise continuous function is permitted. They even allow functions with a singularity of order less than one

These criteria exclude e.g. the piecewise constant (or pulse) function for both basis and testing function. Furthermore the point matching or Dirac

function is not derivable and will not be used here. The second criterion enables the approximation of the singularity of the current along an edge, this singularity always being less than one [59]. Wilton [60] reports a certain, however small improvement of the near field quantities for the quasistatic free-space functions when incorporating special edge functions. As additionally the expressions become considerably more complicated, here no special edge terms were included.

4.1.3. Basis and Testing Functions

Most commonly used functions are today linear functions on triangular supports which allow to mesh arbitrarily shaped objects. As the objects are restricted to have only planar surfaces which are parallel to the coordinate planes and have 90° angles to each other, these functions are not necessary. Other criteria are more important in the present case. They are the mathematical definition, easiness of implementation, rate of convergence of the final result, matrix size, computation time, etc. Mathematically simple functions are piecewise constant, linear, or sinusoidal functions over a strictly local support. This signifies that they have a value different from zero only for a small portion of the object. Functions being defined over the whole surface or at least over slices of the surface of the objects with trigonometric evolution will be called global functions and will finally lead to smaller matrices and therefore faster computation.

Strictly Local Functions

The first class is the mathematically simple class of local functions which require a spatial discretisation of the surface. The mesh is not necessarily regular, the step size can vary on the same object and also between different objects. Meshes with constant mesh sizes Δ_i , $i = x, y, z$ with the first and last mesh point on the edge are generally used. In the following the mesh points being the centre of a cell are denoted as x_i with $i = 1 \dots (N_x - 2)$, the corresponding cell size is Δ_x . The first and last point x_0 and x_{N_x-1} lie on the edge, the cell sizes are $\Delta_x/2$. Let $\hat{x} = \frac{x-x_i}{\Delta_x}$ be normalised and centred in respect to the cell.

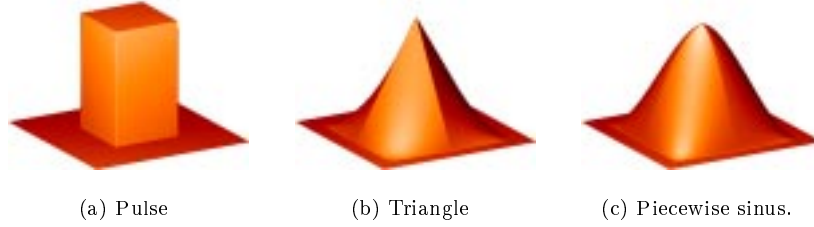


Figure 4.2.: Three possible local functions: 4.2(a) pulse, 4.2(b) piecewise linear (triangle), 4.2(c) piecewise sinusoidal.

Of all possible functions only three will be discussed in the following. The two-dimensional functions which consist of the product of two identical functions in two perpendicular directions are shown in fig. 4.2.

- pulse or piecewise constant (abbreviation C, fig. 4.2(a))

$$C(x) = \begin{cases} 1 & \text{for } |\hat{x}| < 0.5 \\ 0 & \text{elsewhere} \end{cases} \quad (4.8)$$

- triangular or piecewise linear (L, fig. 4.2(b))

$$L(x) = \begin{cases} 1 - \hat{x} & \text{for } |\hat{x}| < 1 \\ 0 & \text{elsewhere} \end{cases} \quad (4.9)$$

- piecewise sinusoidal (S, fig. 4.2(c))

$$S(x) = \begin{cases} \frac{\sin k(\Delta_x - |x - x_i|)}{\sin k\Delta_x} & \text{for } |\hat{x}| < 1 \\ 0 & \text{elsewhere} \end{cases} \quad (4.10)$$

For fine discretisations, i.e. Δ_x small, the piecewise sinusoidal function is well approximated by the piecewise linear functions, the two will then yield the same result.

The well-known roof-top function is in fact the product of the piecewise linear function in direction of the current with the constant function in

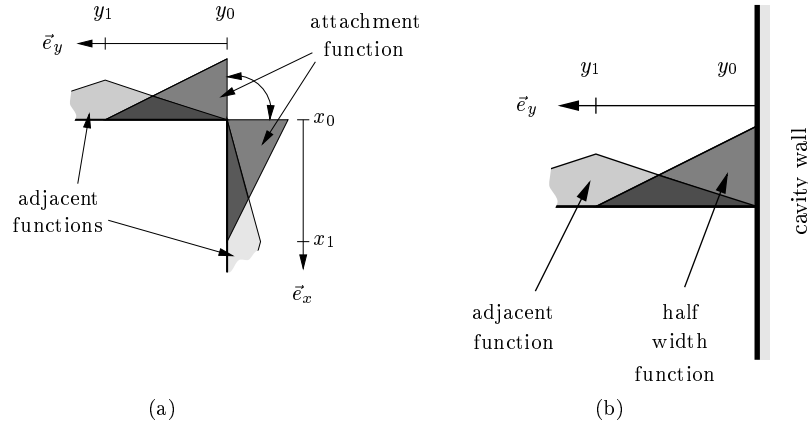


Figure 4.3.: Special functions assuring the continuity over an edge: 4.3(a) across an edge, 4.3(b) at a cavity wall

orthogonal direction. In the following I will however not deal with this function.

For all functions one has to ensure the continuity of the currents normal to an edge. Due to the special position of the first and last mesh point on the edge, the two cells at the edge have only half of the normal width. For isolated plates there is no current normal to an edge, the current is therefore zero on the last cell. The functions for plates touching the cavity walls or being connected to other plates in direction of the current must ensure the continuity of the current, special attachment functions are therefore used. A sketch is shown in fig. 4.3: for the continuity across an edge, two half width functions with the same amplitude compose one attachment function 4.3(a). On an object being in conducting contact with a cavity wall a half width function is used 4.3(b). The testing functions are constructed the same way.

Semi-Global Functions

Another possibility is not to mesh geometrically the object, but to decompose the current on some functional basis. The first choice is a truncated Fourier series, others could be e.g. Chebycheff or Legendre series. The functions are now defined not only on a small portion of the surface, but over the whole object in direction of the current, and assumed constant over a small slice of the surface normal to it. Continuity of current is fulfilled by the appropriate behaviour of the corresponding functions at the boundaries, in our case the sine or cosine function will account for continuity:

- for currents on isolated plates the current is zero at both ends, therefore the sine function is used ($m = 0, 1, \dots$)

$$GI(x) = \sin \left((m+1)\pi \frac{x - x_{min}}{x_{max} - x_{min}} \right) \quad (4.11)$$

- for conductors attached to others at one side, isolated at the other, here the case with isolation at $x = x_{max}$. The current is zero at the end $x = x_{max}$ and non zero at $x = x_{min}$ ($m = 0, 1, \dots$)

$$GO(x) = \cos \left(\frac{2m+1}{2}\pi \frac{x - x_{min}}{x_{max} - x_{min}} \right) \quad (4.12)$$

the first three functions of this type are shown in fig. 4.4.

- for conductors attached to others at both ends, the current is non-zero at both ends ($m = 0, 1, \dots$)

$$GB(x) = \cos \left((m+1)\pi \frac{x - x_{min}}{x_{max} - x_{min}} \right) \quad (4.13)$$

One important property of the global functions must be pointed out. As the discretisation of the objects remains the same when augmenting the number of basis and testing functions, the domains of integration remain the same. Hence, not the entire impedance matrix has to be recalculated. It is sufficient to add the small portion for which the new function pair is responsible. Consider an example: the submatrix Z_{JJ}^3 for 3 functions

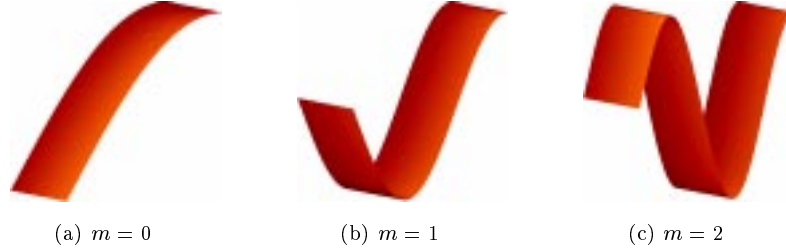


Figure 4.4.: First three global domain functions $GO(x)$

was calculated. Now if the solution is judged to be insufficient, one further function pair can be added. The elements in Z_{JJ}^3 are however independent of the new functions, only one new row due to the additional testing function and one new column must be calculated to obtain the new matrix Z_{JJ}^4 :

$$Z_{JJ}^4 = \begin{pmatrix} Z_{JJ}^3 & \text{new column due to} \\ \text{new row due to} & \text{new basis function} \\ \text{new testing function} & \text{interaction new basis} \\ & \text{and testing function} \end{pmatrix} \quad (4.14)$$

This not only reduces the overall computational cost when fine tuning the modal discretisation, but allows also the use of order recursive matrix solutions [61, 62].

Several sets of the above mentioned functions were applied to a simple test case of a strip in a cavity fig. 4.5 (a), the dimensions are itemised in tab. 4.5 (b), the origin for these values are in the right lower front corner of the cavity. The strip is illuminated at a frequency of 800 MHz by a magnetic dipole in \vec{e}_y placed at the centre of the wall $x = 0$. The strip is cut into two slices in \vec{e}_y (cf. fig. 4.6(a)), the current density J_z is expanded in 3 to 15 functions, corresponding for the local functions to a mesh $\lambda/5$ to $\lambda/25$. The type of the functions is either one of the three proposed local or of the global type (4.12). In fig. 4.6(b) is shown the short circuit current at the base of the strip as the integral of the current density J_y at $z = 0$, the two gray cells in fig. 4.6(a), as a function of matrix size and functions. The abbreviations C (for piecewise constant), L (for piecewise linear) and

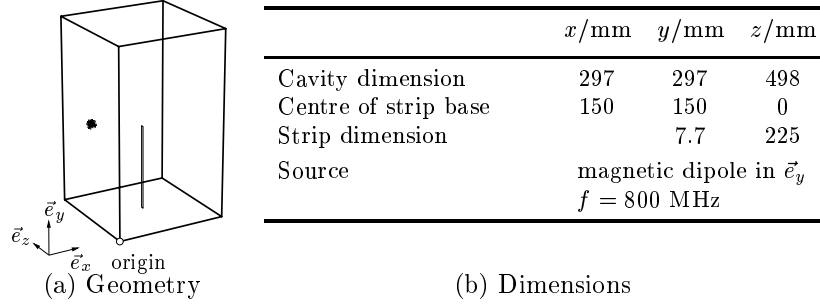


Figure 4.5.: Test case for functions

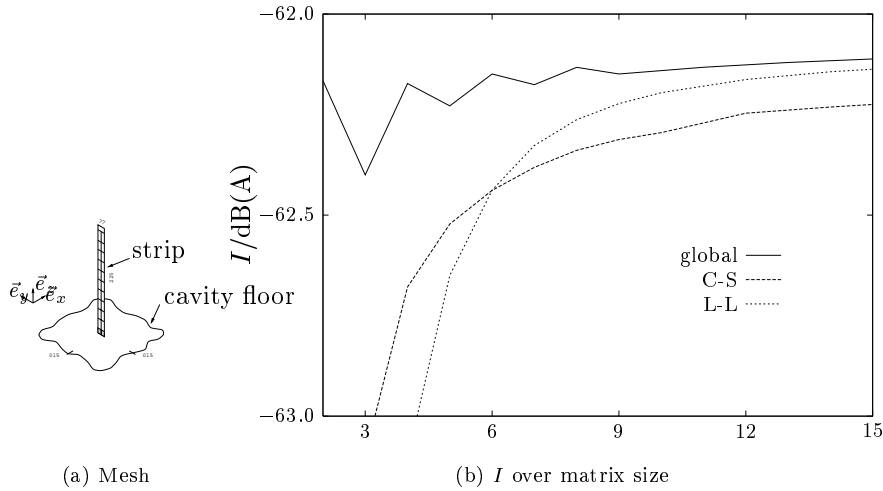


Figure 4.6.: Test case for matrix size

S (for piecewise sinusoidal) denote the function type, first is basis, second is testing function. A discretisation of $\lambda/10$ would need 7 cells, $\lambda/15$ 10 cells. All functions eventually yield the same value, the numbers needed however to achieve a relative convergence of 0.1 % are different: only 9 functions for the global functions, 14 for the constant-linear set.

Summarising, different functions are usable for the method of moments. Two classes were looked at more closely, the local functions as product of two one-dimensional functions with local support, and the global functions as product of a trigonometric function with global support and the constant function with local support. The actual choice of which function to use in a particular case is based on the following: small objects connected to others or to the cavity wall are easier discretised by local elements as these have simple attachment functions. Big objects, connected to the cavity walls or not, are better modelised by global functions as these lead to smaller matrices. Note that the Method of Moments does not constrain to use only one function type for a particular geometry, local and global functions can be mixed, e.g. global for a big plate with local functions for a small scatterer. The following computations use almost exclusively the basic set of the piecewise constant function as basis and the piecewise linear set as expansion function.

4.1.4. Lumped Loads and Sources

A further relationship between the current densities and the fields is added if localised elements like loads or sources are present. The loads can be resistive or reactive as resistors, inductors or capacitors. The input impedance of a measuring instrument of 50Ω , e.g. , must be taken into account during the simulation. On the other hand lumped sources could act as supply sources of equipment inside the cavity.

As the moment matrix associates the fields with the surface currents, lumped loads can be included. For this the impedance is assumed to be distributed over one cell, the current passing through the cell gives rise to a field. This field must be included in the surface integration associated with the testing procedure. A mesh cell with centre x_i shall be affected with a load R . The contribution E_i to the electric field due to the basis element J_i of the surface current density is now by (3.21)

$$\begin{aligned} E_i &= \frac{j}{\omega\epsilon} (\nabla^2 + k^2) \int_{\Gamma_i} \bar{G}_A J_i dr + R_s J_i \\ &= \left(\frac{j}{\omega\epsilon} (\nabla^2 + k^2) \int_{\Gamma_i} \bar{G}_A f_i dr + R_s f_i \right) J_i \end{aligned} \quad (4.15)$$

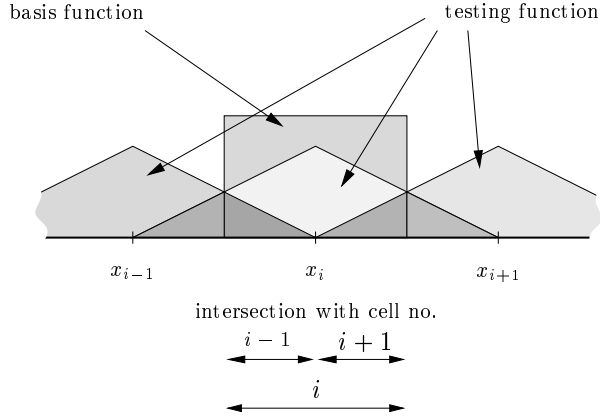


Figure 4.7.: Intersecting basis and testing functions for lumped loads

and is sampled by the testing functions w_j

$$\langle E_i, w_j \rangle = \left\langle \frac{j}{\omega \varepsilon} (\nabla^2 + k^2) \int_{\Gamma_i} \bar{\bar{G}}_A f_i dr + R_s f_i, w_j \right\rangle \quad (4.16)$$

Consider now the one-dimensional case in fig 4.7: the matrix elements of Z_{JJ} (3.35) corresponding to the testing functions $j = i - 1$, $j = i$ and $j = i + 1$ become now complex with the real part $\langle w_j, R_s f_i \rangle$. However as the contribution of the impedance is expressed as simple integration of a constant over a function, this part demands almost no computation time.

Sources can be taken into account by adding an additional voltage gap in one element of the incident field vector. This is however not in the scope of this thesis.

4.1.5. Inversion of the Impedance Matrix

The impedance matrix for the current computation is for a variety of problems quite small. Even with a local discretisation scheme and objects with dimensions of the order of one wavelength the size is rarely larger than 500 or 600. Highly optimised algorithms are therefore not needed for inverting the matrix. A numerical subroutine with an LU factorisation provided

by external sources (IMSL or netlib) gives satisfactory results in negligible computation times.

4.2. Experimental Setup

Comparative measurements were carried out at the SESAME site of the French Government Body DGA at the Centre d'Etudes de Gramat [63]. The setup used hereby is a monoconic antenna with 4 m diameter and 1.865 m height in a circular semi-anechoic chamber, that is a chamber with conducting floor (fig. 4.9(a)). The geometry of the cone over the floor assures a low return loss at the antenna input. A cylindrical wave near the floor of the chamber is radiated, in the test volume which holds the cavities it can be considered as plane [64]. The source for the monoconic antenna (fig. 4.9(a)) is a network analyser HP 8510, the analyser is controlled by a HP 300 computer. The receiver antenna consists of an adjustable set of monopole antennas (fig. 4.9(b)) allowing various lengths. Several sets of cavities, a specimen with circular aperture is shown in fig. 4.10(a), were assembled and tested. For tests with larger objects inside the cavity, additional walls were fixed inside the cavity, the connection of object to wall was done with special conducting tape with naps fig. 4.10(b). The conducting collar at the base of the cavity is taped with conducting napped tape to the floor of the chamber thus ensuring a wide area of contact and preventing measurement errors by fields leaking into the cavity.

In a first measurement the electric field at the cavity front was determined. All subsequent measurements are now normalised to this incident field.

4.3. Sample and Test Cases

In the following the capabilities are investigated and also the limitations of the present method. For this comparisons were drawn with a code treating the wire case [40], and measurements performed at the SESAME site described in the previous section. The sample cases will test the following items:

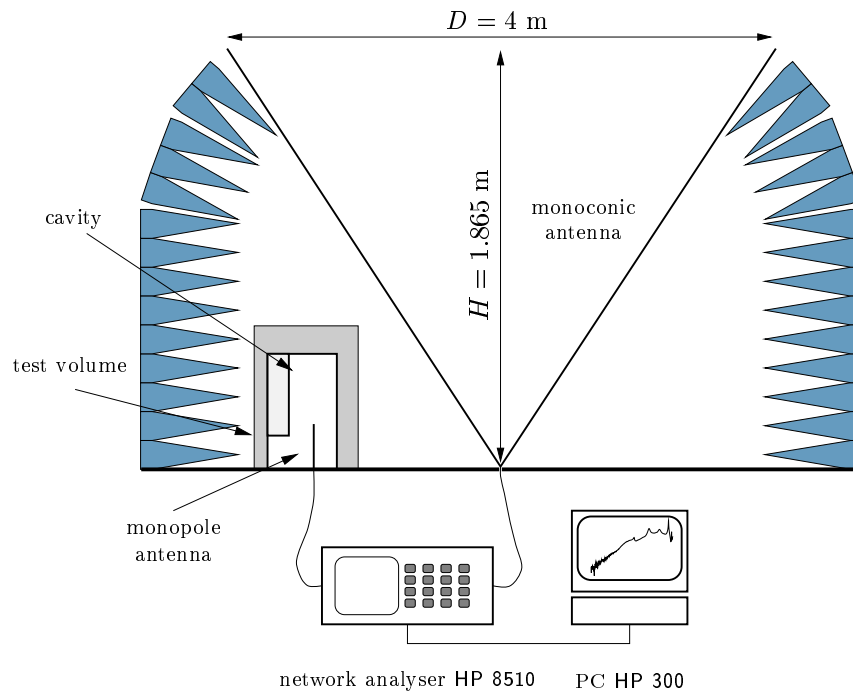


Figure 4.8.: Experimental setup at SESAME



(a) Measurement site SESAME

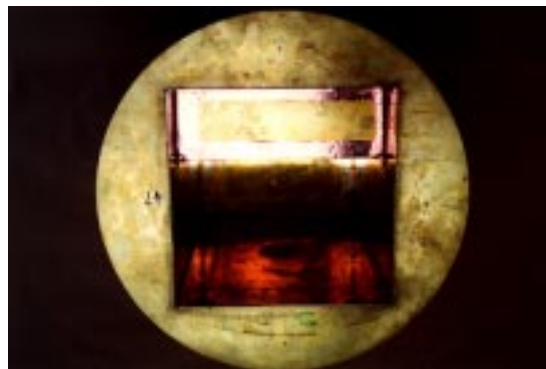


(b) Adjustable set of monopoles

Figure 4.9.: Monocone and monopole antennas



(a) Specimen of test cavity.
Note: numerical figures in this picture are *external* dimensions, not internal ones.



(b) Object in cavity

Figure 4.10.: Test cavity

		x/mm	y/mm	z/mm
Cavity	dimensions	297	297	498
Aperture	circular, $r = 20$ mm	0	152	248
Incident field	a) constant, $H_y = 5.3$ mA/m b) cavity in free space			
Monopole	circular, $r = 1.93$ mm			
	base	150	150	0
	dimensions			225
Equivalent strip	base	150	146.15	0
	dimensions		7.7	225
	mesh points		$N_y = 2$	$N_z = 11$

Table 4.1.: Test case 1: dimensions

- agreement of the three-dimensional code with the wire code
- consistency of the three-dimensional code when changing the shape of the cavity
- deformation of the cavity

4.3.1. The Wire in the Cavity

The first test case compares the performance of the new 3D code to the already established wire code. Measurements were also called on. The test case is a simple single wire in a cavity, the dimensions are shown in tab. 4.1. For the incident field 2 options exist: the assumption that the cavity is flanged behind an infinite plane, so that the exterior fields are assumed to be constant. The other possibility is the rigorous computation of the exterior field by means of a numerical method (cf. 3.3). The measurement monopole antenna is a thin circular wire. As the code presently only uses rectangular objects and no wires, a correspondence between round wires and rectangular plates was used to transform the wire into a rectangular object. This was achieved using the correspondence [65] between a wire with radius r and a thin strip with width w :

$$r = \frac{w}{4} \quad (4.17)$$

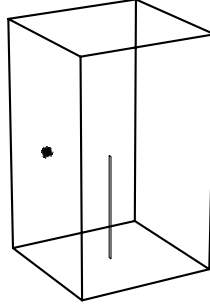


Figure 4.11.: Test case 1: geometry

The incident field is polarised in \vec{e}_z with unit electric field strength, the frequency band is 100 MHz to 995 MHz, which also prescribes the size of the mesh cells. The numbers of mesh points was fixed to 2 in \vec{e}_y and 11 in \vec{e}_z for the whole frequency band, the corresponding discretisation step sizes are hence $\Delta_x = 0.00385$ mm and $\Delta_z = 0.0225$ mm. The step size is $\lambda/10$ at about 1330 MHz. Due to the polarisation, there is only a magnetic dipole in \vec{e}_y .

Fig. 4.11 shows a sketch of the test object, fig. 4.12 and fig. 4.13 show the power received in a 50Ω load at the base of the monopole. During the measurements the monopole antenna was connected to the 50Ω input of the network analyser.

In fig. 4.12 are plotted the experimental curve together with the curves computed with the new 3D code. Differences are at most 3 dB in magnitude. The shift of the resonance lines at 910 MHz is 12 MHz. The computation for the incident field using the free-space Method of Moments is shown here for the first time together with the assumption of constant incident field. Differences are only small, however the rigorous consideration of the incident field agrees well with the experimental data especially for low frequencies. The slight increase of 3 dB between 100 MHz and 250 MHz and between 250 and 500 MHz is due to the incident field dependence on the outer shape of the cavity in the wave field.

The comparison between the old wire code and the new 3D code is

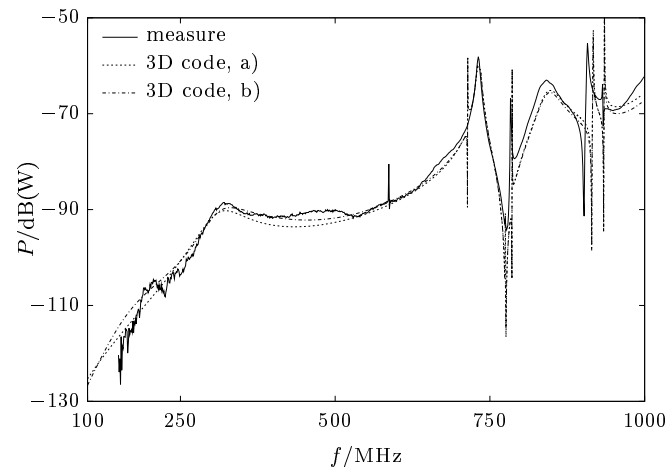


Figure 4.12.: Measure and 3D code. 3D code case a) is with constant incident field, case b) with computed incident field.

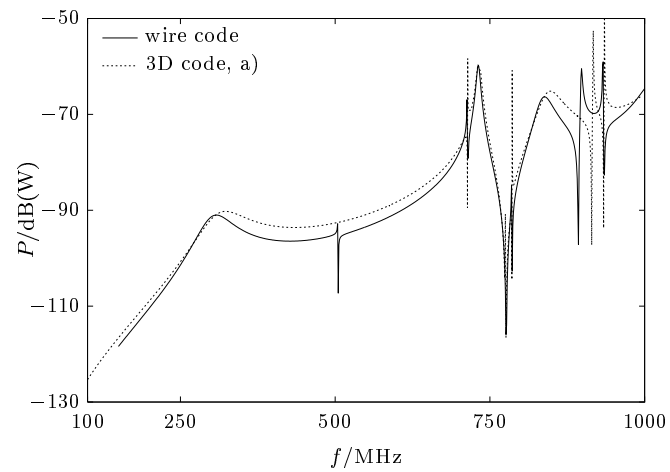


Figure 4.13.: Test case 1: comparison wire and 3D code

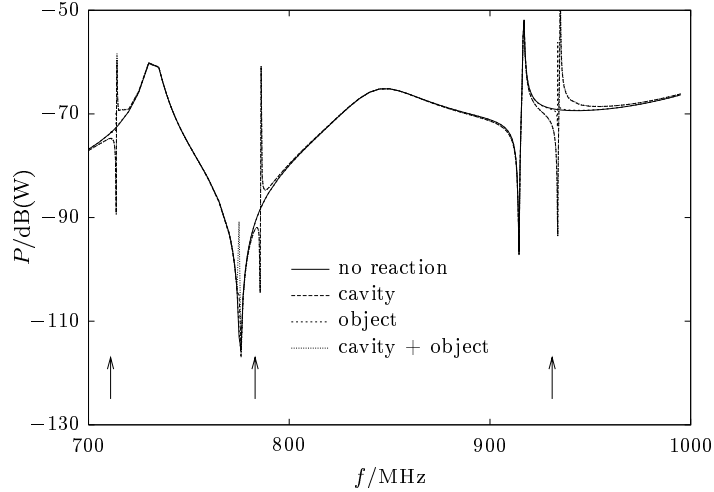


Figure 4.14.: Test case 1: Contributions of reaction terms. Arrows show resonances appearing when including the reaction by the cavity and/or the object

shown in fig. 4.13. The codes agree well, the difference in magnitude is at most 6 dB, the resonance lines are shifted by at most 20 MHz. These differences as well as the spurious resonance at 500 MHz for the wire code are contributed to numerical instabilities during the evaluation of the Green's functions for the wire code.

Fig. 4.14 shows the different contributions of the reaction parts for frequencies above 700 MHz. Below this limit the reaction fields alter the magnitude by at most 0.5 %. Clearly seen are the additional resonances at 711 MHz, 783 MHz and 931 MHz due to internal resonances of the cavity. As a matter of fact, the method of moments allows to include or not the respective expressions so that one has the possibility to investigate the different effects of the reaction terms. If in eqn. (3.35) the matrices Z_{EE} and Z_{HH} are the identity matrices and simultaneously Z_{EH} and Z_{HE} are the null matrices, the reaction of the cavity is not taken into account. One sees that the reaction is only noteworthy at some discrete high frequencies.

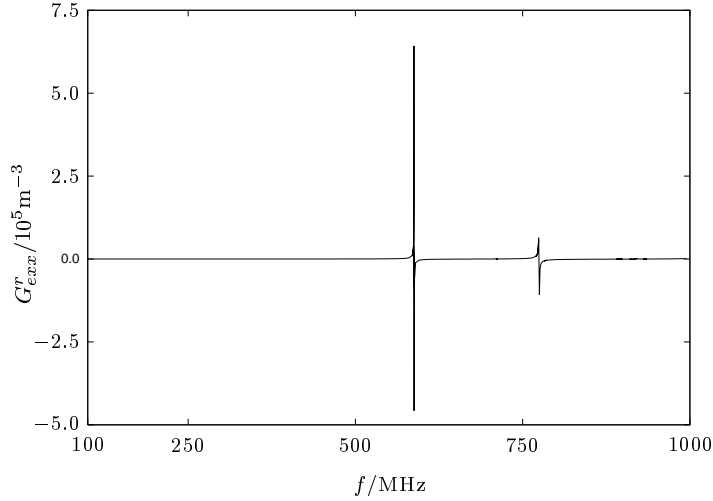


Figure 4.15.: Test case 1: Reaction of the cavity on the electric dipole

The frequencies where this effect occurs are the resonant frequencies of the empty cavity where the reaction of the cavity on the aperture is strong. Compared to the measurements in fig. 4.12 the resonance at $f \approx 586$ MHz ((0, 1, 1) and (1, 0, 1)) is missed in the computations due to the perfect incident field polarised in \vec{e}_z excluding any contribution of the electric dipole in \vec{e}_x or a \vec{e}_z component of the magnetic dipole. However this resonance is readily seen in the reaction terms of the magnetic dipole in \vec{e}_z fig. 4.15, and would appear when including a small electric dipole in \vec{e}_x .

Due to the size of the object the coupling of the object onto the aperture is negligible, in fact the curves for no reaction and the one for only reaction by the object coincide. Finally it is to note that the function set constant-piecewise sinusoidal yields the same result as the linear-linear set.

4.3.2. Plates in the Cavity

The second test case is a preliminary test to show that it is possible to change the shape of the cavity without being obliged to calculate the Green's function of the actual cavity. This is especially interesting when

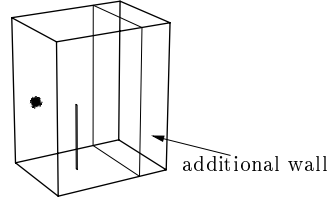


Figure 4.16.: Test case 2: Geometry

non-rectangular or non-cylindrical cavities are involved. Additional metallic objects have then to be placed at the walls of the new cavity, the current on these walls totally shields the space behind making the cavity electrically smaller. The aim is now to simulate the same case as the previous one, this time however with Green's functions of a different cavity. For this (fig. 4.16) a cavity which is longer in \vec{e}_x is chosen, the objects inside are now the strip equivalent to the measuring monopole and a plate covering the whole section of the cavity. This additional wall will now simulate the backside wall of the original cavity. The dimensions are found in tab. 4.2, the cell size is sufficient for simulations up to 1020 MHz and limited by the number of mesh points on the additional wall.

Obviously the same results as in the first case must be obtained. In fig. 4.17 the almost superposing curves are shown. Nevertheless, three discrepancies appear when including the reaction of the cavity. In fig. 4.17 one resonance at 711 MHz is missed, two spurious ones appear at 870 MHz and 902 MHz when including the reaction terms. The discrepancies are due to numerical problems: the high values for the reaction terms of the cavity rend the inversion of the matrix inaccurate.

4.3.3. Changing the Shape of the Cavity

The last verification is a cavity with a reentrant edge. The original cavity has slightly different dimensions as the previous cases, a metallic box is placed in the upper rear corner of the cavity so as to simulate a cavity with reentrant corner. Two comments about the electric size of the objects. The wavelength of the highest simulated frequency $f = 995$ MHz equals

		x/mm	y/mm	z/mm
Cavity	dimensions	400	297	498
Aperture	circular, $r = 20$ mm	0	152	248
Incident field	constant			
Monopole	circular, $r = 1.93$ mm			
	base	150	150	0
	dimensions			225
Equivalent strip	base	150	146.15	0
	dimensions		7.7	225
	mesh points		$N_y = 2$	$N_z = 11$
Second object	base	297	0	0
	dimensions		297	498
	mesh points		$N_y = 12$	$N_z = 18$

Table 4.2.: Test case 2: Dimensions

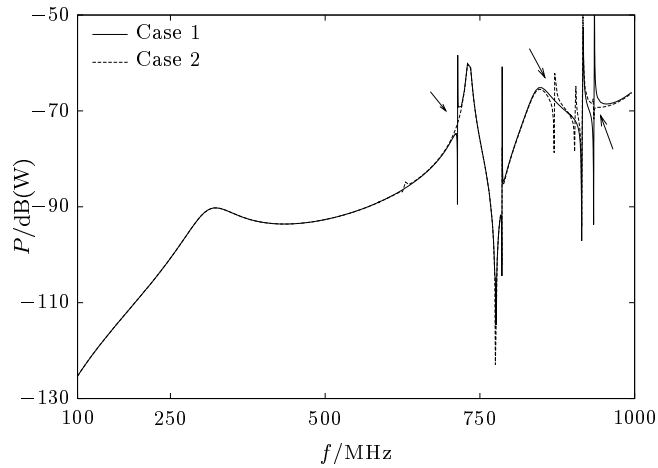


Figure 4.17.: Test case 2: Comparison with test case 1

		x/mm	y/mm	z/mm
Cavity	dimensions	300	300	500
Aperture	circular, $r = 38$ mm	0	150	250
Incident field	constant, $H_y = 5.3$ mA/m			
Monopole	circular, $r = 1.5$ mm			
	base	110	150	0
	dimensions			125
Equivalent strip	base	110	147	0
	dimensions		6	225
	mesh points		$N_y = 2$	$N_z = 11$
Second object	base	190	0	100
	dimensions	300	300	500
	mesh points	$N_x = 5$	$N_y = 12$	$N_z = 16$

Table 4.3.: Test case 3: Dimensions

$\lambda = 301.2$ mm which approaches the size of the additional object. This is hence no longer a low frequency computation, but a computation in the resonance domain. The cell size adopted for the object allows computations up to about 1050 MHz if one requires a cell size smaller than $\lambda/10$. Previous investigations [66] have shown that reasonable results can be achieved with cell size of $\lambda/5$ even though in that case the results must be carefully interpreted. The discretisation is hence with certainty fine enough. On the other hand the dimension of the aperture is no longer in the domain usually asked for when using the equivalent dipole principle. Comparisons of measurements with computations show however that the small aperture theory can be extended to apertures of longest dimensions 0.4λ [40].

The comparison of simulated and measured curves is less favourable as for the previous cases. Differences reach 10 dB. Nevertheless the main features of the curves correspond.

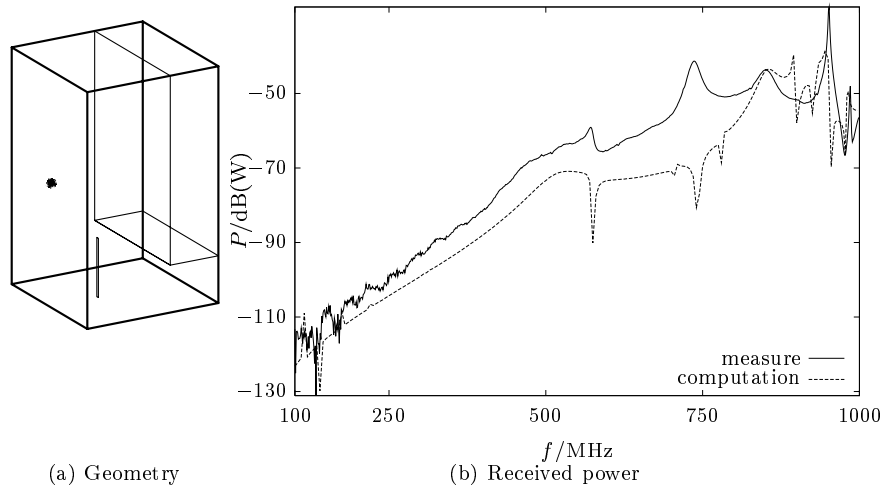


Figure 4.18.: Test case 3: cavity with reentrant corner

4.4. Acceleration of Computation Times

4.4.1. Different Algorithms for Computing Acceleration

Computations of electromagnetic field problems are one of the most resource demanding applications for modern digital computers. Therefore acceleration procedures were investigated for various aspects of the different numerical methods [67]. In the following only those methods are touched upon which are applicable to a Method of Moments in general or for the solution of an integral equation in particular.

Generally speaking, the way a mathematical method is coded contributes to performance, a simple precalculation of various re-used values can save precious processor time. Under this aspect falls also the judicious resorting of the terms in sec. 4.1.1.

The functions involved in the moment solution as basis or testing functions have a further share in computation time. A careful choice of the basis and testing functions helps to reduce computation time as discussed

in sec. 4.1.3. A suitable current representation supports also a rapid convergence and even extrapolation to higher frequencies [68].

Under all circumstances, however, optimal coding will not speed up computation much beyond a limit, it is then more important to reduce the complexity of the algorithm in question. The present algorithm uses analytical expressions to reduce the complexity of the triple indexed sums of the Green's functions in 4.1.1.

Computations needing big matrices were the reason for the development of matrix compression algorithms [69, 70] by constructing either directional functions or wavelets. The procedures for the former are highly adapted to the free-space case, so that they are not applicable to non free-space problems as the present one. Moreover, both methods are better suited for large matrices not encountered in the examples in the present work.

A last class is especially well adapted for the summation of periodic free-space Green's functions occurring for waveguides or stratified media. The convergence of some of their representations can be very slow, convergence accelerating algorithms help to speed up computations. Beside mathematical reformulations as the Poisson formula of the Fourier transform, also proper algorithms for convergence accelerations were derived as the ε -algorithm or Shank's and Levin's transforms [71]. Those algorithms are not applicable to the series constituting the Green's functions of cavities due to their mathematical properties.

For all these methods it is to note that only the computation of a matrix or series at one defined frequency is affected. If the results for a wide band or even only several frequencies are needed, the algorithms will speed up the single computations, the final result however is always the product of number of frequency points and the time needed for every point. Another method to gain fast data over wide range of frequencies will therefore be superior to the above algorithms.

4.4.2. Wide Band Data from Sample Frequencies

An algorithm for the generation of wide band data from computations at some frequency points uses the interpolation of the impedance matrix

between so-called nodes [72]. By using this method, the impedance matrix is only calculated at predefined frequency points, the matrices at the other points are then interpolated. The application of the method to free space uses a mixed linear of the real part and a logarithmic interpolation of the imaginary part of closely spaced elements. The final matrix inversion remains necessary for each frequency point which renders the method rather tedious for large matrices. Another drawback of the method is that the impedance matrices at the nodes need to be stored, whereas the straightforward single step frequency computation allows to remove from the storage medium the matrix for the already solved frequencies. These drawbacks concern less the present case, as the matrix sizes are usually rather small.

The Green's function of the cavity have poles at the resonances of the empty cavity. An interpolation with an linear or logarithmic scheme would inevitably fail if the nodes are spread below and above the resonance frequencies. A polynomial interpolation would not accurately represent the actual Green's function.

Based on [72] a new interpolation method for the Green's functions in resonant structures has been developed and reported [73]. It is well adapted to Green's functions for resonant geometries like cavities, but also waveguides or dielectric resonators. It consists in subdividing the whole frequency band at the resonant frequencies or the poles of the Green's functions and then to interpolate using rational functions to well represent the singular behaviour of the Green's function.

The application of this method to a simple case will be demonstrated briefly in the following. The resonance frequencies of the cavity are calculated by

$$f_i^r(l, m, n) = \frac{c}{2\pi} \sqrt{\left(\frac{l\pi}{A}\right)^2 + \left(\frac{m\pi}{B}\right)^2 + \left(\frac{n\pi}{C}\right)^2} \quad (4.18)$$

Between two frequencies f_i^r and f_{i+1}^r , nodes f_k are chosen. Two possibilities are suggested, the one with an equally spaced distribution of the nodes, the other, more adapted for interpolation purposes and yielding better interpolations especially at the subband limits [74], the distribution of the

nodes according the Chebycheff law

$$f_k = \frac{f_i^r + f_{i+1}^r}{2} + \frac{f_i^r - f_{i+1}^r}{2} \cos\left(\frac{2k+1}{2n+2}\pi\right) \quad (4.19)$$

Then the elements of the impedance matrix Z_{JJ} (3.35) are interpolated by a rational function of order ρ with $\mu + \nu + 1 = \rho + 1$ and $\mu < \nu$

$$R^\rho(x) = \frac{p_0 + p_1 x + \dots + p_\mu x^\mu}{q_0 + q_1 x + \dots + q_\nu x^\nu} \quad (4.20)$$

An interpolation in the usual way would involve the inversion of a very ill-conditioned matrix. Hence the interpolated value calculated by (4.20) would be little accurate. A special algorithm for interpolation [75, 76] by rational functions is faster and yields more accurate results. This algorithm only computes the interpolated values $R^\rho(x)$, and not the coefficients p_i and q_i . The algorithm is highly efficient and very accurate, a brief description can be found also in appendix D.

As an example, consider the wire and plate case in section 4.3. The whole band 100-995 MHz is subdivided into 18 subbands according to the resonances of the empty cavity. Three or five nodes are chosen in each subband, the corresponding curves without reaction of cavity or objects are compared to the rigorous single step computations in fig. 4.19. The agreement between the curves is for three nodes satisfying only for frequencies below 600 MHz. Above this frequency, the curves differ by up to 40 dB. This is due to the fact that with three nodes the rational function in 4.20 has only one pole, whereas the approximation of the Green's function would necessitate two poles.

Five nodes allow to accurately interpolate functions with two poles, hence the curves determined by single step computation and by accelerated computation almost coincide. The maximal difference is 8 dB at the frequency point 935 MHz.

The gain in computation time depends on the number of nodes and of interpolated matrices, in other words the ratio between number of nodes and number of frequency points. In the above case, 180 matrices were needed for a frequency step of 5 MHz. For an interpolation with three

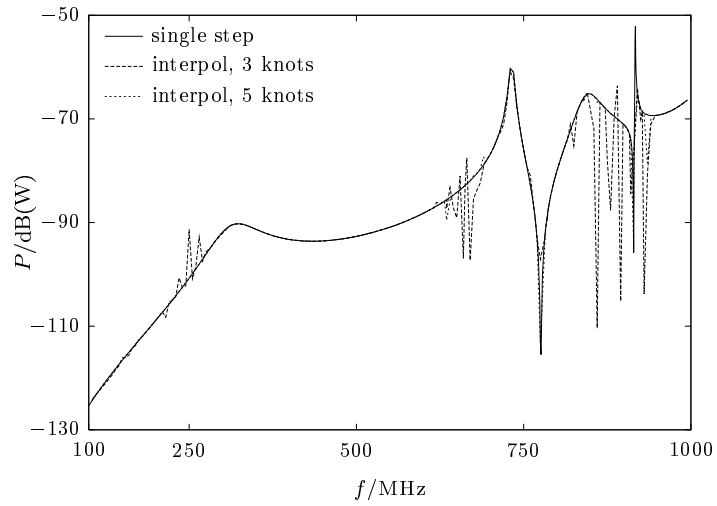


Figure 4.19.: Exact and interpolated curves for the wire/plate case

nodes, 54 matrices must be exactly calculated, the other 126 are interpolated with almost no computation time. The resulting gain is 70 %. This number is reduced to 50 % when interpolating with five nodes.

Chapter 5

Applications

The previous chapter presented details about the implementation of the method I chose based on the considerations stated in chapter 3. In this chapter the computer codes will be applied to two examples. The first example emphasises the necessity of well thought grounding schemes by comparing five different, but similar geometries. The example also introduces why methods are needed which rapidly give an insight into possible perturbations without necessarily supplying exact values. The second example is an application of statistical methods to the generic structure. Statistical methods are intended to give an idea of possible perturbations with only few data. This part is heavily based on a PhD thesis of the University of Paris [77], elaborated at the same research institution as the present work.

5.1. Interaction Plate–Monopole

The careful consideration of connections to ground and/or earth is very important when designing equipments compatible with their environments.

The mutual connection of several devices with shielded cables can cause interferences known as ground loops. They are mainly due to different impedances to the earth potential. In this case, the different devices should be grounded only once so that the ground loop is opened. One hence prevents the interference due to common mode perturbation. For high frequencies, however, the parasitic capacitance to earth of the non-grounded device will close again the loop and ruin the protection.

On printed circuit boards one uses large ground planes to reduce the inductance of the ground connection. Differential mode perturbations are effectively eliminated.

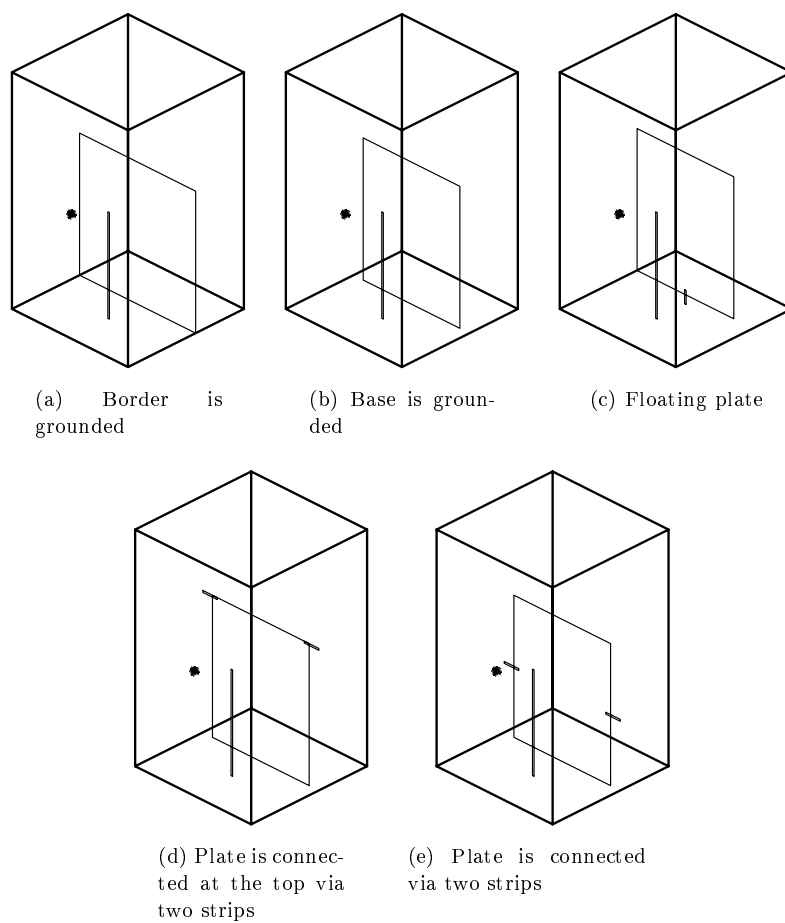


Figure 5.1.: Interaction monopole–plate: various grounding schemes (see text)

This section presents why and how large plates should be grounded inside cavities. For this, two objects are fitted into the usual cavity: the measuring monopole and a thin plate covering a large portion of the cavity section. This large plate is grounded, i.e. connected to the cavity walls, via different schemes:

1. The plate is connected to the base and to two side walls of the cavity, cf. fig. 5.1(a).
2. The plate is only connected to the cavity base, cf. fig. 5.1(b).
3. The plate ‘floats’ in the cavity, but has a conducting connection from the middle of the base to the cavity base, cf. fig. 5.1(c).

With a certain experience in field theory and antennas, the high-frequency-engineer will suppose that at certain frequencies a floating plate or a plate grounded only at an edge will resonate and hence radiate strongly. Two further schemes try to short circuit these resonances:

4. The top edge of the plate is connected to the cavity walls via two short, thin strips, cf. fig. 5.1(d). As the current normally goes to zero at the edges of conductors this scheme does not promise good results.
5. The edges of the plate are connected to the cavity walls via two short, thin strips at mid height of the plate, cf. fig. 5.1(e).

The dimensions of the geometries are summarised in table 5.1. Origin and axes are analog to fig. 4.5.

The structure was chosen to simulate in a simplified form a real, boxed system. A long cable, e.g. a power supply cable, is located close to a multilayer printed circuit board (PCB) in a cavity. The PCB is simplified to its large ground plane (for low inductance, see above), the effects from substrate and various other layers are neglected. Another large layer, e.g. for power supply, would be very close to the ground plane compared to other distances in the cavity. The substrate thickness would also be very small compared, its effect is hence negligible. Therefore, the whole PCB will be considered as a simple conducting plane.

		x/mm	y/mm	z/mm
<u>common characteristics:</u>				
cavity	size	300	300	500
aperture	circular, $r = 20$ mm			
	position	0	150	250
monopole	loaded with $R = 50\Omega$			
	base	100	150	0
	dimension		4	225
<u>scheme 1:</u> plate connected at the border				
plate	base	175	0	0
	dimensions		300	300
<u>scheme 2:</u> plate connected only at the base				
plate	base	175	25	0
	dimensions		250	300
<u>scheme 3:</u> floating plate with grounding strip				
plate	base	175	25	20
	dimensions		250	300
strip	base	175	150	0
	dimension		4	20
<u>scheme 4:</u> plate grounded at the top edge via two strips				
plate	base	175	25	0
	dimensions		250	300
strips	base	175	0	296
		175	300	296
	dimensions		25	4
<u>scheme 5:</u> plate grounded centrally via two strips				
plate	base	175	25	0
	dimensions		250	300
strips	base	175	0	148
		175	300	148
	dimensions		25	4

Table 5.1.: Dimensions of the different grounding schemes

The power in the base impedance of the measuring monopole in the frequency band 100 MHz to 995 MHz for the five grounding schemes was simulated using the method of chapter 4. Here, no reaction terms (neither of the cavity nor of the objects) were taken into account. Only the effects of the resonating plate coupling to the monopole were to be shown without covering them by other effects.

Figure 5.2 shows the received power for the five grounding schemes. Already in these plots over a wide band one sees, that the five schemes yield different results. Scheme 3 with the floating plate constitutes a case apart having differences of 4 to 6 dB to the others. In the following I will discuss more closely some of the phenomena, marked with arrows in the figures.

The first strong resonant effects occur between 120 MHz and 270 MHz. Figures 5.3 show the five curves in this frequency band in detail. Below 130 MHz, the base voltage of the monopole is the same for all cases apart from the one with the almost totally floating plate. Starting at 130 MHz, several resonances occur with a maximum decrease and increase of approximately 35 dB. Above 240 MHz, the curves are again flat with a comparable level. The longer dimension of the plate, 300 mm, is $\lambda/4$ at 250 MHz. For a physical explanation, image the plate at the cavity base, the whole length would now be 600 mm, the corresponding resonance is now $\lambda/2$. All curves except for the one for scheme 1 (complete grounding of the plate) and 5 (central grounding) show at least one resonance, suggesting that the plate resonates and couples to the monopole. Scheme 5 (grounding at mid height) shifted the resonance to 150 MHz, being more efficient to shortcut the above resonance.

The computations assume that losses occur only in the ohmic load of the monopole. The sharp resonances are due to the small losses, in reality they would be less sharp.

A physical interpretation of the remaining frequency band is difficult. Above 600 MHz more than six modes of the cavity are excitable, the different coupling mechanisms are tedious to investigate and to interpret. Different modes are excitable in different ways by the polarisation of the incoming wave and the position of the aperture. The different modes then do not couple uniformly to plate and monopole due to the field config-

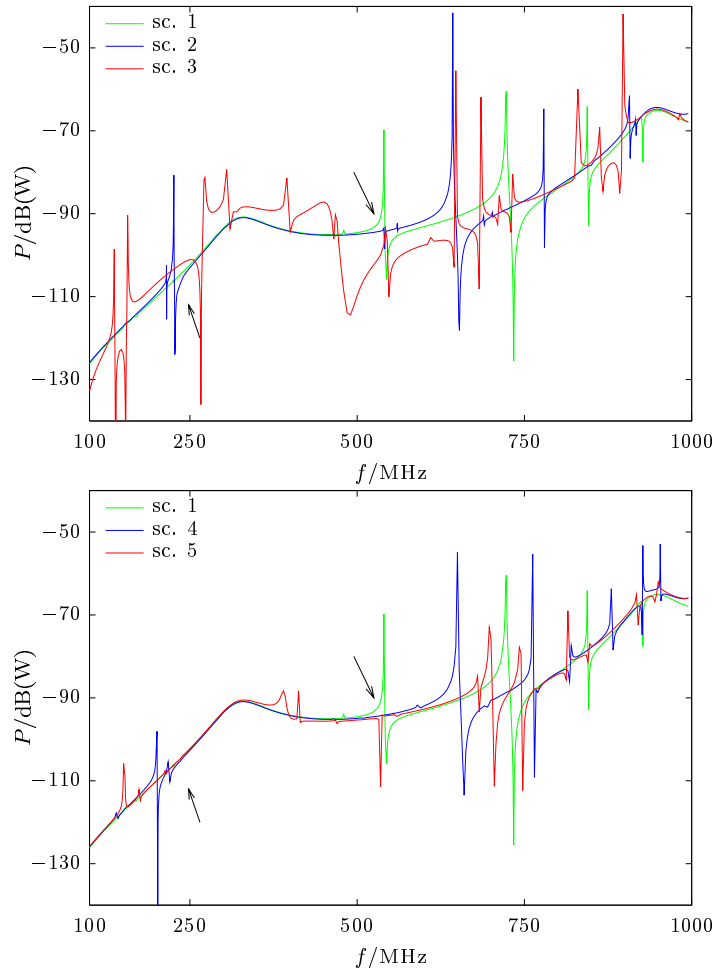


Figure 5.2.: Induced voltage at monopole base for the various grounding schemes. Top schemes 1 to 3, bottom scheme 2 (borders) and 3, 4 (strips)

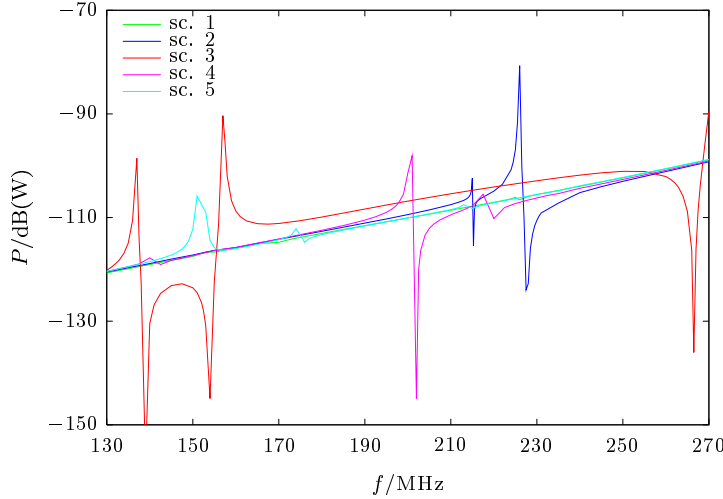


Figure 5.3.: Induced voltage in the frequency band 170 MHz to 270 MHz

uration. A close investigation would also be counterproductive because a small change in the parameters of the cases like dimensions or the position of the grounding wires would yield totally different curves. This can be seen when comparing the two schemes 4 and 5 with the grounding wires to the cavity walls.

Looking at figure 5.2 let us nevertheless conclude that generally the scheme with the plate connected to all possible walls is the one with the least resonances, at least in this frequency band. When considering only this frequency band and only the received power in the monopole, scheme 1 is in fact the best one. But other constraints could be asked for, for instance a maximum perturbation in the frequency band the system is functioning in. If the system functions only in a region from 300 MHz to 500 MHz, all curves are the same, all grounding schemes are appropriate. If however the usable band is in the region 100 MHz to 300 MHz, scheme 2 is necessary.

A resonance at 540 MHz, however, is a different case: only the curve for scheme 1 shows a strong resonance, all others are rather flat. A detailed plot is shown in fig. 5.4. Scheme 5 with grounding at mid-height has also

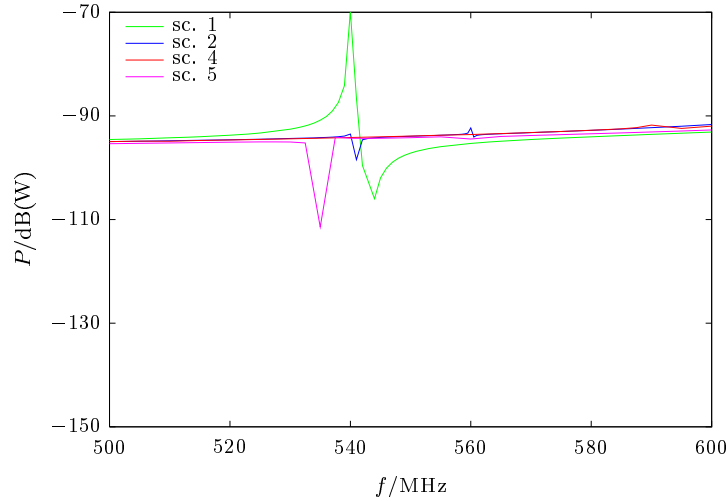


Figure 5.4.: Induced voltage in the frequency band 500 MHz to 600 MHz

a resonance in this region.

Starting with these examples several investigations are possible: changing the dimensions of the plate or its location, grounding by other schemes, etc. and so rapidly making explode the number of structures to investigate. Another factor in such an investigation is the frequency range: is the whole frequency range of 100 MHz to 1 GHz important or only a portion of it? Finally, what is the interesting physical variable? For audio and video applications, this could be a mean of the noise on the input voltage, for digital systems its maximum value. For a fast insight into possible perturbations, statistical methods can be used. One method was developed for an application in EMC [77], and shall be exemplarily applied below.

5.2. Statistical Methods in EMC

By using statistical methods in EMC, developers can gain a fast insight of what can happen if the parameters of a system are modified. The general performance of the system is then judged by measuring some physical vari-

ables like voltages or currents at characteristic places. The methods used below were developed by [77]. For consistency with his work, the variable parameters of a system will be called the factors, the performance of the system will be called the response of the system.

The first step is to choose the factors one would like to investigate, and the response. The mean value of a voltage or a current is a parameter one could be interested in. The mean of the voltage at the base of the monopole $\bar{U}(f)$ constitutes one easily measurable, yet characteristic parameter of the system. Restricted to the frequency band 650 MHz to 1 GHz this response will be considered in the following. The factors are the different geometric dimensions. For the previous case this could be the shape, size and position of the aperture (4 factors), the position and dimensions of the monopole (5 factors), and/or the dimensions of the plate (5 factors). Already with this easy case, fourteen factors possibly vary. For an exemplary description, this number is reduced by using a structure resembling the first test case of chapter 4: the single monopole in a cavity. The aperture will be considered as fixed, the plate will be removed. Of the remaining factors for the monopole only three will vary: the length of the monopole and its position on the cavity base. Considering a totally symmetric geometry with the aperture centred on the front wall, the domains for the three factors are hence reduced to the following intervals:

$$\begin{aligned} 126 \text{ mm} &\leq \text{length } l \text{ of monopole} && \leq 400 \text{ mm} \\ 150 \text{ mm} &\leq \text{position } y \text{ of monopole} && \leq 250 \text{ mm} \\ 50 \text{ mm} &\leq \text{position } x \text{ of monopole} && \leq 250 \text{ mm} \end{aligned}$$

The domain of variation of the position y is reduced to the above range due to the obvious symmetry of the structure: ‘left’ ($y \in [50 \text{ mm} : 150 \text{ mm}]$) will yield the same base voltages as ‘right’ ($y \in [50 \text{ mm} : 150 \text{ mm}]$). The factors are now mapped into normalised intervals and named for an easy identification:

$$\begin{aligned} -1 &\leq x_1 \leq 1 \\ -1 &\leq x_2 \leq 1 \\ -1 &\leq x_3 \leq 1 \end{aligned}$$

x_1 is the length, x_2 and x_3 are the position in x and y of the monopole respectively. One now says that the factors can have levels (= values) between +1 and -1.

For the application of the statistical methods, a so-called design of experiments, or in short just design is now implemented. It lists all possible combinations of all possible levels of the factors. For smaller plans and hence less experimentations, the numbers of levels are reduced. In the present case the number of levels were restricted to two, and 7 points were added so as to obtain the so called composite Δ -optimal design. The normalised factors now have the values -1 and +1, which would correspond to 126 mm and 400 mm and for the length l of the monopole. The above mentioned additional points correspond to the level 0, which is a length of $l = 263$ mm. The design used in the following prescribes 15 simulations. The simulations used the method of chapter 4.

The 15 experimentations are now treated by a numerical method called ordinary Kriging [78, 79], a method which is well known in geostatistics and mining. Jean Lefebvre [77] applied it to the coupling problem. After several steps of computation, the method issues an estimate and the corresponding standard deviation as error of this estimate to the true value. All necessary steps are described in detail in [77]. The estimation of the mean value for the base voltage is shown together with the standard deviation in fig. 5.5, the mean on the left hand side, the standard deviation on the right hand side. The black dots in the graph represent the values at which a simulation took place according to the plan of experimentations. At these places, the estimate is exact (no standard deviation), the plots for the standard deviation show zero. The three charts individually show the values of the perturbation for the three lengths l of 126 mm, 263 mm and 400 mm, each chart shows the estimate for the perturbation at the corresponding position. All three charts are issued by one single application of the Kriging method using all 15 simulations. Charts relating to other monopole lengths l as the shown ones are possible. The present charts also contain the original simulations and are therefore more interesting as the other ones. Note finally that other characteristics of performance are possible. The maximum base voltage could be another important and interesting value. However, the maximum voltage is very dependent on the frequency step

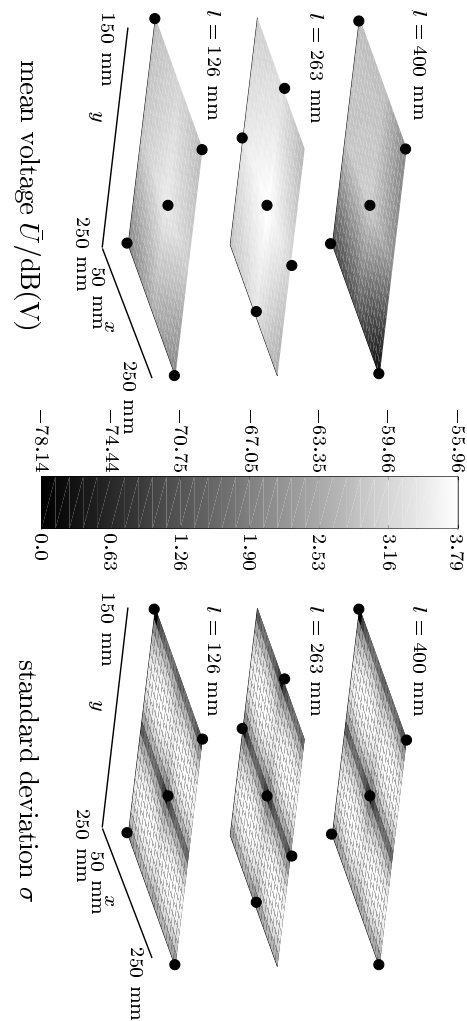


Figure 5.5.: Prediction of the mean base voltage for various lengths and positions

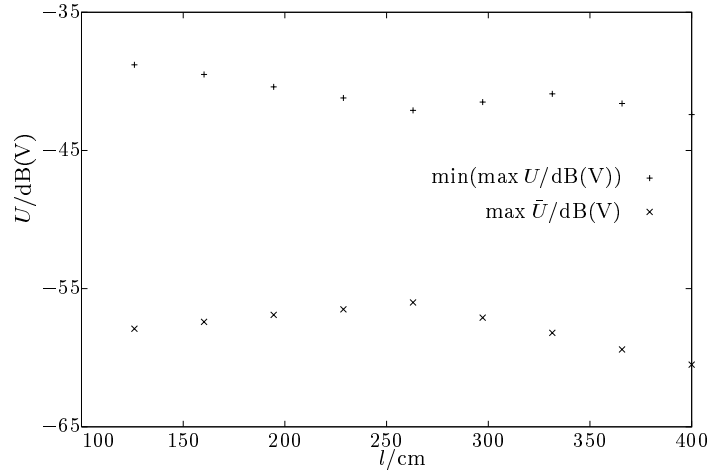


Figure 5.6.: Maximum and mean of the base voltage. Simulation by [77]

used during the calculation or experimentation step preliminary to the statistical method.

The method used for the previously mentioned figure 5.5 is also able to predict two performances important for the EMC engineer: the maximum value and the mean of the voltage for any position as a function of the monopole length. Figure reffig-minmax gives interesting informations for nine different monopole lengths: the maximum base voltage in the considered frequency band will always be between -45 dB(V) and -35 dB(V). At the same time, the mean of the base voltage in the same band will always be lower than -55 dB(V) whichever position for the monopole is chosen. The data is not meant to be exact design data, but provides with orders of magnitude.

5.3. Conclusion

The present chapter presented two applications of the computer codes issued by the present work. The first application was a short investigation

of different grounding schemes. It also showed the need for fast prediction methods without necessarily accurate values. These methods can among others be statistical methods which were shown in the second part of this chapter. With the two methods, an exact method which is also rather fast compared to other exact methods and a statistical method for rapid predictions with a reasonable accuracy, the engineer has tools available which assist in the development of electromagnetic devices.

Chapter 6

Conclusion and Outlook

The determination and investigation of possible coupling paths and mechanisms is important for the design of devices which are to continue to function in an electromagnetic environment possibly hostile. The present work contributes to this by investigating the electromagnetic coupling to objects in cavities. The electromagnetic perturbation is in the present case an electromagnetic wave impinging onto the cavity and entering into it through a small aperture.

The investigations are inserted in the various efforts combined to the catchword Electromagnetic Compatibility (EMC). EMC is a wide field which comprises many disciplines. Engineers specialised in areas as diverse as high voltage and high frequency techniques are needed for today's developments. Whereas until now mainly experimental techniques have been used, numerical methods become more and more important. Still, rigorous solutions need resources in memory and processor speed beyond present day desktop computers. The present work contents to present a fast, but still accurate method for the investigation of various effects which can occur in a generic structure. This generic structure is the coupling to metallic objects in perfectly conducting cavities via a small aperture (cf. chapter 1).

Not only legal obligations, but also possible liability claims nowadays encourage companies to develop and test their products carefully. European standards were elaborated to insure that new products won't interact in a non admissible way. A survey on some of the most representative and important standards is given in chapter 2.

Various tests with commercially available programs showed that these were less effective, or even inappropriate for the solution of the problem (chapter 3). Therefore, an existing method treating wire objects was

extended to include plane conductors. Voluminous objects can be composed by several plates.

The separation of interior and exterior of the cavity is a crucial detail in the present method. The separation is necessary to reduce the complexity of the problem, two small problems being less expensive than one large. Both problems, i.e. the exterior and the interior problem, are tackled with the most appropriate method.

The scattering problem in the exterior, short exterior problem, is solved using two classic methods. The first method is to assume that the cavity is flanged behind an infinite plane, the exterior field is then easily computed. Otherwise a Method of Moments for the free space takes into account the three-dimensional structure. The use of the numerical method for the exterior problem allowed for the first time to investigate the influences of the outer shape of the cavity. The influence is of minor importance compared to other characteristics as position or size of the internal objects.

The interior problem is solved using a specially developed Method of Moments using the dyadic Green's functions of the cavity. The mathematical form of these Green's functions needs a particular treatment, described in chapter 4. The reaction of the objects and the cavity on the aperture is evaluated by an improved technique. Further details of the numerical implementation show also a comparison of global and local function types. The experimental setup used for measurements is described before comparing computations and measurements.

Interior and exterior are related by the equivalent dipole principle. The aperture is metallized and replaced by two dipoles, an electric one and a magnetic one. The calculation of the dipole moments necessitates the determination of the short-circuit fields at both sides of the wall. The numerical evaluation of the exterior fields removes restrictions on the position of the aperture, it can now be placed anywhere on a cavity wall. The determination of the interior field involves the evaluation of Green's functions close to the source and an extrapolation.

Computations for wide frequency bands need long computation times. A new method for fast wide band computations of scattering problems in resonant structures is set out at the end of chapter 4. The method demands

more memory than a simple step-by-step computation, is, however, much faster.

Exemplary computations of wave interaction with cavities are found in chapter 5 where the interaction of a monopole and a plate is looked at. In the example a large plate is connected to the cavity walls by various schemes. The numerical results give evidence that grounding is a difficult task in EMC. It also underlines that techniques are needed in EMC which predict rapidly possible perturbations without involving long computations. Statistical methods, shown in the second part of the chapter, can contribute to fast predictions.

A work, what extensive it may be, is always incomplete and should stimulate to further research. Further work is possible in the physical area and the numerical area.

Further investigations may be done on the actual symptoms the generic structure exhibits. A study involving various parameters appears useful to gain understanding of physical phenomena. Hereby a simple generic structure permits a study of effects of aperture size and shape or cavity shape and size.

More theoretical work is still needed for the transmission of electromagnetic energy through small, medium, and large sized apertures. Both numerical and experimental work need to be conducted to obtain ideally expressions for large apertures as simple as the ones of the equivalent dipole approximation.

The procedure of separating interior and exterior is a necessary step when computing coupling through apertures. The implementation of the continuity/discontinuity of the E/H field is straightforward when using Integral Equations, but needs more theoretical work to be applicable in combination with other methods like the Finite-Difference Time-Domain or Finite Element Method.

Already now with the conjunction of the present rigorous numerical methods and statistical methods, the engineer has tools for the investigation of coupling problems. The present method also has the advantage that by including or excluding in a well defined way the various contributions, the user will gain more understanding of the coupling phenomena, and is hence able to react and to prevent strong interactions.

Appendix A

Polarisabilities of Small Apertures

The aperture considered in the following has a normal in \vec{e}_x , the two half axis for the elliptic ones and the major directions for the rectangular ones are in \vec{e}_y and \vec{e}_z respectively. Dimensions and orientation are sketched in fig. A.1.

Butler [80] resumes the polarisabilities for small circular, elliptic and narrow elliptic apertures. His notation is used here. Please note, that the values differ from his by a factor of 2 due to a different definition of fields radiated by the equivalent dipoles.

A.1. Circular Aperture

$$\alpha_e = \frac{4}{3}r^3 \quad \alpha_{myy} = \frac{8}{3}r^3 \quad \alpha_{mzz} = \frac{8}{3}r^3 \quad (\text{A.1})$$

A.2. Elliptic Aperture

$$\alpha_e = \frac{2}{3} \frac{\pi w^2 l}{E(\epsilon)}$$
$$\alpha_{myy} = \frac{2}{3} \frac{\pi l^3 \epsilon^2}{K(\epsilon) - E(\epsilon)} \quad \alpha_{mzz} = \frac{2}{3} \frac{\pi l^3 \epsilon^2}{\left(\frac{l}{w}\right)^2 E(\epsilon) - K(\epsilon)} \quad (\text{A.2})$$

K and E are the complete elliptic integrals of the first and second kind respectively: $K(\epsilon) = \int_0^{\pi/2} \frac{d\Phi}{\sqrt{1-\epsilon^2 \sin^2 \Phi}}$, $E(\epsilon) = \int_0^{\pi/2} \sqrt{1-\epsilon^2 \sin^2 \Phi} d\Phi$, ϵ is the ellipse eccentricity $\epsilon = \sqrt{1 - (w/l)^2}$.

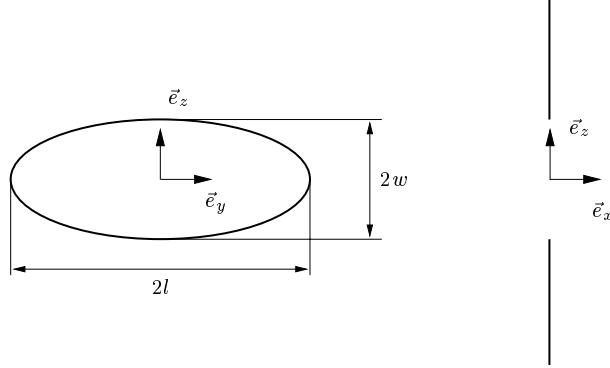


Figure A.1: Aperture dimensions and orientation

A.3. Narrow Elliptic Aperture ($w \ll l$)

$$\alpha_e = \frac{2}{3}\pi w^2 l \quad \alpha_{myy} = \frac{2}{3} \frac{\pi l^3}{\ln\left(\frac{4l}{w}\right) - 1} \quad \alpha_{mzz} = \frac{2}{3}\pi w^3 l \quad (\text{A.3})$$

A.4. Narrow Slit ($w \ll l$)

Lee [54] cites the polarisabilities for a narrow slit.

$$\alpha_e = \pi w^2 l \quad \alpha_{myy} = \frac{2}{3} \frac{\pi l^3}{\ln\left(\frac{4l}{w}\right) - 1} \quad \alpha_{mzz} = \pi w^3 l \quad (\text{A.4})$$

A.5. Various Shapes

When normalising the polarisabilities by $A^{3/2}$ with A surface of the aperture, the resulting values for a rectangular, cross, or rectangular with rounded corners are very close (at most 3%) to the elliptic ones [54]. Slightly different values are obtained for the losange. By this normalisation, apertures with almost arbitrary shapes can be considered.

Appendix B

Reaction of Cavity and Objects

Topic of this appendix is the derivation of the reaction field of the cavity to the aperture. For the free-space case the reaction fields were derived in [81]. In the general case, consider an electric dipole in \vec{e}_z , shown in fig. B.1, and in a similar way a magnetic dipole in \vec{e}_z . The spherical and Cartesian coordinate system are shown in the same figure along with the corresponding angles and unit vectors.

B.1. Electric Dipole

The electric and magnetic field radiated by an electric dipole $\vec{p} = p_0\vec{e}_z$ are [82]:

$$E_r = \frac{p_0 k^2}{2\pi\epsilon} \cos\theta \left(\frac{1}{k^2 r^2} + \frac{j}{kr} \right) \frac{1}{r} e^{-jkr} \quad (\text{B.1})$$

$$E_\theta = -\frac{p_0 k^2}{4\pi\epsilon} \sin\theta \left(1 - \frac{1}{k^2 r^2} - \frac{j}{kr} \right) \frac{1}{r} e^{-jkr} \quad (\text{B.2})$$

$$H_\phi = \frac{j p_0 \omega k \sin\theta}{4\pi} \frac{1}{r} \left(\frac{1}{kr} + j \right) e^{-jkr} \quad (\text{B.3})$$

Very close to the source (r small), the exponential can be approximated by

$$e^{-jkr} = 1 - jkr - \frac{k^2 r^2}{2} + j \frac{k^3 r^3}{6} \quad (\text{B.4})$$

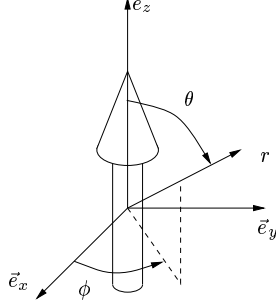


Figure B.1.: Electric dipole in spherical and Cartesian coordinate system

With this, (B.1-B.3) become

$$\begin{aligned} E_r &= \frac{p_0 k^2 \cos \theta}{2\pi\epsilon} \frac{1}{r} \left(\frac{1}{k^2 r^2} + \frac{j}{kr} \right) \left(1 - jkr - \frac{k^2 r^2}{2} + j \frac{k^3 r^3}{6} \right) \\ &= \frac{p_0 k^2 \cos \theta}{2\pi\epsilon} \frac{1}{r} \left(\frac{1}{k^2 r^2} + \frac{1}{2} - \frac{k^2 r^2}{6} - j \frac{kr}{3} \right) \end{aligned} \quad (\text{B.5})$$

$$\begin{aligned} E_\theta &= -\frac{p_0 k^2 \sin \theta}{4\pi\epsilon} \frac{1}{r} \left(1 - \frac{1}{k^2 r^2} - \frac{j}{kr} \right) \left(1 - jkr - \frac{k^2 r^2}{2} + j \frac{k^3 r^3}{6} \right) \\ &= \frac{p_0 k^2 \sin \theta}{4\pi\epsilon} \frac{1}{r} \left(\frac{1}{k^2 r^2} - \frac{1}{2} + \frac{k^2 r^2}{3} + j \frac{2kr}{3} \right) \end{aligned} \quad (\text{B.6})$$

and

$$\begin{aligned} H_\phi &= \frac{jp_0 \omega k \sin \theta}{4\pi} \frac{1}{r} \left(\frac{1}{kr} + j \right) \left(1 - jkr - \frac{k^2 r^2}{2} + j \frac{k^3 r^3}{6} \right) \\ &= jp_0 \frac{\omega k \sin \theta}{4\pi} \frac{1}{r} \left(\frac{1}{kr} + \frac{kr}{2} - j \frac{k^2 r^2}{3} \right) \end{aligned} \quad (\text{B.7})$$

With this the electric field in \vec{e}_z is

$$\begin{aligned} E_z &= E_r \cos \theta - E_\theta \sin \theta \\ &= \frac{p_0}{4\pi\epsilon} \frac{k^2}{r} \left(\frac{2 \cos^2 \theta - \sin^2 \theta}{k^2 r^2} + \frac{k^2}{2} (2 \cos^2 \theta + \sin^2 \theta) - j \frac{2kr}{3} \right) \end{aligned} \quad (\text{B.8})$$

Please note that the imaginary part of the electric field remains bounded at the source. The real part diverges with r^{-3} and r^{-1} .

Similar for the magnetic field:

$$\begin{aligned}
 H_x &= -H_\phi \sin \phi \\
 &= -jp_0 \frac{\omega k r \sin \theta \sin \phi}{4\pi r^2} \left(\frac{1}{kr} + \frac{kr}{2} - j \frac{k^2 r^2}{3} \right) \\
 &= -jp_0 \frac{\omega k y}{4\pi r^2} \left(\frac{1}{kr} + \frac{kr}{2} - j \frac{k^2 r^2}{3} \right) \tag{B.9}
 \end{aligned}$$

$$\begin{aligned}
 H_y &= H_\phi \cos \phi \\
 &= jp_0 \frac{\omega k r \sin \theta \cos \phi}{4\pi r^2} \left(\frac{1}{kr} + \frac{kr}{2} - j \frac{k^2 r^2}{3} \right) \\
 &= -jp_0 \frac{\omega k x}{4\pi r^2} \left(\frac{1}{kr} + \frac{kr}{2} - j \frac{k^2 r^2}{3} \right) \tag{B.10}
 \end{aligned}$$

The real parts vanish at the source. The choice $y = r$ and $x = r$ respectively simplifies the expressions and is therefore the direction of extrapolation.

To simplify the expression for the E_z choose now $\cos \theta = \frac{1}{\sqrt{3}}$, so that eqn. (B.8) becomes

$$E_z = \frac{p_0 k^2}{6\pi\epsilon r} \tag{B.11}$$

and hence

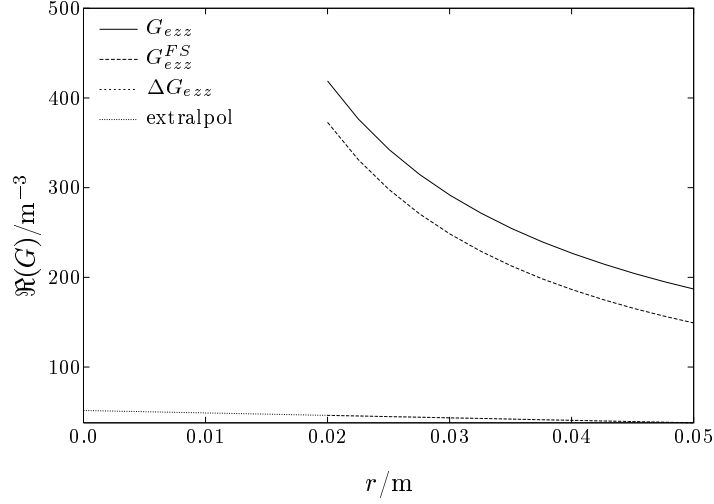
$$G_{ezz}^{FS} = \frac{k^2}{6\pi r} \tag{B.12}$$

The Green's function for the magnetic field close to the source are

$$G_{hxz}^{FS} = -\frac{k y}{4\pi r^2} \left(\frac{1}{kr} + \frac{kr}{2} \right) \tag{B.13}$$

$$G_{hyz}^{FS} = \frac{k x}{4\pi r^2} \left(\frac{1}{kr} + \frac{kr}{2} \right) \tag{B.14}$$

With a simple coordinate transform, the expressions for an electric dipole $\vec{p} = p_0 \vec{e}_x$ are readily found.

Figure B.2.: Extrapolation procedure for $E_z(p_0\vec{e}_z)$

B.2. Magnetic Dipole

Babinet's principle now states that if \vec{E}' and \vec{H}' are solution of Maxwell's equations in a homogeneous, lossless and chargefree space, then also

$$\vec{E} = -Z\vec{H}' \quad (\text{B.15})$$

$$\vec{H} = +\frac{1}{Z}\vec{E}' \quad (\text{B.16})$$

with $Z = \sqrt{\mu/\varepsilon}$ are solution of Maxwell's equation, hence the expressions for the electric and magnetic field in the vicinity of the source are expressed analogously.

B.3. Example

The field radiated by the images of the two dipoles which replaced the aperture is now the difference between the field radiated by a dipole in free space and the field radiated by a dipole in a cavity. Both fields diverge

at the aperture, however the difference is bounded. This value was previously determined by the extrapolation of \bar{G}_A and \bar{g}_F and a subsequent numerical finite difference scheme. The values for \bar{G}_e , \bar{G}_h , \bar{g}_e and \bar{g}_h are, however, very inaccurate. More accurate is the direct extrapolation of the difference of the Green's function of free space and of the cavity proposed here. In fig. B.2 is shown the Green's function for free space and for the cavity evaluated for $\cos \theta = 1/\sqrt{3}$. Both curves show the $1/r$ behavior of eqn. (B.11), the difference is now extrapolated to the source point (numerical values for the figure: $A = 297$ mm, $B = 297$ mm, $C = 498$ mm, $(x_{aper}, y_{aper}, z_{aper}) = (0, 152; 0, 248)$ mm, $f = 400$ MHz).

Appendix C

The Elements of the Impedance Matrix

Equation (3.35) shows the linear system to be solved. This equation is recalled here for clarity:

$$(3.35): \quad \begin{pmatrix} Z_{JJ} & Z_{JE} & Z_{JH} \\ Z_{EJ} & Z_{EE} & Z_{EH} \\ Z_{HJ} & Z_{HE} & Z_{HH} \end{pmatrix} \cdot \begin{pmatrix} J \\ \Delta E \\ \Delta \vec{H} \end{pmatrix} = \begin{pmatrix} 0 \\ \vec{E}^- \cdot \vec{n} \\ \vec{H}^- \end{pmatrix}$$

The different elements were described in section 3.5, and are recalled here together with a more detailed description of the actual implementation.

C.1. Z_{JJ} : Moment Matrix

The elements of the Moment Matrix relate the field radiated by a current element, hence the basis function of this current element, with the testing or sampling function. Mathematically, a double surface integration of the Green's function with basis and testing function yield the matrix elements. The domains of integration are firstly the domain Γ_b for the basis functions f_b and secondly Γ_t , domain of the testing functions f_t . Numerical issues of the Green's functions as well as the double surface integration are listed in chapter 4. The integrations again are carried out term by term, they converge sufficiently to be allowed to do this.

$$(Z_{JJ}) = \int_{\Gamma_b} \int_{\Gamma_t} f_t \bar{\bar{G}}_e f_b d\Gamma_t d\Gamma_b \quad (C.1)$$

The elements $Z_{J_y J_y}$ for the current J_y on a surface normal to \vec{e}_x are:

$$\begin{aligned} \langle G_{e_{yy}} f_{by}, f_{ty} \rangle &= \frac{j}{\omega \varepsilon} \sum_{k_x} \sum_{k_y} \sum_{k_z} \\ &\quad \sin(k_x x) \sin(k_x x') \\ &\quad (k^2 - k_y^2) \int_{\Gamma_t} \cos(k_y y) f_t(y) d\Gamma_t \int_{\Gamma_r} \cos(k_y y') f_b(y') d\Gamma_b \\ &\quad \int_{\Gamma_t} \sin(k_z z) f_t(z) d\Gamma_t \int_{\Gamma_r} \sin(k_z z') f_b(z') d\Gamma_b \end{aligned}$$

The part for x is reduced by using one of the expressions (4.1) - (4.4).

The other elements Z_{JJ} are computed in the same way.

C.2. Z_{JE} : Sampled Incident Field Due to Electric Dipole

The sampled incident electric field is the electric field radiated by the electric dipoles representing the aperture.

$$(3.28): \quad \vec{E}_{inc} = \frac{1}{\varepsilon} \vec{G}_e(\vec{r}, \vec{r}') \vec{p}_e$$

This incident field is sampled by a testing function. For a current J_x , (3.28) becomes:

$$(Z_{J_x E}) = \alpha_e \int_{\Gamma_t} f_{tx} G_{exx}(\vec{r}, \vec{r}_{aper}) d\Gamma_t \quad (C.2)$$

f_{tx} is constructed depending on the normal vector of the surface with no integration in the normal direction. Similar for J_y and J_z .

C.3. Z_{JH} : Sampled Incident Field Due to Magnetic Dipole

The sampled incident electric field is the electric field radiated by the magnetic dipoles representing the aperture.

$$(3.28): \quad \vec{E}_{inc} = +j \mu \omega \bar{g}_e(\vec{r}, \vec{r}') \vec{p}_m$$

This incident field is sampled by a testing function.

$$\begin{aligned} (Z_{J_x H_y}) &= -j \mu \omega \int_{\Gamma_t} f_t g_{exy}(\vec{r}, \vec{r}_{aper}) d\Gamma_t \alpha_{myy} \\ &\quad - j \mu \omega \int_{\Gamma_t} f_t g_{exz}(\vec{r}, \vec{r}_{aper}) d\Gamma_t \alpha_{mzy} \end{aligned} \quad (C.3)$$

$$\begin{aligned} (Z_{J_y H_y}) &= -j \mu \omega \int_{\Gamma_t} f_t g_{eyy}(\vec{r}, \vec{r}_{aper}) d\Gamma_t \alpha_{myy} \\ &\quad - j \mu \omega \int_{\Gamma_t} f_t g_{eyz}(\vec{r}, \vec{r}_{aper}) d\Gamma_t \alpha_{mzy} \end{aligned} \quad (C.4)$$

$$\begin{aligned} (Z_{J_z H_y}) &= -j \mu \omega \int_{\Gamma_t} f_t g_{ezy}(\vec{r}, \vec{r}_{aper}) d\Gamma_t \alpha_{myy} \\ &\quad - j \mu \omega \int_{\Gamma_t} f_t g_{ezz}(\vec{r}, \vec{r}_{aper}) d\Gamma_t \alpha_{mzy} \end{aligned} \quad (C.5)$$

Similar for H_z .

C.4. Z_{EJ} : Reaction of Surface Currents onto Electric Dipole

When neglecting the reaction of the surface currents on the objects, these elements equal zero.

$$(Z_{EJ}) = \left(-\frac{j}{\omega \varepsilon} \int_{\Gamma_b} G_{exx} f_{bx} d\Gamma_b, -\frac{j}{\omega \varepsilon} \int_{\Gamma_b} G_{exy} f_{by} d\Gamma_b, -\frac{j}{\omega \varepsilon} \int_{\Gamma_b} G_{exz} f_{bz} d\Gamma_b \right) \quad (C.6)$$

In a Galerkin scheme (basis and testing functions are identical), the sampled incident field (C.2) and the reaction of the surface currents (C.6) are proportional by a factor of $-\frac{j}{\varepsilon \omega} \frac{1}{\alpha_e \Delta E}$.

C.5. Z_{EE} : Reaction of the Electric Field onto Electric Dipole

Unity if reaction is neglected. The exact derivation of the elements of the so-called reaction Green's \bar{G}_e^r functions is in appendix B.

$$(Z_{EE}) = (1 + \alpha_e G_{eex}^r) \quad (\text{C.7})$$

C.6. Z_{EH} : Reaction of the Magnetic Field onto Electric Dipole

Zero if reaction is neglected. The exact derivation of the elements of the so-called reaction Green's functions \bar{g}_e^r is in appendix B.

$$(Z_{EH}) = (Z_{E_x H_y}, Z_{E_x H_z}) = (-j\omega\mu g_{exy}^r - j\omega\mu g_{exz}^r) \quad (\text{C.8})$$

C.7. Z_{HJ} : Reaction of Surface Currents onto Magnetic Dipole

When neglecting the reaction of the surface currents on the objects, these elements equal zero.

$$(Z_{H_y J}) = \left(+ \int_{\Gamma_b} G_{hyx} f_{bx} d\Gamma_b, + \int_{\Gamma_b} G_{hyy} f_{by} d\Gamma_b, + \int_{\Gamma_b} G_{hyz} f_{bz} d\Gamma_b \right) \quad (\text{C.9})$$

Similar for $Z_{H_z J}$. In a Galerkin scheme (basis and testing functions are identical), the sampled incident field and the reaction of the surface currents (C.2) are proportional by a factor of $-j\mu\omega\alpha_m\Delta H$.

C.8. Z_{HE} : Reaction of the Electric Field onto Magnetic Dipole

Zero if reaction is neglected. The exact derivation of the elements of the so-called reaction Green's functions \bar{G}_h^r is in appendix B.

$$(Z_{HE_x}) = (Z_{H_y E_x}, Z_{H_z E_x}) = (j\omega\varepsilon\alpha_e G_{hyx}^r, j\omega\varepsilon\alpha_e G_{hzx}^r) \quad (\text{C.10})$$

C.9. Z_{HH} : Reaction of the Magnetic Field onto Magnetic Dipole

Unity if reaction is neglected. The exact derivation of the elements of the so-called reaction Green's functions \bar{g}_h^r is in appendix B.

$$(Z_{H_y H}) = (Z_{H_y H_y}, Z_{H_y H_z}) = ((1 - g_{h_y y}^r \alpha_{m_y y}), -g_{h_y y}^r \alpha_{m_y z}) \quad (\text{C.11})$$

Similar for $Z_{H_z H}$.

C.10. One Dimensional Integrations of Sine/Cosine and Basis/Testing Functions

The following expressions list the expressions of the integrals encountered during the expansion as well as the testing step. The appropriate expressions are used in the appropriate elements above.

According to the distinction made in section 3.5 for the type of basis or testing functions the expressions for local and global functions are listed.

The following expression contain the variables x_i , x_{i+1} and x_{i-1} which are the present sampling point and the two adjacent sampling points. If $i = 0$, the sampling point is on the edge, x_{i-1} does not exist in that case. The last point on the edge is x_{N-1} with $i = N - 1$. The sampling rate is $x_i - x_{i-1} = \Delta_x$. Some terms can be precalculated and stored to reduce the computational effort.

C.10.1. Local Basis Functions

- piecewise constant function with sine:

$$i = 0 : \quad \int_{x_i}^{x_{i+1}} \sin k_x x \, dx = \frac{1}{k_x} \sin k_x \frac{\Delta_x}{4} \sin k_x (x_0 + \frac{\Delta_x}{4}) \quad (\text{C.12})$$

$$i \neq 0, N - 1 : \quad \int_{x_{i-1}}^{x_{i+1}} \sin k_x x \, dx = \frac{2}{k_x} \sin k_x \frac{\Delta_x}{4} \sin k_x x_i \quad (\text{C.13})$$

$$i = N - 1 : \quad \int_{x_{i-1}}^{x_i} \sin k_x x \, dx = \frac{1}{k_x} \sin k_x \frac{\Delta_x}{4} \sin k_x (x_{N-1} - \frac{\Delta_x}{4}) \quad (\text{C.14})$$

with cosine:

$$i = 0 : \quad \int_{x_i}^{x_{i+1}} \cos k_x x \, dx = \frac{1}{k_x} \sin k_x \frac{\Delta_x}{4} \cos k_x \left(x_0 + \frac{\Delta_x}{4} \right) \quad (\text{C.15})$$

$$i \neq 0, N-1 : \quad \int_{x_{i-1}}^{x_{i+1}} \cos k_x x \, dx = \frac{2}{k_x} \sin k_x \frac{\Delta_x}{4} \cos k_x x_i \quad (\text{C.16})$$

$$i = N-1 : \quad \int_{x_{i-1}}^{x_i} \cos k_x x \, dx = \frac{1}{k_x} \sin k_x \frac{\Delta_x}{4} \cos k_x \left(x_{N-1} - \frac{\Delta_x}{4} \right) \quad (\text{C.17})$$

- piecewise linear function with sine:

$$i = 0 : \quad \int_{x_i}^{x_{i+1}} \sin k_x x \left[1 - \frac{|x - x_i|}{\Delta_x} \right] dx = + \frac{\cos k_x x_i}{k_x} - \frac{2 \sin k_x \frac{\Delta_x}{2} \cos k_x \left(x_i + \frac{\Delta_x}{2} \right)}{k_x \Delta_x} \quad (\text{C.18})$$

$$i \neq 0, N-1 : \quad \int_{x_{i-1}}^{x_{i+1}} \sin k_x x \left[1 - \frac{|x - x_i|}{\Delta_x} \right] dx = \Delta_x \left(\frac{2 \sin k_x \frac{\Delta_x}{2}}{k_x \Delta_x} \right)^2 \sin k_x x_i \quad (\text{C.19})$$

$$i = N-1 : \quad \int_{x_{i-1}}^{x_i} \sin k_x x \left[1 - \frac{|x - x_i|}{\Delta_x} \right] dx = - \frac{\cos k_x x_i}{k_x} + \frac{2 \sin k_x \frac{\Delta_x}{2} \cos k_x \left(x_i - \frac{\Delta_x}{2} \right)}{k_x \Delta_x} \quad (\text{C.20})$$

with cosine:

$$\begin{aligned}
 i = 0 : \\
 \int_{x_i}^{x_{i+1}} \cos k_x x \left[1 - \frac{|x - x_i|}{\Delta_x} \right] dx &= - \frac{\sin k_x x_i}{k_x} \\
 &\quad - \frac{2 \sin k_x \frac{\Delta_x}{2}}{k_x \Delta_x} \frac{\sin k_x (x_i + \frac{\Delta_x}{2})}{k_x}
 \end{aligned} \tag{C.21}$$

$$\begin{aligned}
 i \neq 0, N - 1 : \\
 \int_{x_{i-1}}^{x_{i+1}} \cos k_x x \left[1 - \frac{|x - x_i|}{\Delta_x} \right] dx &= \Delta_x \left(\frac{2 \sin k_x \frac{\Delta_x}{2}}{k_x \Delta_x} \right)^2 \sin k_x x_i
 \end{aligned} \tag{C.22}$$

$$\begin{aligned}
 i = N - 1 : \\
 \int_{x_{i-1}}^{x_i} \cos k_x x \left[1 - \frac{|x - x_i|}{\Delta_x} \right] dx &= + \frac{\sin k_x x_i}{k_x} \\
 &\quad - \frac{2 \sin k_x \frac{\Delta_x}{2}}{k_x \Delta_x} \frac{\sin k_x (x_i - \frac{\Delta_x}{2})}{k_x}
 \end{aligned} \tag{C.23}$$

- piecewise sinusoidal with sine:

$$\begin{aligned}
 i = 0 : \int_{x_i}^{x_{i+1}} \sin k_x x \frac{\sin k (\Delta_x - |x - x_i|)}{\sin k \Delta_x} dx &= \\
 \frac{k \sin k_x x_i \cos k_x \Delta_x - \cos k \Delta_x}{k^2 - k_x^2} - \frac{\cos k_x x_i k_x \sin k \Delta_x - k \sin k_x \Delta_x}{k^2 - k_x^2} \frac{1}{\sin k \Delta_x}
 \end{aligned} \tag{C.24}$$

$$\begin{aligned}
 i \neq 0, N - 1 : \int_{x_{i-1}}^{x_{i+1}} \sin k_x x \frac{\sin k (\Delta_x - |x - x_i|)}{\sin k \Delta_x} dx &= \\
 \frac{2k \sin k_x x_i \cos k_x \Delta_x - \cos k \Delta_x}{k^2 - k_x^2} \frac{1}{\sin k \Delta_x}
 \end{aligned} \tag{C.25}$$

$$\begin{aligned}
i = N - 1 : \int_{x_{i-1}}^{x_i} \sin k_x x \frac{\sin k (\Delta_x - |x - x_i|)}{\sin k \Delta_x} dx = \\
\frac{k \sin k_x x_i \cos k_x \Delta_x - \cos k \Delta_x}{k^2 - k_x^2} + \frac{\cos k_x x_i k_x \sin k \Delta_x - k \sin k_x \Delta_x}{\sin k \Delta_x}
\end{aligned} \tag{C.26}$$

with cosine:

$$\begin{aligned}
i = 0 : \int_{x_i}^{x_{i+1}} \cos k_x x \frac{\sin k (\Delta_x - |x - x_i|)}{\sin k \Delta_x} dx = \\
\frac{k \cos k_x x_i \cos k_x \Delta_x - \cos k \Delta_x}{k^2 - k_x^2} + \frac{\sin k_x x_i k_x \sin k \Delta_x - k \sin k_x \Delta_x}{\sin k \Delta_x}
\end{aligned}$$

$$\begin{aligned}
i \neq 0, N - 1 : \int_{x_{i-1}}^{x_{i+1}} \cos k_x x \frac{\sin k (\Delta_x - |x - x_i|)}{\sin k \Delta_x} dx = \\
\frac{2k \cos k_x x_i \cos k_x \Delta_x - \cos k \Delta_x}{k^2 - k_x^2}
\end{aligned} \tag{C.27}$$

$$\begin{aligned}
i = N - 1 : \int_{x_{i-1}}^{x_i} \cos k_x x \frac{\sin k (\Delta_x - |x - x_i|)}{\sin k \Delta_x} dx = \\
\frac{k \cos k_x x_i \cos k_x \Delta_x - \cos k \Delta_x}{k^2 - k_x^2} + \frac{\sin k_x x_i k_x \sin k \Delta_x - k \sin k_x \Delta_x}{\sin k \Delta_x}
\end{aligned} \tag{C.28}$$

$$\tag{C.29}$$

C.10.2. Global Basis Functions

- floating plate, function $GI(x) = \sin \left((m+1)\pi \frac{x-x_{min}}{x_{max}-x_{min}} \right)$ with $k_m = \frac{(m+1)\pi}{x_{max}-x_{min}}$

$$\begin{aligned}
\int_{x_{min}}^{x_{max}} \sin k_x x GI(x) dx = \\
\frac{k_m}{k_m^2 - k_x^2} (\sin k_x x_{min} - (-1)^{m+1} \sin k_x x_{max}) \tag{C.30}
\end{aligned}$$

$$\int_{x_{min}}^{x_{max}} \cos k_x x \, GI(x) \, dx = \frac{k_m}{k_m^2 - k_x^2} (\cos k_x x_{min} - (-1)^{m+1} \cos k_x x_{max}) \quad (C.31)$$

- plate at one end, function $GO(x) \cos\left(\frac{2m+1}{2}\pi\frac{x-x_{min}}{x_{max}-x_{min}}\right)$, with $k_m = \frac{2m+1}{2} \frac{\pi}{x_{max}-x_{min}}$

$$\int_{x_{min}}^{x_{max}} \sin k_x x \, GO(x) \, dx = \frac{-k_x}{k_m^2 - k_x^2} \cos k_x x_{min} + (-1)^m \frac{k_m}{k_m^2 - k_x^2} \sin k_x x_{max} \quad (C.32)$$

$$\int_{x_{min}}^{x_{max}} \cos k_x x \, GO(x) \, dx = \frac{k_x}{k_m^2 - k_x^2} \sin k_x x_{min} + (-1)^m \frac{k_m}{k_m^2 - k_x^2} \cos k_x x_{max} \quad (C.33)$$

Appendix D

Algorithm for the Interpolation by Rational Functions

The Neville type algorithm for the interpolation by rational functions [75, 76] is well suited for the interpolation of functions which are not well approximated by polynomials, but well approximated by rational functions.

Let R^ρ be a rational function of order $\rho + 1$ with

$$R^\rho = R_{i(i+1)\cdot(i+\rho)} = \frac{p_0 + p_1 x + \cdots + p_\mu x^\mu}{q_0 + q_1 x + \cdots + q_\nu x^\nu} \quad (\text{D.1})$$

with $\rho + 1 = \mu + \nu + 1$. It denotes a rational function passing through the $\rho + 1$ data doublets (x_i, y_i) with $R^\rho(x_i) = y_i$. Note that the zeros and the poles of (D.1) can be both real or complex, so that an approximation of real functions with singular continuation in the complex plane is possible.

The proposed algorithm performs a Neville type rational function extrapolation on tabulated data. The recurrence relation is the following:

$$R_{i(i+1)\cdot(i+\rho)} = R_{(i+1)\cdot(i+\rho)} + \frac{R_{(i+1)\cdot(i+\rho)} - R_{i(i+1)\cdot(i+\rho-1)}}{\frac{x-x_i}{x-x_{i+\rho}} \left(1 - \frac{R_{(i+1)\cdot(i+\rho)} - R_{i(i+1)\cdot(i+\rho-1)}}{R_{(i+1)\cdot(i+\rho)} - R_{i(i+1)\cdot(i+\rho-1)}} \right) - 1} \quad (\text{D.2})$$

and generates the rational functions through the $\rho + 1$ points using the ones through the ρ and $\rho - 1$ points. The first elements are

$$R_i = y_i \quad (\text{D.3})$$

and

$$R_{i(i+1)\cdot(i+m)} = 0 \quad \text{when } m = -1 \quad (\text{D.4})$$

Finally please note that the *Padé-approximation* is a method where the first $\rho + 1$ terms of the power series expansion of (D.1) correspond to the first $\rho + q$ terms of the power series expansion of the desired function $f(x)$. The presented algorithm however is not using this property.

Bibliography

- [1] T. H. Hubing, "Practical EMI/EMC design and modeling," *Short Course, Annual Review of Progress in Appl. Comp. EM*, 1997.
- [2] D. Mittler, "Wiederbelebungsgerät setzt aus," *Süddt. Zeitung*, 5./6./7. January 1995.
- [3] Bayr. Staatsministerium für Landesentwicklung und Umweltfragen, *Stichwort Mobilfunk*, 1/1997.
- [4] Standard DIN 5 December 1970, "Axonometrische Projektionen."
- [5] Standard DIN 461 March 1973, "Graphische Darstellung in Koordinatensystemen."
- [6] Standard DIN 1324 Mai 1988, "Elektromagnetisches Feld."
- [7] A. Schwab, *Elektromagnetische Verträglichkeit*. Berlin: Springer Verlag, 1996.
- [8] M. Mardiguian, *Manuel Pratique de Compatibilité Électromagnétique*. Les Ulis: Prâna Recherche et Developpement, 1992.
- [9] D. A. Weston, *Electromagnetic Compatibility*. New York: Marcel Dekker, Inc, 1991.
- [10] P. Degauque and J. Hamelin, eds., *Compatibilité Électromagnétique*. Collection Technique et Scientifique des Télécommunications, Paris: Dunod, 1990.

-
- [11] T. Hubing, "Calculating the currents induced on wires attached to opposite sides of a thin plate," in *The ACES Collection of Canonical Problems* (H. A. Sabbagh, ed.), vol. 1, pp. 9–13, App. Comp. Elmag. Soc., 1990.
- [12] V. Levillain, "Un aperçu de la compatibilité électromagnétique dans le groupe AEROSPATIALE," *Congrès National d'Analyse Numérique, CANICE 96*, May 1996.
- [13] Aerospatiale, *Compatibilité Électromagnétique : Nous avons l'expérience et les moyens pour savoir faire décoller vos produits*, 1996.
- [14] B. Archambeault, "Modeling of EMI emissions from microstrip structures with imperfect reference planes," *App. Comp. Elmag. Soc., Monterey*, pp. 1058–1063, 17 – 21 March 1997.
- [15] C. Fuchs, *Effiziente Modellierung leitfähiger Schirme im Zeitbereich*. PhD thesis, Institut für Elektroenergiesysteme und Hochspannungstechnik, University of Karlsruhe, Germany, 1996.
- [16] C. Fuchs, P. Fischer, and A. J. Schwab, "Parallelization of a 3d-TLM-algorithm on a workstation cluster," *App. Comp. Elmag. Soc., Monterey*, pp. 1437–1443, 17 – 21 March 1997.
- [17] B. Archambeault, "Pre-construction evaluation modeling of Open Area Test Sites (OATS)," *App. Comp. Elmag. Soc., Monterey*, pp. 1064–1069, 17 – 21 March 1997.
- [18] C. Bornkessel, *Analyse und Optimierung der elektrodynamischen Eigenschaften von EMV-Absorberkammern durch numerische Feldberechnung*. PhD thesis, Institut für Höchstfrequenztechnik und Elektronik, University of Karlsruhe, Germany, 1993.
- [19] A. Taflové, *Computational Electromagnetics: The Finite-Difference Time-Domain Method*. Boston, London: Artech House, 1995.
- [20] R. Mittra, ed., *Computer Techniques for Electromagnetics*. Pergamon Press, 1973.

-
- [21] R. F. Harrington, *Field Computation by Moment Methods*. New York: The Macmillan Company, 1968.
- [22] K. S. Kunz and R. J. Luebbers, *The Finite Difference Time Domain Method for Electromagnetics*. Boca Raton, Ann Arbor: CRC Press, 1993.
- [23] T. Sarkar and J. Kong, eds., *Special Issue on Numerical Methods*, vol. 1 of *J. Electromag. Waves Appl.*, May 1987.
- [24] J. Achenbach, ed., *Special Issue on Numerical Methods for Electromagnetic Wave Interactions*, vol. 10 of *Wave Motion*, Dec. 1988.
- [25] J. W. Bandler, ed., *Special Issue on Advanced Numerical Techniques in Electromagnetics*, vol. 45, nr. 5 of *IEEE Trans. Ant. Prop.*, May 1997.
- [26] K. S. Yee, "Numerical solution of initial boundary value problems involving Maxwell's equations in isotropic media," *IEEE Trans. Ant. Prop.*, vol. 14, no. 3, pp. 302–307, May 1966.
- [27] T. Weiland, "Eine Methode zur Lösung der Maxwell'schen Gleichungen für sechskomponentige Felder auf diskreter Basis," *Archiv für Elektronik und Übertragungstechnik*, vol. 31, no. 3, pp. 116–120, March 1977.
- [28] A. Taflove and K. Umashankar, "The Finite-Difference Time-Domain (FDTD) Method for electromagnetic scattering and interaction problems," *J. Electromag. Waves Appl.*, vol. 1, no. 3, pp. 243–267, 1987.
- [29] K. R. Umashankar, A. Taflove, and B. Beker, "Calculation and experimental validation of induced currents on coupled wires in an arbitrary shaped cavity," *IEEE Trans. Ant. Prop.*, vol. 35, no. 11, pp. 1248–1257, Nov. 1987.
- [30] W. C. Chew and J. Jin, eds., *Special Issue on Absorbing Boundary Conditions (ABC)*, vol. 16, nr. 4 of *Electromagnetics*, Jul-Aug 1996.
- [31] J.-P. Bérenger, "Calcul de la diffraction à l'aide d'une méthode aux différences finies," *Colloque CEM, Trégastel, France*, June 1983.

-
- [32] J.-P. Bérenger, "Perfectly matches layer for the FDTD solution of wave-structure interaction problems," *IEEE Trans. Ant. Prop.*, vol. 44, no. 1, pp. 110–117, Jan. 1996.
- [33] A. Taflove, K. R. Umashankar, B. Beker, F. Harfoush, and K. S. Yee, "Detailed FD-TD analysis of electromagnetic fields penetrating narrow slots and lapped joints in thick conducting screens," *IEEE Trans. Ant. Prop.*, vol. 36, no. 2, pp. 247–257, Feb. 1988.
- [34] DGA, *GORF 3D, Version 3.0*, 1 ed., 1996.
- [35] The MAFIA collaboration, *T3 - The 3D Time Domain Solver*, Apr. 1996.
- [36] A. Taflove and K. Umashankar, "A hybrid moment method/finite-difference time-domain approach to electromagnetic coupling and aperture penetration into complex geometries," *IEEE Trans. Ant. Prop.*, vol. 30, no. 4, pp. 617–627, July 1982.
- [37] Hewlett Packard, *HP 85180A High-Frequency Structure Simulator, User's Reference, Release 3.0*, 1 ed., Dec. 1994.
- [38] Hewlett Packard, *HP 85180A High-Frequency Structure Simulator, Discovering the System, Release 3.0*, 1 ed., Dec. 1994.
- [39] S. D. Gedney and R. Mittra, "A hybrid method for the solution of the electromagnetic scattering by an inhomogeneously filled through or slit in a thick conducting screen," *IEEE Ant. Prop. Soc. Int. Symp.*, vol. 4, pp. 1730–1733, 1990.
- [40] D. Lecoq, *Détermination du couplage d'une onde électromagnétique avec un câble situé dans une cavité métallique*. PhD thesis, University of Paris VI, France, 1995.
- [41] R. Harrington, "The method of moments in electromagnetics," *J. Electromag. Waves Appl.*, vol. 1, no. 3, pp. 181–200, March 1987.
- [42] K. R. Umashakar, "Numerical analysis of electromagnetic wave scattering and interaction based on frequency-domain integral equation

- and method of moments techniques," *Wave Motion*, vol. 10, no. 6, pp. 493–525, Nov-Dec 1988.
- [43] R. E. Collin, *Field Theory of Guided Waves*. New York, Toronto, London: McGraw-Hill, 1960.
- [44] E. H. Newman, "An overview of the hybrid MM/Greens's function method in electromagnetics," *Proceedings of the IEEE*, vol. 76, no. 3, pp. 270–282, March 1988.
- [45] C.-T. Tai, "On the Eigenfunction expansion of dyadic Green's functions," *Proceedings of the IEEE*, vol. 61, no. 4, pp. 480–481, Apr. 1973.
- [46] Y. Rahmat-Samii, "On the question of computation of the dyadic Green's function at the source region in waveguides and cavities," *IEEE Trans. Micro. Theo. Tech.*, vol. 23, no. 9, pp. 762–765, Sept. 1975.
- [47] C.-T. Tai and P. Rozenfeld, "Different representations of dyadic Green's functions for a rectangular waveguide," *IEEE Trans. Micro. Theo. Tech.*, vol. 24, no. 9, pp. 597–601, Sept. 1976.
- [48] D. B. Seidel, "Aperture excitation of a wire in a cavity," PhD-thesis, University of Arizona, Arizona, 1977.
- [49] S. Schelkunoff, "Kirchhoff's formula, its vector analogue, and other field equivalence theorems," *Communications on Pure and Applied Mathematics*, vol. 4, no. 1, pp. 43–59, June 1951.
- [50] J. van Bladel, "Small-hole coupling of resonant cavities and waveguides," *Proceedings of the IEE*, vol. 117, no. 6, pp. 1098–1104, June 1970.
- [51] F. de Meulenaere and J. van Bladel, "Polarizability of some small apertures," *IEEE Trans. Ant. Prop.*, vol. 25, no. 2, pp. 198–205, March 1977.
- [52] J. van Bladel, "Field penetration through small apertures: The first-order correction," *Radio Science*, vol. 14, no. 2, pp. 319–331, March-April 1979.

-
- [53] Y. Rahmat-Samii and R. Mittra, "Electromagnetic coupling through small apertures in a conducting screen," *IEEE Trans. Ant. Prop.*, vol. 25, no. 2, pp. 180–187, March 1977.
- [54] K. S. H. Lee, ed., *EMP Interaction: Principles, Techniques, and Reference Data*. Washington, Berlin: Hemisphere Publishing Company, Springer Verlag, 1986.
- [55] W. Wiesbeck, "Hochfrequenztechnik I." lecture notes, Institut für Höchstfrequenztechnik und Elektronik, University of Karlsruhe, Germany, 1990.
- [56] J. Bolomey and W. Tabbara, "Numerical aspects on coupling between complementary boundary value problems," *IEEE Trans. Ant. Prop.*, vol. 21, no. 3, pp. 356–363, May 1973.
- [57] V. G. Daniele and M. Orefice, "Dyadic Green's functions in bounded media," *IEEE Trans. Ant. Prop.*, vol. 32, no. 2, pp. 193–196, Feb. 1984.
- [58] M. Aksun and R. Mittra, "Choices of expansion and testing functions for the Method of Moments applied to a class of electromagnetic problems," *IEEE Trans. Micro. Theo. Tech.*, vol. 41, no. 3, pp. 503–509, March 1993.
- [59] J. Meixner, "The behavior of electromagnetic fields at edges," *IEEE Trans. Ant. Prop.*, vol. 20, no. 4, pp. 442–446, July 1972.
- [60] D. Wilton and S. Govind, "Incorporation of edge conditions in moment method solutions," *IEEE Trans. Ant. Prop.*, vol. 25, no. 6, pp. 845–850, Nov. 1977.
- [61] P. Misra and K. Naishadham, "Order-recursive gaussian elimination (ORGE) and efficient CAD of microwave circuits," *IEEE Trans. Micro. Theo. Tech.*, vol. 44, no. 12, pp. 2166–2173, Dec. 1996.
- [62] K. Naishadham and P. Misra, "Order recursive Method of Moments (ORMoM) for iterative design applications," *IEEE Trans. Micro. Theo. Tech.*, vol. 44, no. 12, pp. 2595–2604, Dec. 1996.

-
- [63] J. v. Hagen, D. Leconte, J.-L. Lasserre, J.-L. Lavergne, and W. Tabbara, "Coupling into non-rectangular cavities: simulation and experiments," *App. Comp. Elmag. Soc., Monterey*, pp. 1086–1093, 17 – 21 March 1997.
- [64] J. Andrieu, "L'étude des caractéristiques large bande d'un monocône placé sur un plan parfaitement conducteur," tech. rep., I.R.C.O.M, University of Limoges, France, 1989.
- [65] O. Einarsson, "The Wire," in *Electromagnetic and Acoustic Scattering by Simple Shapes* (J. Bowman, T. Senior, and P. Uslenghi, eds.), Amsterdam: North-Holland Publishing Company, 1969.
- [66] J. von Hagen, W. Tabbara, and D. Leconte, "Coupling to strip-type objects in cavities: A rigorous Method of Moments approach," *PIERS, Innsbruck*, p. 423, 8 – 12 July 1996.
- [67] E. K. Miller, "Solving bigger problems – by decreasing the operation count and increasing the computation bandwidth," *Proceedings of the IEEE*, vol. 79, no. 10, pp. 1493–1504, Oct. 1991.
- [68] Z. Altman, R. Mittra, O. Hashimoto, and E. Michielssen, "Efficient representation of induced currents on large scatterers using the generalized pencil of function method," *IEEE Trans. Ant. Prop.*, vol. 44, no. 1, pp. 51–57, Jan. 1996.
- [69] F. X. Canning, "Improved impedance matrix localization method," *IEEE Trans. Ant. Prop.*, vol. 41, no. 5, pp. 659–667, May 1993.
- [70] Z. Baharav and Y. Leviatan, "Impedance matrix compression using adaptively constructed basis functions," *IEEE Trans. Ant. Prop.*, vol. 44, no. 9, pp. 1231–1238, Sept. 1996.
- [71] R. Singh and S. Singh, "Efficient evaluation of singular and infinite integrals using the \tanh transformation," *IEE Proceedings - Microwave Antennas and Propagation*, vol. 141, no. 6, pp. 464–466, Dec. 1994.
- [72] E. H. Newman, "Generation of wide-band data from the method of moments by interpolating the impedance matrix," *IEEE Trans. Ant. Prop.*, vol. 36, no. 12, pp. 1820–1824, Dec. 1988.

-
- [73] J. von Hagen and W. Tabbara, "Méthode d'analyse large bande du couplage onde-structure," *CANICE, La Londe-Les Maures*, 28 – 31 May 1996.
- [74] R. Bulirsch and H. Rutishauser, "Interpolation und genäherte Quadratur," in *Mathematische Hilfsmittel des Ingenieurs* (R. Sauer and I. Szabó, eds.), no. H in Teil III, Berlin, Heidelberg: Springer-Verlag, 1968.
- [75] J. Stoer, "Über zwei Algorithmen zur Interpolation mit rationalen Funktionen," *Numerische Mathematik*, vol. 3, pp. 285–304, 1961.
- [76] W. H. Press, S. A. Teukolsky, W. T. Vetterling, and B. P. Flannery, *Numerical Recipes in C*. Cambridge, New York and Melbourne: Cambridge University Press, 1992.
- [77] J. Lefèbvre, *Apport des statistiques aux études des phénomènes de couplage en compatibilité électromagnétique*. PhD thesis, University of Paris VI, Nov. 1997.
- [78] A. G. Journel and C. J. Huijbregts, *Mining Geostatistics*. New York: Academic Press, 1978.
- [79] N. Cressie, *Statistics for Spatial Data*. Wiley: Springer-Verlag, 1991.
- [80] C. M. Butler, Y. Rahmat-Samii, and R. Mittra, "Electromagnetic penetration through apertures in conducting surfaces," *IEEE Trans. Ant. Prop.*, vol. 26, no. 1, pp. 82–93, Jan. 1978.
- [81] R. E. Collin, "Rayleigh scattering and power conservation," *IEEE Trans. Ant. Prop.*, vol. 29, no. 5, pp. 795–798, Sept. 1981.
- [82] D. A. Mlynski, "Elektrodynamik." lecture notes, Institut für Theoretische Elektrotechnik und Meßtechnik, University of Karlsruhe, Germany, 1985.

Curriculum Vitae

Persönliche Daten:

Name: Jürgen Christian v. Hagen
Geburtsdatum: 1. Februar 1968
Geburtsort: München, Bayern
Familienstand: ledig

Schulbildung:

1974 - 1976 Guardini Schule in München
1976 - 1978 Grundschule Wolfratshausen
1978 - 1987 Gymnasium Icking (Abschluß: Abitur)

Studium:

1988 - 1994 Studium der Elektrotechnik an der Universität Karlsruhe
Europäisches Gemeinschaftsstudium für Elektroingenieure
1992 - 1993 Ecole Supérieure d'Ingenieurs en Electronique et
Electrotechnique, Paris
1993 - 1994 University of Essex, Colchester
1994 - 1997 Doktorand des
Insitut für Höchsfrequenztechnik und Elektronik
und des
Laboratoire des Signaux et Systèmes, Gif-sur-Yvette